University of Alberta

A Wireless 3D Posture Monitor for Adolescent Idiopathic Scoliosis

by

Christopher Woloschuk

A thesis submitted to the Faculty of Graduate Studies and Research in partial fulfillment of the requirements for the degree of

Master of Science

in

Biomedical Engineering

Department of Electrical and Computer Engineering

Abstract

Scoliosis affects 2.5% of adolescents and 90% of these adolescents have mild curves of less than 25°. These adolescents do not currently have any active treatments to prevent curve progression. Literature suggests that exercise-based treatment may be able to help patients with mild scoliosis. Current posture monitoring systems measure posture along the sagittal and/or coronal planes, but neglect the transverse plane. The objective of this research was to develop a 3D posture monitoring system to study the effects of posture training. The developed system used a wireless distributed computing network of orientation sensors and a master processing and feedback unit to compute an individual's posture, provided feedback if correction was required, and stored session information for later analysis. Testing demonstrated that the system possessed sufficient accuracy to measure posture. Volunteers who used the developed system for posture training spent less time in poor posture when feedback was provided for correction.

Acknowledgements

This thesis would not be possible without the assistance and support of many individuals. I would like to begin by expressing my gratitude to both of my supervisors, Dr. Vicky Zhao and especially Dr. Edmond Lou for his guidance and help in navigating the academic world.

I would like to thank the members of my committee for their time and feedback in helping to improve this work.

NSERC and the Government of Alberta for generously providing me with funding to undertake my research.

I owe a great deal to Mr. Eric Chalmers, Mr. Fraaz Kamal, and Mr. Jacob Ortt for their technical support and friendship. I am especially grateful to the volunteers who wore the posture monitoring system during testing.

I would like to acknowledge all staff members at the Glenrose Rehabilitation Research Centre. It was a privilege working with you all. Thank you for the coffee.

I would also like to thank the staff at the Glenrose Rehabilitation Hospital, espcially Mr. Justin Lewicke for his assistance and expertise in the motion capture camera laboratory.

I am grateful to Ms. Kayleigh Cline for her assistance in proof reading the first few chapters of this thesis and for providing an outsider's perspective of the realm of scoliosis research.

To my family - this is what I was up to for the past two years. Thank you so much for all of your support.

And finally I would like to thank Ms. Laura Doyle for her unconditional support, patience, and understanding throughout all the stages of my degree. I could not have done it without you.

Table of Contents

List of Tables

List of Figures

List of Abbreviations

ADC	*Analog to Digital Converter*
AIS	*Adolescent Idiopathic Scoliosis*
BLE	*Bluetooth Low Energy*
CPU	*Central Processing Unit*
DPS	*Degrees Per Second*
dBm	*Decibels Relative to 1 Milli Watt*
EM	*Electromagnetic*
FITS	*Functional Individual Therapy of Scoliosis*
G	*Gauss*
GPIO	*General Purpose Input / Output*
I^2C	*Inter-Integrated Circuit*
IEEE	*Institute of Electrical and Electronics Engineers*
IMU	*Inertial Measurement Unit*
ISM	*Industrial, Science and Medical*
kB	*Kilo Byte*
LSB	*Least Significant Bit*
LiPo	*Lithium Polymer*
LED	*Light Emitting Diode*
mAh	*Milli Amp Hour*
MEMS	*Micro-Electrical-Mechanical Systems*
PAN	*Personal Area Network*
PCB	*Printed Circuit Board*
POF	*Plastic Optical Fiber*
RTC	*Real-Time Clock*
RMS	*Root Mean Square*
SIG	*Bluetooth Special Interest Group*
SIR	*Scoliosis In-Patient Rehabilitation*
SoC	*System on a Chip*
SOSORT	*Society on Scoliosis Orthopaedic Rehabilitation and Treatment*

SPI	*Serial Peripheral Interface*
SRS	*Scoliosis Research Society*
TLSO	*Thoraco-Lumbo-Sacral-Orthosis*
UART	*Universal Asynchronous Receiver/Transmitter*
UAV	*Unmanned Aerial Vehicles*
WPAN	*Wireless Personal Area Networks*

Chapter 1

Introduction

Scoliosis is a condition where the spine possesses an abnormal curvature along the coronal, sagittal and/or transverse planes. Scoliosis affects approximately 2.5% of adolescents [1]. Adolescent Idiopathic Scoliosis (AIS) is the most common form of scoliosis and it has no known causes. There are no known cures for AIS, but treatments have been developed to prevent the condition from deteriorating further for the patient.

While AIS does not significantly increase an individual's mortality rate [1, 2], severe curves can alter the appearance of the patient and cause him/her undue psychological stress. AIS can also cause the patient additional pain in their back due to the uneven loading on the spinal column and the hips.

Treatments for AIS aim to stop the progression of the patient's curve. The most intense treatment option available is surgical correction of the curve. Surgery is seen as the last and least desirable treatment option for patients with scoliosis. The surgery involves the placement of metal rods along the side of the spine, which are attached to the spine using special screws and hooks. The orthopedic surgeon will manually force the spine into a more correct form and then, using metal rods and hooks to hold the spine in place, applies a bone graft in order to fuse the selected vertebrae and to halt the curve progression. The fusion of the vertebrae results in a permanent loss of mobility for the patient. As well, major surgery can be dangerous and the recovery time for patients can be quite lengthy.

A less invasive treatment option for AIS is to have the patients wear an external brace to force their spine into a more 'natural' position until they reach maturity. For some patients, it may be years before they reach maturity and they will need to wear their brace every day in order to have the highest likelihood of a positive outcome. Bracing can be uncomfortable as the brace is constantly applying corrective force to the patient's body. These braces can be large and rigid, which can limit the movement of patients and can decrease their self-image.

Brace treatment does not guarantee that there will be no curve progression. There are many factors that can affect the brace treatment, such as the initial curvature and the age of the patient [3, 4]. These factors make it difficult for therapists and other medical professionals to predict whether the brace treatment will be effective or not. If the brace treatment is not effective and the curve is deteriorating, surgery may be recommended to the patient to correct his/her curve.

There is another type of treatment for AIS, similar to bracing, that can be recommended for patients with mild curves of less than 25°. In exercise-based treatments, the patient uses his/her own body to halt the curve progression. These exercises strengthen the core muscles of the patient, so that the muscles can act as a natural brace. The exercises are also designed to teach patients to be more self-aware of their own posture and to correct it when they have assumed a poor posture. Maintaining a correct posture throughout the day can be quite challenging and difficult to self-regulate. Patient compliance also plays a critical factor in determining whether the exercise-based treatment will be successful. Without compliance information, determining if treatment failure is the result of the specific treatment itself or due to patient non-compliance can be difficult.

Requiring a therapist to monitor patients continuously in order to ensure that they are maintaining a correct posture can be tedious and not very efficient. The therapist may only be available for specific times during the week and exercise-based treatment requires that the patient be performing his/her exercises or posture improving exercises on a regular basis. An external system that could continuously monitor the posture of a patient while he/she is performing the exercises and also provide feedback to the patient would be of considerable benefit. The benefit to the patients would be the capability of performing their exercises on their own schedule and in the privacy of their own home. The benefit for the therapist and/or researcher is that the system would be able to monitor the compliance of the patient towards the exercise treatment and the frequency at which he/she use the treatment. Feedback provided by the system to the patient would aid the patient in developing correct posture.

This research seeks to determine the effectiveness of monitoring the posture of a patient and providing feedback when the patient has not adopted a correct posture. The final goal of this research is to determine whether exercise-based treatments are effective at treating patients with mild scoliosis. Although the use of exercise in the treatment of scoliosis has been reported, a randomized clinical trial has not been performed to validate the true effectiveness of exercise for the treatment of mild scoliosis. This evaluation of the effectiveness of an exercise-based treatment will necessitate the design and construction of a system that is able to both monitor a patient's posture and to provide feedback to that patient if his/her posture requires correction.

1.1 Application of Posture Monitoring for Patients with Mild AIS

Posture monitors have been utilized extensively by researchers as a means of monitoring the posture of patients during their normal day to day lives [5–14]. Compared to other systems that utilize high-speed cameras and markers placed on the patient to detect motion and orientation, posture monitors are smaller, less intrusive, and often mobile. The ability for the posture monitor to be utilized by the patient and by researchers outside of a clinical setting is greatly beneficial. With respect to the application being discussed in this thesis, a posture monitor would allow patients with AIS to perform specific exercises aimed at stopping their curve from progressing. This posture monitor would also act as a feedback mechanism, triggering only when it detects incorrect posture, with the goal of training the patient to recognize and adopt a correct posture.

The posture monitoring system could also be beneficial to researchers and clinicians to evaluate the effectiveness of different types of exercise regimes as well as patient acceptance and compliance towards those exercises. Individualized exercises programs may be developed to maximize the likelihood of a positive outcome from the treatment.

1.2 Objectives

The objectives of this thesis are:

- To research and determine the most suitable type of sensors for use in a posture monitoring system.
- To design and validate the developed 3D posture monitoring system.
- To determine the accuracy of the pitch, roll, and yaw angles measured by the system.
- To evaluate the immediate response of a subject on using the 3D posture monitoring system.

1.3 Scope of Work

As mentioned before, there have been many posture monitoring systems previously developed by researchers. These posture monitors have been designed with many different types of sensors such as inductive sensors, electromagnetic transmitters and receivers, accelerometers, and gyroscopes. These sensors will be examined in order to determine the most appropriate sensor for this posture monitoring system. The sensors must be small and consume low power.

As well, research will be required to determine the most effective method for communication between the sensors and the processing unit. To increase patient acceptance, wireless communication is recommended as this will allow for the flexibility of monitoring different locations along the patient's back. Furthermore, using wireless communication can eliminate wires between the sensor units and the processing unit will improve the robustness of the system.

Once the communication protocol and the sensors have been chosen, a wireless distributed computing network will be developed to determine the posture of the patient. As the system is aimed to be small, light weight, and portable, the selection of electronic components will be considered carefully. In addition, as wireless communication consumes more power than wired communication, a compromise between the battery life and overall size has been performed. A larger battery will allow the system to operate for a longer period of time but a smaller battery will be lighter and more easily integrated into a garment.

Overall, one of the major requirements of the system is that it is does not interfere significantly in the patient's daily activities in order to keep compliance high.

The integrated system will then be tested to determine the accuracy and reliability of the angle measurements from the sensor units. The system will also be used by volunteers to calculate their posture. In this thesis, the posture monitor will undergo a few short term tests to evaluate the effectiveness of posture training using the posture monitoring system.

1.4 Thesis Overview

This thesis contains six chapters. It begins by reviewing scoliosis and the current treatment options. After this, a comprehensive literature review of posture monitors have been reported. The theory behind the system and the design of the system is presented. Finally, the complete posture monitoring system has been used to investigate its effectiveness at monitoring and correcting the posture of a patient.

Chapter 1 contains an introduction to AIS and reports the use of exercise as a treatment option for scoliosis. This chapter also describes the objective and the scope of the thesis.

Chapter 2 provides a review of scoliosis and the current treatment options that are available. Also, an in-depth literature review of posture monitoring systems has also been reported.

Chapter 3 describes the theories behind the different types of sensors that are being used in this thesis. The wireless protocol IEEE's 802.15.4 is presented and it has been compared to other existing low power wireless protocols, namely Bluetooth and ANT. This chapter also contains information detailing how the sensor fusion algorithm works in order to combine the data from the sensors into an accurate orientation of the sensor unit.

Chapter 4 provides a detailed description of the design of the 3D posture monitor. This includes the sensor units, the master control unit, and their integration into the full posture monitoring system.

Chapter 5 reports the laboratory test procedures and results for the sensor units, the master control unit, and the full posture monitoring system.

Chapter 6 summarizes the work performed in this thesis and provides some future recommendations for using the posture monitoring system in long-term clinical trials, as well as to further improve the system to increase the usability and effectiveness of the system.

Chapter 2

Background

2.1 Human Anatomy

The human spine is an important structure inside the body as it maintains an upright posture when standing or sitting, and it supports the head, neck, and trunk by transferring their weight to the lower limbs. As well, the spine protects the spinal cord and nerves. In all, it is composed of 26 individual bones, called vertebrae, and separated into five different regions as shown in Figure 2.1. Starting from the base of the head and counting downwards, the regions are called cervical, thoracic, lumbar, sacral, and coccygeal. The seven vertebrae in the cervical region form the neck. There are twelve vertebrae in the thoracic region and they form the mid-back. Five lumbar vertebra form the lower back. The sacral region consists of a single vertebrae called the sacrum. The sacrum begins as a series of five smaller vertebrae that fuse together by the age of 25. Similarly, the coccygeal region also only consists of a single vertebra called the coccyx which initially starts out as three to five smaller vertebrae that fuse together later in life [15]. When referencing specific vertebra, the convention is to write the first letter of the region in question, followed by the number (for example: the fifth vertebra in the thoracic region would be labeled "T5"). Each vertebra in the spine is separated by intervertebral discs, which are made up of fibrocartilage [15]. The parts of the vertebra that are connected to the intervertebral discs are called the endplates.

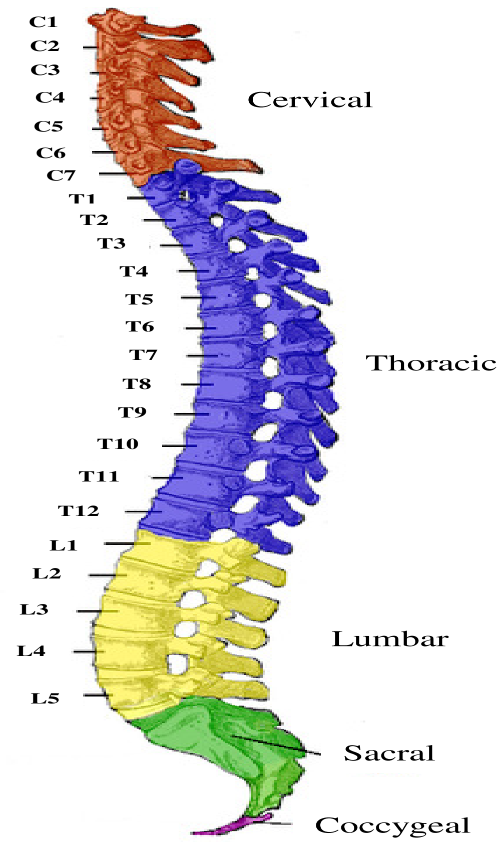

Figure 2.1: Lateral view of spinal column
[16]

Planes are often used when describing the orientation and position of the human body. The standard cartesian coordinate system used by the Scoliosis Research Society (SRS) originates at the superior (upper) endplate of S1 [17]. The positive X axis goes towards the anterior (front) of the patient while the positive Y axis goes to the left of the patient. The positive Z axis goes towards the superior part of the body.

The commonly used terminology of the three planes that bi-sect the human body are shown in Figure 2.2. The coronal plane runs vertically through the body (YZ plane) and separates the posterior (back) from the anterior regions. The sagittal plane (XZ plane) divides the left and right sides and the transverse plane (XY plane) separates the superior region from the inferior (lower) region.

The "balance" of a patient's spine refers to the head being correctly positioned over top of the sacrum and pelvis in both the sagittal and coronal planes [17].

Balance also implies that the shoulders of the patient are both at the same height and that the mass of his/her trunk is evenly distributed around an imaginary axis passing through the sacrum in the spine [17]. The process of a patient attempting to become balanced is termed compensation while decompensation is the failure of the patient to achieve balance [17].

The amount of rotation about the vertebrae about the Z axis is defined as the vertebral axial rotation [17]. The vertebral lateral rotation is the amount of rotation the vertebra has undergone about the X axis and the vertebral flexion/extension rotation is the amount of rotation about the Y axis [17]. Flexion is the term used when an angle is decreasing while extension is used when the angle is increasing [17].

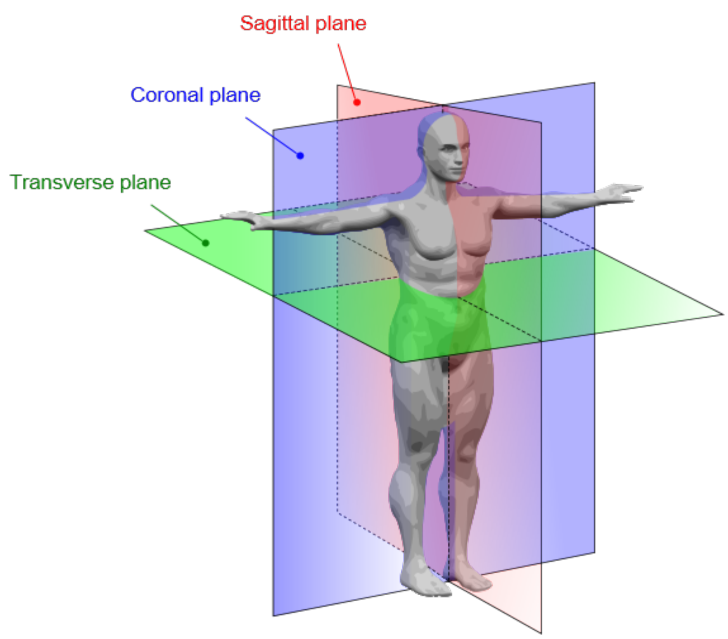

Figure 2.2: Anatomy planes of the human body
[18]

2.2 Adolescent Idiopathic Scoliosis

Scoliosis is a condition that affects the spine and it is characterized by an abnormal curvature along the coronal, sagittal, and/or transverse planes. Scoliosis that is diagnosed without any known cause is referred to as idiopathic scoliosis [1,3,19,20]. Idiopathic scoliosis is divided into three categories based on the age of onset - infantile (up to three years old), juvenile (three to ten years old) and adolescent (ten to sixteen years old) [1]. As the age of onset is often not easily determined, there can be some overlap between the three stages [1, 3, 4]. Infants with idiopathic scoliosis are often diagnosed within the first six months of life [1]. AIS is the most common spinal deformity seen by spinal surgeons and primary care physicians [2–4]. AIS affects between 1% to 3% of the population between ten and sixteen years old [2, 19, 21] and is more common in females [4, 19]. Factors and indicators of curve progression are much studied areas [22–24], and many researchers believe that there could be a genetic component to the disorder as AIS is often seen in multiple members of one family, but no pattern of susceptibility has been uncovered [1, 4, 19, 22, 25, 26].

Puberty is a critical stage for those with AIS because they experience a significant amount of growth which can cause their curve to increase rapidly [4,19,27]. The greater the initial curve and the lesser the skeletal and/or sexual maturity of the patient, the higher the risk of curve progression [19]. Significant curve progression is problematic since it can lead to future cardiopulmonary problems, back pain, and psychological concerns brought upon by the patient's own views on his/her appearance [19, 27]. Significant curve progression can lead to continuous asymmetric loading on the spine which can cause the curve to progress further [27]. AIS does not significantly increase an individual's mortality rate [1, 2], but for curves that are very large ($\geq 80°$) and left untreated, AIS can lead to cardiopulmonary failure which can result in death [1].

Due to the idiopathic nature of scoliosis, the only available treatments for the condition deal with either preventing curve progression or correcting more serious curves. Treatments are recommended for patients who have curves of $20°$ or greater [2]. The treatments for AIS can affect the quality of the life of the patient [2, 28]. Some studies have shown that patients perceive themselves to be less healthy than those around them and as a result have restricted their social and physical activities [19, 20]. Adolescents who have been diagnosed with scoliosis also have to contend with puberty, a sensitive stage in life where self-image becomes a paramount factor in the adolescent's daily life as relationships with peers becomes more important [28]. A diagnosis of AIS requires some major lifestyle changes such as visiting specialists, wearing a brace, and/or performing specific exercises [28]. These lifestyle changes can lead to feelings of fear, depression, hopelessness, self-doubt, and segregation from the adolescent's peers [28]. This feeling of being different and deviating from the norm can lead to many AIS patients developing a sense of shame and the wish to hide or obscure their deformity from the rest of the world [28]. Depending on the treatment provided, adolescents may have a difficult time hiding their condition, especially in young girls because of current fashion trends that focus on body-emphasizing clothing [28]. Untreated idiopathic scoliosis in adults can also possibly lead to social isolation and limited job opportunities [2].

A common term used in identifying the severity of the curve along the coronal plane is called the Cobb angle [29]. The Cobb angle is defined as the angle formed between a parallel line drawn from the top of the most tilted vertebra above the curve and a second parallel line drawn from the bottom of the most tilted vertebra below the curve [29]. The larger the Cobb angle, the more severe the curve as can be seen in Figure 2.3. The value of the Cobb angle, when measured by a trained specialist, can vary in magnitude by 5° [30, 31].

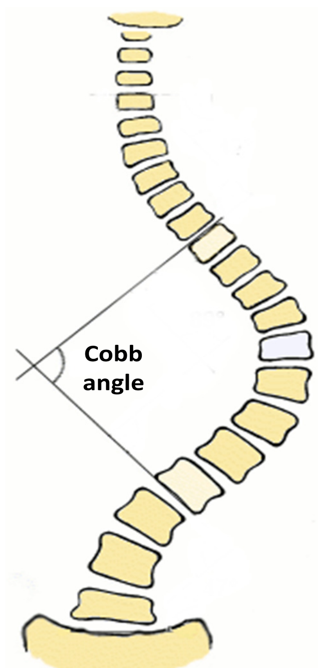

Figure 2.3: Measurement of the Cobb angle
[32]

Two other common measurements for patients with AIS are the kyphotic angle and the lordotic angle on the sagittal plane. The kyphotic angle (K) is formed by the intersection of one line that is parallel to the top plate of the most upper tilted vertebra and a second line running parallel from the base plate of the lowest tilted vertebra in the thoracic region as seen in Figure 2.4. The lordotic angle (L) is calculated in a similar manner to that of the kyphotic angle except that the tilted vertebrae are located in the lumbar region.

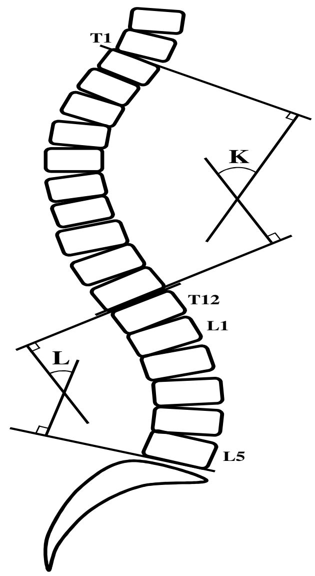

Figure 2.4: Kyphotic (K) and Lordotic (L) Angles

2.3 Surgery

There are two primary treatments for AIS - surgery and conservative treatments [2]. Surgical treatment is considered the least desirable and last possible option that can be prescribed to a patient with AIS. Surgery would be recommended for patients with curves over 45° or if there was significant progression with a prior non-operative treatment such as bracing [2, 4, 19]. Non-operative treatments are also referred to as conservative treatments and will be discussed in Section 2.4. The surgical treatment differs from the non-operative treatments in that the purpose of surgery is to stop the progression of the curve through vertebral fusion in the spine [19]. Metal rods are placed along the side of the spine and attached to the vertebra using special screws and hooks. The rods keep the spine in the corrected position while the bone graft is applied in order to fuse the vertebra together. The surgical treatment therefore causes a loss of movement and flexibility for the patient for the rest of his/her life and a very long recovery period. Surgery is a better option at the adolescent stage than the adult stage as he/she is at a lower risk for developing complications [3].

2.4 Conservative Treatments

The vast majority of AIS patient will undergo a conservative treatment [2]. The goal of conservative treatment is to stop the progression of the curve [19]. Two common conservative treatments are bracing and exercise.

2.4.1 Bracing

Bracing involves the use of a rigid (or soft) brace that is worn by the adolescent for a significant portion of the day in order to mechanically halt his/her curve from progressing. A value of $5°$ is often used as a threshold for progression [33]. Some researchers believe that bracing is only an effective treatment when the patient has reached puberty and is growing at an increased rate [4, 34]. The brace is prescribed to be worn until the patient has reached skeletal maturity [19, 34, 35]. The more hours per day that an adolescent wears his/her brace, the more effective the treatment will be [34]. Skeletal maturity is measured using the Risser sign, which is based upon the amount of calcification of the human pelvis. A grade of 0 indicates no skeletal maturity while a grade of 5 indicates that skeletal maturity has been reached [35]. Achieving skeletal maturity greatly reduces the risk of further curve progression [19].

The prescribed amount of time that a brace is to be worn depends on the type of brace used. The Thoraco-Lumbo-Sacral-Orthosis (TLSO) brace is prescribed for full-time wear (approximately 23 hours per day) [36]. It can be custom moulded to the patient's trunk or fabricated using a pre-made brace with custom interior pads [36]. It uses both passive and active correction to halt the patient's curve [36]. Passive correction occurs from the brace applying a force to the patient's body, while active correction entails the patient themselves adjusting his/her body away from the interior pads to relieve pressure. Another brace that is prescribed for full-time wear is the Milwaukee Brace (Cervico-Thoraco-Lumbo-Sacral-Orthosis) [36]. The Milwaukee brace consists of a neck ring that is connected to a plastic pelvic section through two posterior and a single anterior upright, which are rigid vertical bars [36]. Pads are connected to the uprights to provide corrective force [36]. The Charleston brace is different from the TLSO or Milwaukee braces in that it is a part-time brace that is meant to be worn by patients at night [36]. The Charleston brace bends the spinal column towards the convexity of the curve [36].

Although bracing has been used for 45 years, the effectiveness of the brace treatment is still debatable [2, 19]. Those who disbelieve the effectiveness of bracing say that there is poor correlation between success and failure of bracing treatment [19] and that clinical studies need to have longer follow-up times (ideally from start of treatment until maturity) in order to determine the treatments long-term effects [2]. The definition of success is also disputed as some state that the measure of success is in limiting the amount of curve progression while others state that a successful treatment would prevent the adolescent from having to undergo corrective surgery to repair the curve [19]. Furthermore, patient compliance can be a major issue affecting the treatment outcome. Lenssinck *et al.* suggested that in order to determine the effectiveness of the brace treatment, the patient's compliance should be recorded [2]. Due to the numerous factors involved in brace treatment such as the type of brace, patient compliance, skill of the orthotist who made the brace, and the skeletal maturity of the patient, it is very difficult to predict the brace treatment outcome [3]. In 2005, Richards *et al.* proposed a set of standardized criteria that should be used in order to properly determine the effectiveness of bracing [37]. This study has become the gold standard for determining brace effectiveness. The effectiveness of bracing needs to take into account the amount of curve progression that the patient experiences as well as if he/she have undergone surgery within two years of completion of the brace treatment. The SRS then suggested that these criteria should be used in any future brace study. The effectiveness of the brace treatment should be determined after two years of completion of the brace treatment.

In addition, Upadhyay *et al.* conducted a study of 85 AIS patients who were treated with bracing [23]. The goal of the study was to determine if there are any radiological features that can be identified in order to predict the effectiveness of the brace early on in the treatment. In this study, no change was deemed to be when the change in Cobb angle was within $\pm 5°$. They found that patients who experienced an increase in Cobb angle and/or vertebral rotation within the first two months of wearing their brace had a significantly higher chance for their brace treatment to fail (93%) and to require surgery to correct their curve (79%). For patients who had a reduction in both vertebral rotation and Cobb angle within the first two months, they had a 97% likelihood of having a positive outcome from the treatment.

This finding from [23] can potentially prevent those patients who are unlikely to benefit from brace treatment from needing to wear the brace for a prolonged period of time. Bracing requires a big commitment from patients as braces are uncomfortable, must be worn for long periods of time, and are quite visible. It is also a difficult decision for adolescents as the brace is worn during puberty when their body image is important [28, 34]. Wearing a brace can limit movement and cause a social withdrawal from normal leisure and recreational activities [28]. If a patient has a low likelihood of a positive outcome from the brace treatment, does it make any sense for the patient to wear the brace until the end of treatment period? The brace may just add another complication to his/her daily life with no real benefit. Similarly, if a patient is told that he/she has a much higher chance of a positive outcome from his/her brace treatment, the patient may be more likely to fully comply with the treatment. As well, Bunge *et al.* found that patients were more likely to undergo brace treatment if treatment decreased the probability of requiring surgery [38].

2.4.2 Exercise

The aim of using exercise as a treatment for AIS is to prevent the aggravation of the curve and potentially to work in conjunction and enhance the brace treatment [19]. Exercise is favoured in European nations, such as France, Spain, and Germany [19]. Some studies have shown that patients who are prescribed an exercise-based treatment experience less progression than those who did not have any sort of treatment [27, 39, 40]. While some literature has stated that exercise-based treatments have not been proven to be effective [3,4], a systematic review of the literature conducted by Weiss *et al.* has shown that there is no evidence to support the ineffectiveness of exercise-based therapies at treating scoliosis [27].

Kenanidis *et al.* [22] found that there was no significant increase in risk of developing AIS in relation to the athletic ability of the children. The study involved 2593 children who were asked to identify if they considered themselves to be 'athletic' or 'non-athletic' and examined to determine if they have AIS. This study showed that exercise itself did not increase the risk of curve progression for AIS patients.

A preliminary report by Mooney *et al.* [41] found that strength training exercises for AIS patients was able to reduce the curve or halt its progression. They investigated the effect of muscle asymmetry on AIS patients. A total of twelve patients (ten female) were involved in the study and each performed trunk rotations to the left and right twice a week for four months. Only one of the patients progressed by more than 5° and that patient started out with a curve of 60°. The remaining patients had their curves stabilize and four patients had their curves decrease. Although the results of this study showed promise, a conclusive statement could not be made. The major reasons were that the study time was short and the sample size was small. It was difficult to confirm if the effects of the strength exercises were better than natural history [25].

Schroth [42] introduced a specific exercise regime called the Schroth Method, for the treatment of scoliosis for all ages. The Schroth Method recognizes that scoliosis is a three dimensional deformity and that treatments must address each dimension. It uses a technique called rotational breathing that allows the patient to selectively inflate the concavity of his/her curve in order to act against it. As well, the patients are taught to mirror their curves, and by doing so, creating the opposite shape of their curve, so to prevent the curve from progressing. The Schroth Method teaches patients how to help themselves by performing specific exercises and maintaining a correct posture during their daily activities. Weiss *et al.* conducted a controlled study [40] to determine the effectiveness of the Schroth Method. One group of 181 patients underwent the scoliosis in-patient rehabilitation (SIR) treatment while the control group consisted of a natural history study that was performed in the same geographical area. They found that there was a lower risk of progression for patients under the age of twelve with curves of less than 30° in the treatment group (46.7%) than when compared to the natural history group (71.2%). Progression was deemed to be an increase of 5° or more of the curve. Jelaĉić *et al.* conducted a study on the short-term effects on back symmetry using the Schroth Method [43]. A total of 47 patients were treated exclusively with exercise for three hours per day, five times per week for four weeks. The results of the study indicated that the treatment improved both the back asymmetry and the spinal imbalance in the coronal plane of the patients. A long-term study would need to be conducted to determine if the treatment has a lasting effect on the asymmetry of the patient's back.

Negrini *et al.* [39] undertook a study to examine the effectiveness of two different exercise-based treatments on preventing brace prescription and curve progression for patients with AIS. One treatment involved a personalized exercise program while the second treatment involved more standard exercises. Patients in both groups were required to participate in sports activities as part of the treatment. The results of the study found that only 6.1% of patients in the personalized exercise group required bracing compared to 25% in the standard group. The authors claim that the Cobb angle in the personalized group improved while the standard group worsened, but the actual changes were -0.67°and +1.38°respectively. These changes in the Cobb angle were too small from which to draw any definite conclusions [25]. As well, Negrini *et al.* did not mention what the criteria were for assigning brace treatment to the patients so it is difficult to determine if the bracing was a direct result of the exercise program failing or if the patients already started out with a larger curve than the rest of the patients in the study. An important result of this study is the reduction in the number of patients requiring brace treatment. Brace treatment is a more intense treatment when compared to exercise and so it would be advantageous for the patient to only require an exercise-based treatment.

Some researchers have investigated the use of exercises in conjunction with brace treatment to determine if exercises can enhance the effect of bracing and improve the outcome. Maruyama *et al.* [35] investigated the effects of conservative treatment as it related to reducing the incidence of surgical treatment. Their study involved 328 female patients. Patients who possessed curves of less than 25° or were skeletally mature (Risser sign of 4 or 5) were treated only with exercise. The remaining patients were treated with a combination of part-time brace wear (eight hours per day) and exercise. The two exercises that the patients performed were the side shift and the hitch exercise. The side shift involved the patient shifting his/her trunk into the concavity of his/her curve from a neutral position. The hitch exercise consisted of the patient starting in a neutral position, lifting his/her heel on the side with the dominant curve while keeping his/her leg straight, and then returning to the neutral position. Of the 328 patients in the study, only 20 required surgical treatment as their curve had progressed beyond 50°. These 20 patients all started off with a much larger curve (48.5°±9.3°). The remaining patients showed no significant progression (average curve of 31.2°±10.2°). From the 328 patients in the study, 299 of them were followed until after the age of 15. Their results led the authors to recommend using the brace full-time in conjunction with part-time exercise using the side shift and hitch exercise.

Negrini *et al.* [44] investigated how the criteria for conservative treatment of scoliosis put forth by the Society on Scoliosis Orthapedic and Rehabilitation Treatment (SOSORT) compared to the criteria for selecting patients to be included in research studies put forth by the SRS in a retrospective study. The SRS criteria [37] states that for inclusion in a brace study the patients must be ten years old or older, have a Risser sign of 0-2, have curves between $25°$ to $40°$, have received no prior treatments, and for female patients, be less than one year post-menarcheal. The authors believed that the combination of SOSORT and SRS criteria would offer the best combination of clinical and methodological quality for studies. The study consisted of 48 patients (44 female) who had an average age of 12.8 ± 1.6 years old with an average Cobb angle of $30.4° \pm 4.4°$. Only two patients were treated with exercise only, and these exercises were designed with strength and stabilization as the focus. For the remaining brace-wearing patients, the exercises were designed to increase the correction provided by the brace and, as well, to avoid the loss of correction when weaning off the brace once they reached Risser sign 3. Treatment lasted on average 4.2 ± 1.4 years. At the end of the study, no patient progressed beyond $45°$ and only 15% required surgery in the two year follow up of the patients. The conclusion of the study was that patients who fit into the SRS inclusion criteria could be successfully treated with conservative treatments. The study reported that for patients who are undergoing brace treatment, the inclusion of specific exercises during the brace treatment and afterwards was shown to be beneficial in preventing moderate curves over $25°$ from deteriorating.

Bialek [21] studied the effects of the Functional Individual Therapy of Scoliosis (FITS) concept, which is a conservative treatment that aims to teach patients techniques and postures to correct scoliosis. Bialek believes that it is important to make the patient a partner of the treatment and not simply a subject. In this way, the motivation of the patient to exercise is significantly increased and this will lead to the treatment producing better results. Not a single patient out of the 115 involved in the study required surgery. For 78 patients who had a curve between $10°$ to $25°$, 50% improved their curve by more than $5°$, 46.2% stabilized their curve, (which was defined as changing by no more than $\pm 5°$), and the remaining patients progressed more than $5°$. The remaining 37 patients, who had larger curves between $26°$ to $40°$, were treated with a combination of bracing and FITS. For these 37 patients, 20% showed improvement of curve reduction by more than 5° while the remaining 80% showed that their curve stabilized. This study shows that exercise is a viable treatment by itself for AIS patients who posses a curve of less than 25° and exercise can improve the outcome of patients who have larger curves and use a combination of bracing and exercises.

In 2008, Negrini published a paper [45] that discussed the trend of scoliosis research being skewed to favour surgery compared to conservative treatments. Negrini argued that scoliosis is a complex condition and patient treatment requires "... continuous multi-disciplinary (and in rehabilitation also multi-professional) interactions". He hypothesized that a large prevalence of orthopedic surgeons in the field of scoliosis treatment could be creating false impressions with regard to patient care and in treatments themselves. Negrini advised that specialists of conservative treatments should become more involved in the scoliosis field in order to "create better teams". That is not to say that all orthopedic surgeons do not support conservative treatments; however, after performing a bibliometric analysis of available literature online, Negrini noted that there was an increase in surgical research while the effectiveness of conservative treatments were criticized. While he acknowledged that surgery can be unavoidable for severe curves, curves causing additional symptoms or where conservative treatments have failed, it is hard to believe that surgery is considered preventive. He also claimed that vertebral fusion did not have any proof that it was beneficial to patients in the long-term, though he only cited one paper [46] to back up that claim. The question at this point is why conservative treatments are more heavily criticized than surgery? Negrini suggested three possible reasons for the preference of surgical treatments. The first was that orthopedic surgeons have the greatest interest in studying AIS and with that would naturally come more research with a focus on surgery. His second suggestion was that the lack of proof for the efficacy of conservative treatments in the 1980s through to the 1990s pushed researchers to focus on surgical treatments. Finally, his third suggestion was that surgery may be more socially acceptable compared to conservative treatments.

Negrini *et al.* [47] performed a systematic review of the literature to examine the efficacy of exercise-based treatments for AIS. The aim of the review was to provide proof for the scoliosis treatment community that exercise is a positive influence for those suffering from the deformity. The authors concluded that the exercise can be recommended for reducing the progression of scoliosis.

However, the authors do suggest that the evidence is not completely conclusive as there are still questions regarding the long-term effects of exercise-based treatments. As well, it is not possible to state which exercises are the most effective, so more clinical trials will need to be performed. This review highlights the need for more standardized clinical trials of exercise-based treatments to prove the validity of exercises.

For all exercise-based treatments, the patients must rely on their sense of proprioception in order to correctly perform the exercises for maximum effectiveness. Proprioception is the sense of one position of your body in relation to another part of your body. Proprioception is important for an exercise-based treatment as when the patient is no longer under the supervision of a therapist, the patient will need to rely on his/her own senses to determine if he/she are currently in a good posture or a bad posture. Barrack *et al.* conducted a study on proprioception in patients with idiopathic scoliosis [48]. They found that patients with scoliosis had a much more difficult time reproducing specific movements of their limbs. The results of this study showed patients with idiopathic scoliosis might have difficulty in monitoring their own posture, which might reduce the effectiveness of the exercise treatment.

One possible solution to the problem of proprioception in AIS patients involves a physiotherapist working with the patient to ensure that the exercises are done correctly [21, 40, 41, 43]. For example, patients using the Schroth Method undergo weeks of intensive exercise training with therapists [40, 42]. However, it is not practical or efficient to have a therapist available at all times to monitor a patient while he/she is performing his/her exercises. If patients required a therapist to monitor their exercises, patients may not partake in their exercises as frequently. Fewer opportunities for performing their exercises could lead to reducing the effectiveness of the treatment.

Another solution may be the use of a device to act as a neutral observer which can monitor the patient as he/she performs his/her exercises and provide feedback when the patient is not performing the exercise correctly. This device could be constructed using a series of sensors to monitor the position of various points on the patient's body. These sensors would be able to calculate and compare the motions of the patient to a predefined 'ideal' motion and provide feedback in order for the patient to correct themselves. Designing this observer, henceforth known as a posture monitor, is an area of where extensive research has been made and a good portion of this research has been directed at developing posture monitors specifically for treatment of AIS.

Exercise-based treatments have been shown to be quite effective at treating mild cases of AIS, where the curve is less than 25°. One type of exercise used in an exercise-based treatment is posture training. Posture training involves the patients adopting a more correct posture for a prolonged period of time in order to strengthen the muscles in their back. Using a posture monitor may help to improve the effectiveness of posture training by providing feedback to the patient when he/she is not adopting the correct posture so the patient can correct it. The next section examines the current state of posture monitors and investigates the different types of posture monitors that have been developed.

2.5 Literature Review of Posture Monitors

A posture monitor is a system that can gather information pertaining to an individual's posture in real-time and make decisions about the current state of the individual's posture. The results of these decisions could be used to apply biofeedback to the patient in order for the patient to correct his/her posture. Many posture monitors have been developed by researchers for rehabilitation [14, 49–51], context awareness [52], lower back pain research [53], and for posture and activity detection systems [54].

Posture monitoring systems can be classified according to the number of sensors that are used to measure the posture of an individual. Dunne *et al.* [5] proposed a posture monitor for computer users that utilized a plastic optical fiber (POF) integrated along the back of a garment. The POF was abraded along one side in order to allow light to escape depending on the bend of the POF. Using a light sensor and a light source, the authors were able to direct a beam of light through one end of the POF and measure the intensity of the light at the other end. Therefore, the intensity of the light passing through the POF was directly related to any bending of the POF and this value was used to calculate the posture of the wearer. The system proposed by Dunne *et al.* is an example of a single sensor posture monitoring system.

Sardini *et al.* proposed another single sensor posture monitoring system that used an inductive sensor to detect changes in posture [6]. The inductive sensor was integrated into a garment and it varied its impedance when a mechanical deformity was applied. Conductive wire was sewn into the back and front of the garment. The impedance of the wire was monitored using a conditioning system to convert the impedance into a voltage that was sampled using the analog to digital converter (ADC) peripheral of a microcontroller. The microcontroller processed the data acquired from the inductive sensors directly to provide either audio or vibration feedback to the wearer to encourage him/her to improve his/her posture. Other single sensor systems have been proposed in the literature [52, 55].

A disadvantage of using a single sensor based posture monitor is these systems often require the use of a complex processing unit, such as a computer. The POF system from [5] requires a connection to a computer in order to calculate the posture from the POF sensor and to provide feedback in the form of visual cues displayed on the monitor. The posture monitor from [55] required that a smartphone process the data which was transmitted via Bluetooth. The need of the complex processing unit may limit the flexibility and portability of the posture monitor.

The other type of posture monitoring system uses multiple sensors to calculate posture. These systems either use sensors placed upon the back of the individual to measure posture or a combination of different types of sensors to form a picture of an individual's current posture. Bazzarelli *et al.* developed a low-power posture monitoring system that used a combination of electromagnetic (EM) coils and accelerometers [7–9]. This 'hybrid' approach, as the authors state, used the EM coils to obtain distance measurements from multiple receivers mounted on the patient with respect to a single transmitter. Roll and pitch angles were computed from the outputs of the accelerometers. The system provided feedback when the patient's posture deviated from the preset threshold. This posture monitor system consisted of a single control unit, multiple receivers, and one EM transmitter. The receivers and EM transmitter were mounted on the patient's back while the control unit was carried by the patient. The distance between the transmitter and receivers was calculated based on the received strength of the EM field. As each receiver contained its own microcontroller, sampling was done in parallel which allowed for the possibility of additional receivers to be implemented without decreasing the sampling rate.

Instead of using EM coils, Ding *et al.* [49] developed an upperlimb posture monitor that used two inertial measurement units (IMUs) which were attached to a patient's arm. Each IMU contained a 2-axis accelerometer, a 3-axis magnetometer, and two 2-axis gyroscopes. One posture monitor was worn by a therapist and a second system was worn by the patient. The goal was for the patient to match the arm movements of the therapist as closely as possible. If the difference between the orientation of the therapist's arm and the patient's arm was not within a pre-determined range, then vibration feedback was provided. The intensity of the feedback applied was proportional to the difference of the two movements. This allowed for specific, targeted feedback to the patients in order to better aid them in determining how to correct the posture of their arm.

A posture monitor developed by Lou *et al.* in [10] was specifically designed to measure the kyphotic angle of adolescent patients and to provide feedback when their kyphotic angle was above a pre-determined threshold. The complete system consisted of two 3-axis accelerometers, a microcomputer, and a spandex halter-top garment that was custom made for the patient to ensure a tight fit. The garment contained pockets on the back that was used to hold the electronics. When the system detected that the kyphotic angle was above the threshold, it would apply vibration feedback for two seconds. The length of the feedback times was increased when the patients did not correct their posture for a consecutive three minute interval. In addition, the difference of the kyphotic angle measurements between the system and a Minolta laser scanner camera system (Model, Japan) was less than 2°. A drawback to this system was that it could only measures posture along the sagittal plane. As well, each of the accelerometer sensors was connected to the microcomputer unit by a cable which could become tangled. Another disadvantage of the system was the difficulty in upgrading the size of the memory.

Silva *et al.* proposed a unique posture monitoring system that was waterproof [56]. Their system was used to monitor body kinematics and physiological data such as heart and respiratory rate during hydrocinesiotherapy classes, in which the exercises were performed in water. Each suit contained a heart rate monitor, a respiratory sensor, and five posture sensors that were all stored in waterproof containers. The posture sensors were placed on each shoulder, on the outside of each leg below the hips laterally, and one unit on the back between the shoulder blades. The unit on the back measured the inclination of the spine along the sagittal plane and was also used as a reference for the other four sensors to measure the angle of articulation at their respective locations. The results of this study showed that the system has a resolution of 1° for yaw, pitch, and roll. The power consumption of the system was not reported in the paper, so it was impossible to calculate how long the system would last on a single set of AA batteries. There was also very little information regarding the size of the sensors on the suit and how the sensors are integrated into the system. As the system was being used in an underwater environment, it was critical that the system was embedded in a waterproof case.

Lou *et al.* developed another posturing monitoring system specifically aimed at improving the patient's posture along the sagittal plane [11]. The system consisted of two sensor units and a harness worn on the upper body like a backpack. When the system detected that the kyphotic angle of the patient was above a pre-determined threshold, feedback would be applied to the patient. Results from a preliminary test of four volunteers over a four day period found that using this system improved the volunteer's kyphotic angle by more than 5° [11].

Wong *et al.* developed a posture monitoring system that could monitor the posture of a patient in both the sagittal and coronal planes [12–14, 57]. The system consisted of a garment, three sensor units, a digital data acquisition and feedback system, and a battery pack. The sensors were attached to the acquisition system through a wired connection. Laboratory results showed that the system had an root mean square (RMS) error of less than 1° for static measurements and less than 1.5° for dynamic measurements. In a four day preliminary study [13], the authors found that there was approximately a 26% reduction in time spent in a poor posture in the thoracic region and approximately 65% in the lumbar region, depending on the threshold used for feedback. The subjects in the study would wear the system for two hours continuously per day. On the first day and the last day, there was no feedback applied to the subjects. On day two and three, feedback was provided if the posture of the subjects were poor. All the subjects would spend the two hours sitting down at a computer or watching TV.

A common problem associated with all mulit-sensor style posture monitoring systems is repeatability of the sensor measurements. It can be very difficult to place the sensors in the exact same position between tests and this can affect when feedback is applied. False positives and negative errors may occur.

The connection between the sensors and the central processing unit can be either wired or wireless. Using a wired connection is much easier to implement in hardware and software, can reduce the size of the integrated sensor unit, and can reduce the power required to operate the sensor unit. However the connected wires may become tangled or damaged. The damaged wires may require experienced technicians to repair, which can be costly and time consuming. A wired connection also limits the flexibility of the placement of the sensor units on the patient's back. On the other hand, using wireless communication allows for much greater flexibility in placing the sensors. As well, it may be much easier to add additional wireless sensors for monitoring.

The use of posture monitors as a treatment option for AIS patients has been researched before with varying levels of success [5–10,12–14]. The contribution of this research is to develop a posture monitoring system that can provide three-dimensional measurements of a patient's posture, is small in size, consumes low power, can be easily integrated into a garment, and can be used anywhere at anytime. The developed system may then be used to identify whether exercise is an effective treatment for mild cases of AIS.

Chapter 3

System Theory

This chapter begins by examining the physical appearance of patients with AIS. Next, a review of the motion analysis of the human torso has been conducted. The number of sensors that are required to capture the patient's posture is then discussed. The selection criteria for the sensors are then examined and the operational theory for the chosen sensors is described briefly in Section 3.3. A few key mathematical constructs that are used to represent the orientation of a rigid body in three-dimensional space are introduced. The theory of the sensor fusion algorithm to obtain an accurate orientation estimate has been reviewed and explained. In order to increase the flexibility of the placement of the sensors, wireless communication is implemented using the IEEE 802.15.4 standard. A comparison of the IEEE 802.15.4, Bluetooth, and ANT standards has been provided.

3.1 Cosmetic Features

The most significant concern for patients with AIS is their body image. Theologis *et al.* published a study about quantifying the cosmetic appearance of patients with AIS [58]. The study found that the rib hump, formed by excessive rotation of the thoracic vertebrae, had a direct correlation to the patient's cosmetic spinal score. A score of 10 related to the most cosmetically acceptable back while a score of 0 was the worst [58]. A more prominent rib hump resulted in a lower cosmetic spinal score. The study did note that the rib hump was not the only deformity that affected the patient's cosmetic appearance but varied with the deformity. An example of how a severe curve can cause a visible deformity is shown in Figure 3.1.

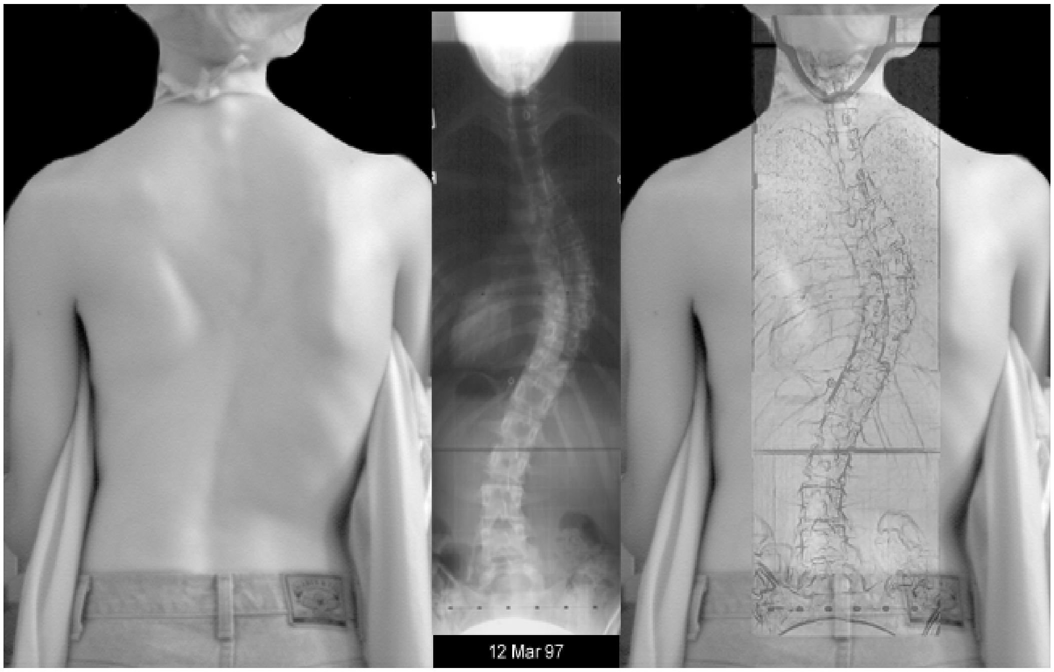

Figure 3.1: Cosmetic back appearance due to scoliosis

3.2 Torso Motion Analysis

In order to accurately measure the movements of the patient's posture, it is required to understand the range of motion that the patient's torso is capable of making. It is known that the torso can move in the sagittal, coronal, and transverse planes, but the minimum number of sensors that are needed to adequately capture these motions is unclear. The following sections provide a review of the existing literature and help to determine the number of sensors required to capture the motion of the patient's torso.

3.2.1 Movements along the Sagittal Plane

The vast majority of posture monitoring systems record motion along the sagittal plane [10–13]. One reason for the popularity of the plane is that the forward flexion (bending) can be easily measured. This forward flexion can lead to rounding of the upper back and is more commonly referred to as postural kyphosis [11]. The severity of the postural kyphosis can be quantified using the kyphotic angle shown previously in Figure 2.4. As the patient bends forward, the kyphotic angle will increase and can be easily monitored. Previous posture monitoring systems [10–13] have measured the kyphotic angle using only two sensors placed on the patient's back.

Another common condition along the sagittal plane is lordosis, which is the inward curving of the lower back in the lumbar region of the spine. It may be possible to monitor the lordotic angle, shown in Figure 2.4, in a similar way as the kyphotic angle, therefore two sensors will be needed to measure that angle. Therefore, the primary motions along the sagittal plane may be monitored using a minimum of three sensors.

3.2.2 Movements along the Coronal Plane

There are many different curvature types along the coronal plane. Different curvatures of the spine will require different sensor placements for measurement. Lenke *et al.* published a paper [59] that outlines a standard classification for AIS. The classification outlines six types of curves ranging from a single thoracic curve (Type 1) to a triple curve (Type 4). To go along with these six types, there are three lumbar spine modifiers that describe the curvature of the lumbar region. The main thoracic curve (Type 1) is the most prevalent curve type for AIS [59] and so the sensor placement was based around that curve type. In order to capture the movement of a Type 1 curve, at least three sensors are required.

Among all the topographical features of an AIS's patient back, shoulder asymmetry is one of the most common cosmetic asymmetries. Measuring the orientation of the patient's shoulders may allow us to detect the upper portion of his/her posture along the coronal plane. If the slope of the shoulder angles are different, lateral flexion of the patient's trunk may result.

3.2.3 Movements along the Transverse Plane

Measuring the rotation of a patient's trunk along the transverse plane during his/her daily activities has significant challenges. There is no portable device that has been reported from the literature that can provide accurate measurements on axial rotation. However, measuring the rotation of the patient's trunk is important as it has been found that there is a high correlation between trunk rotation and vertebral rotation [60]. A measurement of the overall rotation of the torso will suffice for the purposes of distinguishing 'good' posture versus 'poor' posture. In order to measure any change in the transverse plane, two sensors will be needed.

In summary, from examining the different motions that may occur along the patient's torso, it appears that the posture monitoring system would require a minimum of five sensors in order to monitor the different motions along all the planes. Two sensors are suggested to be placed on the shoulders while three sensors will be placed along the spinal column. An important consideration is that the sensors must be mounted inside a skin-tight garment in order to detect the most proxy motion.

3.3 Sensors

From the literature review in Chapter 2, many different methods have been utilized to measure the posture of individuals. All of these different methods also make use of a variety of sensors for measuring posture. Dunne *et al.* implemented a POF into a garment that measured the changing intensity of light based on the shape of the POF [5]. Sardini *et al.* used an inductive sensor that measured changes in resistance based on the mechanical forces applied to conductive wire [6]. Bazzarelli *et al.* utilized EM coils and accelerometers to obtain distance measurements from multiple receivers mounted on the back of a patient [7–9].

However, from the literature it is quite clear that the dominant sensors used in posture monitoring systems consist of a combination of accelerometers and gyroscopes [10–14, 49, 51, 56]. Due to advances in mico-eletrical-mechanical systems (MEMS) technology, accelerometers and gyroscopes can be fabricated in very small packages and require very low operating currents, making them ideal for battery powered applications such as a portable posture monitoring system.

3.3.1 Accelerometers

An accelerometer is a sensor that is able to measure its own acceleration and acceleration forces [61]. The acceleration forces that the sensor experience may be static and/or dynamic in nature. Of primary importance is the ability of the accelerometer to detect the acceleration due to gravity, which is constant in magnitude. Accelerometer measurements are often described in units of g where 1 g = 9.81 m/s^2. Accelerometers are used extensively in posture monitoring systems and other areas of research such as human motion tracking [62] and in Unmanned Aerial Vehicles (UAVs) [63].

Figure 3.2 consists of a 2-axis accelerometer with mass m placed on an tilted surface with only the force of gravity (F_g) acting upon it. To calculate the angle of inclination θ_i, the measured force values along the accelerometer's X_A and Y_A axes are used in equation (3.1). The measured force in the senor's X_A and Y_A axes are F_x and F_y respectively. In this example, θ_i can be thought of as the angle to which the accelerometer's frame of reference, X_A and Y_A, is rotated compared to the Earth's reference frame shown by X_E and Y_E.

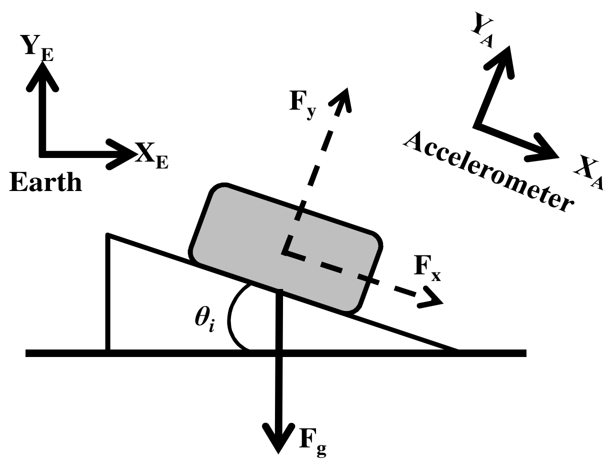

Figure 3.2: 2-axis accelerometer on tilted surface

$$\theta_i = atan\left(\frac{F_x}{F_y}\right) \tag{3.1a}$$

$$F_x = F_g sin(\theta_i) \tag{3.1b}$$

$$F_y = -F_g cos(\theta_i) \tag{3.1c}$$

Both F_x and F_y both have units of N. Equation (3.1) is only valid when $\sqrt{F_x^2 + F_y^2} = mg$. This is because it is assumed that the only force applied to the accelerometer is F_g. If an additional acceleration force F_a is applied to the accelerometer, the assumption that the norm of the forces is equal to mg

is no longer valid. Only with knowledge of the magnitude and direction of F_a can the correct orientation of the sensor be determined from F_x and F_y.

An advantage of using an accelerometer in a posture monitoring system is that accelerometers perform very well in static situations where $F_a = 0$. The accuracy decreases during dynamic situations where $F_a \neq 0$. Accelerometers are sensitive to small changes in tilt when the sensing accelerometer is perpendicular to gravity (i.e: horizontal to the earth's surface). Past 45°, the sensitivity decreases. For this reason, it is common to use a multiple axes accelerometer. However, accelerometers are not able to measure the changes in orientation along the plane perpendicular to gravity as the change of the tilt angle is related to the sine function. Therefore, accelerometer based posture monitoring systems are not able to monitor changes along the transverse plane.

3.3.2 Gyroscopes

A gyroscope is a sensor that is able to measure angular rate using the Coriolis force [61]. With knowledge of the sampling rate of the gyroscope, it is possible to integrate the angular rate to provide positional data which can be used to determine the orientation of the sensor. The output of a gyroscope is in rad/s, so integrating the output over the duration of the rotation will result in the change in orientation along the axis of rotation. In digital systems that make use of discrete signals, this can be accomplished by multiplying the measured angular rate $\dot{\omega}$ by the time interval ΔT and summing all of k samples of the rotation as seen in equation (3.2).

$$\omega = \int_{i=0}^{k} \dot{\omega} dT = \sum_{i=0}^{k} \dot{\omega}_i \Delta T \tag{3.2}$$

An advantage of using a gyroscope is that they perform well in dynamic situations, such as human motion. However, errors accumulated during the summation process shown in equation (3.2) will cause ω to "drift" and become increasingly inaccurate as time progresses. One solution to combat the integration errors is to pair up the gyroscope with other sensors [12]. The most common additional sensor is the accelerometer, which as mentioned previously has better performance during static situations. Using a combination of accelerometers and gyroscopes for posture monitoring is quite prevalent in the literature [11–14, 49, 64]. However, even with the addition of an accelerometer, it is still difficult to accurately measure rotations about the transverse plane as this measurement will rely completely upon the gyroscope. The drift in the gyroscope will result in erroneous measurements. In order to combat the drift about the transverse plane, an additional sensor is required and for most researchers, the magnetometer is suggested.

3.3.3 Magnetometers

A magnetometer is a senor that is able to measure the strength of the surrounding magnetic field. The magnetic field is determined by monitoring the change of resistance of magnetoresistive sensing elements [65]. For the posture monitoring system, the magnetometer is used to measure the Earth's magnetic field. The advantage of using a magnetometer is its capability of measuring orientation changes along the plane perpendicular to gravity unlike the accelerometer. However, a major challenge in using the magnetometer is in calibrating the sensor to only detect the Earth's magnetic field. Permanent magnetic fields and magnetic permeable materials that are near the magnetometer can drastically affect the measurements of the sensor and cause inconsistent and incorrect results. The effects of permanent magnetic fields are referred to as hard iron effects while magnetic fields generated by magnetically permeable materials are referred to as soft iron effects [66]. Proper calibration of the magnetometer is critical to ensure accurate and consistent sensor readings.

3.4 Sensor Calibration

When using any type of sensor, it is highly advisable to calibrate them in order to ensure the accuracy of the measurements. Accelerometers, gyroscopes, and magnetometers all require different calibration methods which are described below.

3.4.1 Accelerometer Calibration

Calibration of an accelerometer is a relatively straightforward process. Calibration requires applying ± 1 g of force to each axis and measuring the maximum output. This can be done by placing the sensor on a horizontal surface. The maximum and minimum output values along each axis will be equal to 1 g, so with the measurements from the six faces, the scale factor $\boldsymbol{S}_a$ and offset $\boldsymbol{O}_a$ from equation (3.3) can be computed.

$$[a_{cx}, a_{cy}, a_{cz}] = \begin{bmatrix} S_{ax} & 0 & 0 \\ 0 & S_{ay} & 0 \\ 0 & 0 & S_{az} \end{bmatrix} \begin{bmatrix} a_{ux} - O_{ax} \\ a_{uy} - O_{ay} \\ a_{uz} - O_{az} \end{bmatrix} \tag{3.3}$$

From equation (3.3), $\boldsymbol{a}_u$ are the raw accelerometer measurements and $\boldsymbol{a}_c$ are the calibrated measurements. For simplicity, $\boldsymbol{S}_a$ is a scaling matrix and each axis of the accelerometer is assumed to be orthogonal with one another.

3.4.2 Gyroscope Calibration

Calibrating a gyroscope is important as it can reduce drift in the integrated angle ω. To calibrate a gyroscope, one can apply a known angular rotation to the gyroscope along each axis in order to obtain the scale factor $\boldsymbol{S}_\omega$ and offset $\boldsymbol{O}_\omega$ in a similar manner to which the accelerometer was calibrated. A second method to calibrate the gyroscope is to rotate the gyroscope by a known angle such as 90° or 180°. Integrating the calibrated gyroscope measurements $\dot{\boldsymbol{\omega}}_c$ using equation (3.2), where $\dot{\boldsymbol{\omega}}_c$ is calculated using

$$[\dot{\omega_{cx}}, \dot{\omega_{cy}}, \dot{\omega_{cz}}] = \begin{bmatrix} S_{\omega x} & 0 & 0 \\ 0 & S_{\omega y} & 0 \\ 0 & 0 & S_{\omega z} \end{bmatrix} \begin{bmatrix} \dot{\omega_{ux}} - O_{\omega x} \\ \dot{\omega_{uy}} - O_{\omega y} \\ \dot{\omega_{uz}} - O_{\omega z} \end{bmatrix} \tag{3.4}$$

where $\dot{\boldsymbol{\omega}}_u$ is the raw angular rate from the gyroscope. Like $\boldsymbol{S}_a$, $\boldsymbol{S}_\omega$ assumes that each axis of the gyroscope is orthogonal to each other.

3.4.3 Magnetometer Calibration

Magnetometers require more frequent calibrations as they can be severely affected by the surrounding environment more so than either accelerometers or gyroscopes. Any surrounding ferrous objects such as computer equipment, metal furniture, appliances, the design of the printed circuit board (PCB), and the nearby electronic components mounted on the same PCB can affect its measurements [67]. Many different research groups have developed methods for magnetometer calibration [66, 68, 69]. The popular procedure for calibrating the magnetometer is to record the sensor readings while rotating the magnetometer along its X, Y, and Z axes. If the readings from the magnetometer were to be plotted as shown in Figure 3.3, the ideal readings shown in blue would be a sphere centered at the origin. A plot of the real measurements obtained by the magnetometer would actually show an ellipsoid with an offset from the origin as shown in red in Figure 3.3. The hard iron effects create an offset of the measured magnetic readings while the soft iron matrix is responsible for causing the readings to appear to be a tilted ellipsoid.

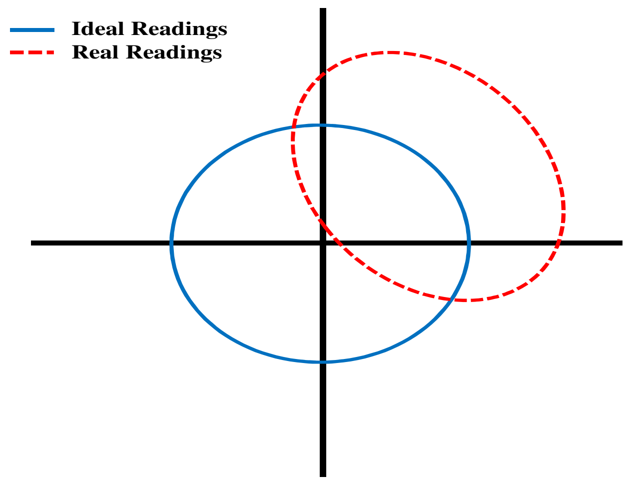

Figure 3.3: Real vs Ideal magnetometer readings

The calibration of the magnetometer is performed using the method proposed in [68]. Equation (3.5) shows the linear relationship between the calibrated magnetometer data $\boldsymbol{w}$ and the uncalibrated data $\boldsymbol{m}$

$$\boldsymbol{w} = \boldsymbol{A}_m(\boldsymbol{m} - \boldsymbol{O}_m), \quad \boldsymbol{A} = \begin{bmatrix} a_{11} & a_{12} & a_{13} \\ 0 & a_{22} & a_{23} \\ 0 & 0 & a_{33} \end{bmatrix} \tag{3.5}$$

where $\boldsymbol{A}_m$ contains information pertaining to the sensitivity of the axes of the magnetometer as well as their non-orthogonality to each other. $\boldsymbol{A}_m$ is used to compensate for the soft iron effects that are present around the magnetometer. $\boldsymbol{O}_m$ is a 3x1 matrix that relates to the hard iron effects.

The combination of accelerometers, gyroscopes, and magnetometers for measuring the orientation of a rigid body is a fairly well established area of research [70–77], making the use of those three sensors the most logical for a posture monitoring system. In the following section, a brief review of the different methods and terminology that are used to represent the orientation of a rigid body will be conducted.

3.5 Orientation Representation of Rigid Bodies

3.5.1 Euler Angles

Euler angles are a commonly used representation for orientation of an object in three-dimensional space [78]. Euler angles are comprised of three angles, pitch (ϕ), roll (θ), and yaw (ψ) that pertain to the angles formed along the X, Y, and Z axes as shown in Figure 3.4. Euler angles are often used as they are intuitively easy to understand and visualize. However, due to the nature of the computation of Euler angles, they can suffer from singularities, more commonly referred to as gimbal lock [78]. Gimbal lock is discussed in more detail in the next section.

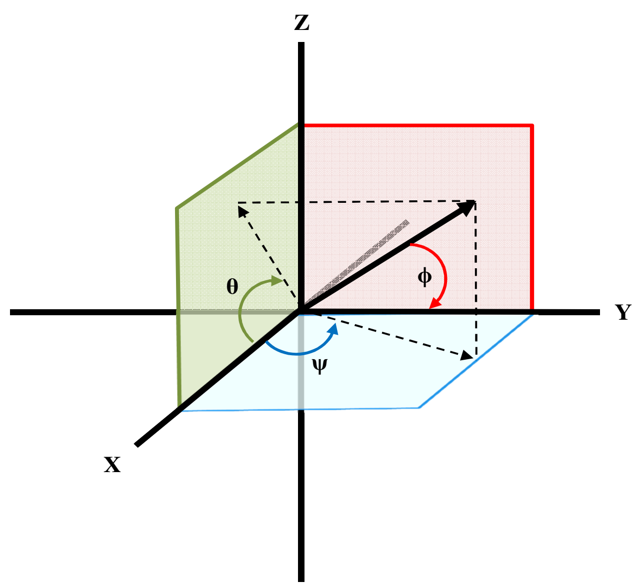

Figure 3.4: Visual representation of defined Euler angles

3.5.2 Rotation Matrix

A rotation matrix, also referred to as a direction cosine matrix [78], is a 3x3 matrix that can rotate a vector while preserving its length [78]. A rotation matrix $\boldsymbol{R}$ is composed of three separate rotations each about a single axis. Let $\boldsymbol{R}_\phi$, $\boldsymbol{R}_\theta$, and $\boldsymbol{R}_\psi$ represent rotations about the X, Y, and Z axes respectively and they are shown in equation (3.6).

$$\boldsymbol{R}_\phi = \begin{bmatrix} 1 & 0 & 0 \\ 0 & cos(\phi) & -sin(\phi) \\ 0 & sin(\phi) & cos(\phi) \end{bmatrix} \tag{3.6a}$$

$$\boldsymbol{R}_\theta = \begin{bmatrix} cos(\theta) & 0 & sin(\theta) \\ 0 & 1 & 0 \\ -sin(\theta) & 0 & cos(\theta) \end{bmatrix} \tag{3.6b}$$

$$\boldsymbol{R}_\psi = \begin{bmatrix} cos(\psi) & -sin(\psi) & 0 \\ sin(\psi) & cos(\psi) & 0 \\ 0 & 0 & 1 \end{bmatrix} \tag{3.6c}$$

Therefore $\boldsymbol{R}$ is defined by

$$\boldsymbol{R} = \boldsymbol{R}_\psi \boldsymbol{R}_\theta \boldsymbol{R}_\phi = \begin{bmatrix} R_{1,1} & R_{1,2} & R_{1,3} \\ R_{2,1} & R_{2,2} & R_{2,3} \\ R_{3,1} & R_{3,2} & R_{3,3} \end{bmatrix}$$

$$= \begin{bmatrix} c_\psi c_\theta & (c_\psi s_\theta s_\phi - s_\psi c_\phi) & (c_\psi s_\theta c_\phi + s_\psi s_\phi) \\ s_\psi c_\theta & (s_\psi s_\theta s_\phi + c_\psi c) & (s_\psi s_\theta c_\phi - c_\psi s_\phi) \\ -s_\theta & c_\theta s_\phi & c_\theta c_\phi \end{bmatrix} \tag{3.7}$$

where c_ϕ is equal to *cos(θ)*, etc [63]. Conversely, equation (3.8) allows for ϕ, θ, and ψ to be obtained from $\boldsymbol{R}$.

$$\phi = atan2(R_{3,2}, R_{3,3}) \tag{3.8a}$$

$$\theta = -atan\left(\frac{R_{3,1}}{\sqrt{1 - R_{3,1}^2}}\right) \tag{3.8b}$$

$$\psi = atan2(R_{2,1}, R_{1,1}) \tag{3.8c}$$

From equations (3.7) and (3.8), it can be seen that there exists certain critical angles for θ that can cause ϕ and ψ to become undefined (gimbal lock) [78]. For example, when $\theta = 90°$, the terms $R_{1,1}$, $R_{2,1}$, $R_{3,2}$, and $R_{3,3}$ are all equal to 0, causing ϕ and ψ to be undefined [78].

3.5.3 Unit Quaternion

Quaternions were first introduced by William Hamilton in 1843 as a way of representing complex numbers with a rank of greater than two [79]. Quaternions are another method for representing rotations in three-dimensions. A quaternion $\boldsymbol{q}$ can be defined as

$$\boldsymbol{q} = q_1 + \mathbf{i}q_2 + \mathbf{j}q_3 + \mathbf{k}q_4 = [q_1, q_2, q_3, q_4] \tag{3.9}$$

where $\boldsymbol{q} \in \mathbb{R}^4$. The complex conjugate of quaternion $\boldsymbol{q}$ can be represented as

$$\boldsymbol{q}^* = q_1 - \mathbf{i}q_2 - \mathbf{j}q_3 - \mathbf{k}q_4 = [q_1, -q_2, -q_3, -q_4] \tag{3.10}$$

As the name suggests, the norm of the unit quaternion is defined by equation (3.11).

$$||\boldsymbol{q}|| = 1 = \sqrt{q_1^2 + q_2^2 + q_3^2 + q_4^2} \tag{3.11}$$

Multiplication of quaternions is not commutative [63]. The value of quaternion $\boldsymbol{a} = \boldsymbol{b} \times \boldsymbol{c}$, where $\boldsymbol{b}$ and $\boldsymbol{c}$ are also quaternions, is shown in Equation (3.12) [63].

$$\boldsymbol{a} = \boldsymbol{b} \times \boldsymbol{c} = [b_1, b_2, b_3, b_4] \times [c_1, c_2, c_3, c_4] = \begin{bmatrix} (b_1c_1 - b_2c_2 - b_3c_3 - b_4c_4) \\ (b_1c_2 + b_2c_1 + b_3c_4 - b_4c_3) \\ (b_1c_3 - b_2c_4 + b_3c_1 + b_4c_2) \\ (b_1c_4 + b_2c_3 - b_3c_2 + b_4c_1) \end{bmatrix}^T \tag{3.12}$$

Since $\boldsymbol{q}$ contains information about a rotation, $\boldsymbol{q}$ can be applied to a vector $\boldsymbol{u}$ to rotate it to a new vector $\boldsymbol{v}$. Equation (3.13) defines the rotation from $\boldsymbol{u} \rightarrow \boldsymbol{v}$ [79]. For both $\boldsymbol{u}$ and $\boldsymbol{v}$, the first element is set to zero to make them four element vectors [80].

$$\boldsymbol{v} = \boldsymbol{q} \times \boldsymbol{u} \times \boldsymbol{q}^* \tag{3.13}$$

Equation (3.13) is only valid if both $\boldsymbol{u}$ and $\boldsymbol{v}$ share the same origin. If not, the origin of $\boldsymbol{v}$ must be subtracted from equation (3.13) [78].

Obtaining $\boldsymbol{R}$ from $\boldsymbol{q}$ is accomplished using equation (3.14) [80].

$$\boldsymbol{R} = \begin{bmatrix} 2q_1^2 - 1 + 2q_2^2 & 2q_2q_3 + 2q_1q_4 & 2q_2q_4 - 2q_1q_3 \\ 2q_2q_3 - 2q_1q_4 & 2q_1^2 - 1 + 2q_3^2 & 2q_3q_4 + 2q_1q_2 \\ 2q_2q_4 + 2q_1q_3 & 2q_3q_4 - 2q_1q_2 & 2q_1^2 - 1 + 2q_4^2 \end{bmatrix} \tag{3.14}$$

Using equations (3.8) and (3.14), the Euler angles can be computed from $\boldsymbol{q}$.

As it can be seen, there are advantages to using quaternions to represent orientation. The orientation can be stored in a four element array as compared to a rotation matrix which is a nine element array [79]. As well, quaternions do not suffer from any singularities that are present in an Euler angle representation [78]. However, quaternions suffer from requiring that they must have a norm equal to one [78]. In embedded systems, normalizing a quaternion can become computationally expensive due to the square root term. Another disadvantage of using quaternions is that it is the difficulty to visualize the physical Euler angles [78].

Despite these disadvantages, quaternion representations are commonly used when performing human body orientation tracking [62, 70–72] and as a result, a quaternion-based representation of orientation was deemed to be the best suited for the development of the posture monitoring system.

Since quaternions are used to represent orientation, it is necessary to refer to a quaternion with respect to another frame of reference. The notation system that will be used henceforth is with the use of super and subscripts preceding the quaternion $\boldsymbol{q}$ [81]. For example, an orientation in the sensor frame S relative to the frame of the earth E would be denoted as ${}^{E}_{S}\boldsymbol{q}$. Likewise, $\boldsymbol{q}$ in E relative to S would equal ${}^{S}_{E}\boldsymbol{q}$ and the two are related by equation (3.15).

$$ {}^{E}_{S}\boldsymbol{q} = {}^{S}_{E}\boldsymbol{q}^{*} \tag{3.15} $$

3.6 Review of Select Sensor Fusion Algorithms

Sensor fusion algorithms combine the data received by the accelerometer, gyroscope, and magnetometer to determine the orientation and position of the sensor. The kalman filter and complementary filter are two common types of sensor fusion algorithms.

3.6.1 Kalman Filter

A sensor fusion algorithm that is often implemented successfully in the literature is the kalman filter [63, 70, 73, 77, 82–84]. Essentially, a kalman filter is a set of mathematical equations that is used to estimate the state of a linear discrete-time controlled process [85]. The filter aims to minimize the estimated error covariance between the estimated state and the actual state.

The kalman filter has two primary components - a time update (*Predictor*) step and a measurement update (*Corrector*) step. The *Predictor* step uses the previous state and error covariance to make a prediction about the future state and error covariance. These estimates are referred to as the *a priori* estimates [85]. The *Corrector* step takes the *a priori* estimate and incorporates the new measurement values of the state to generate an *a posteriori* estimate of the state and error covariance. This *a posteriori* estimate is then fed back to the *Predictor* for a new *a priori* estimate of the upcoming state [85]. Thus, the *Predictor* and the *Corrector* steps forms a recursive loop [85].

The proliferation of kalman filter based orientation estimation systems is a testament to their accuracy, however they do posses a few disadvantages. One disadvantage is the recursive nature of the filter, which requires very high sampling rates for the sensors that may exceed their bandwidth [81]. Another disadvantage is that the state space for a kalman filter for orientation estimation may require very large matrices and state vectors [81] which can become very computationally expensive and slow if the kalman filter is running on an embedded device such as an 8-bit microcontroller.

3.6.2 Complementary Filter

Due to the large computational load that a kalman filter implementation would require, researchers investigated alternate approaches to the fusion of sensor data for orientation estimation. As mentioned previously, some sensors have a higher accuracy in certain situations. An example would be that an accelerometer is much more accurate at calculating orientation in static situations when compared to a gyroscope. Likewise, the gyroscope is much more accurate in more dynamic situations compared to the accelerometer. A complementary filter aims to fuse the data from multiple sensors in such a way that each sensor "complements" one another, increasing the overall accuracy of the system [74]. Suppose that there is a hypothetical IMU that consists of a single 3-axis accelerometer and a 3-axis gyroscope. A complementary filter algorithm would weight the data from the accelerometer more highly than that of the data from the gyroscope to calculate orientation of pitch and roll when the system was static. However, when the system begins to move, the weight of the accelerometer data would decrease and the results from the gyroscope would have more significance for calculating orientation. By placing higher emphasis on the data output from the sensor that is more reliable for the given situation, this will minimize the error [74].

Complementary filters have been used in many human limb tracking based systems [62, 71, 74]. An important advantage that a complementary filter has over a kalman filter is that the implementation of the complementary filter is more intuitive [74], though the complementary filter implementation may not be as accurate as the kalman filter [62, 74].

The authors of [62] found that the accuracy of a complementary filter was comparable to that of a kalman filter. Therefore, because of the reasonable accuracy and reduced computational complexity, a complementary filter would be the ideal choice for fusing data from the sensors of a posture monitoring system. In the following section, the chosen complementary filter will be reviewed.

3.6.3 Complementary Filter for Sensor Fusion

The complementary filter that was used for the developed posture monitoring system was fully described in [86]. The filter operation is shown in Figure 3.5.

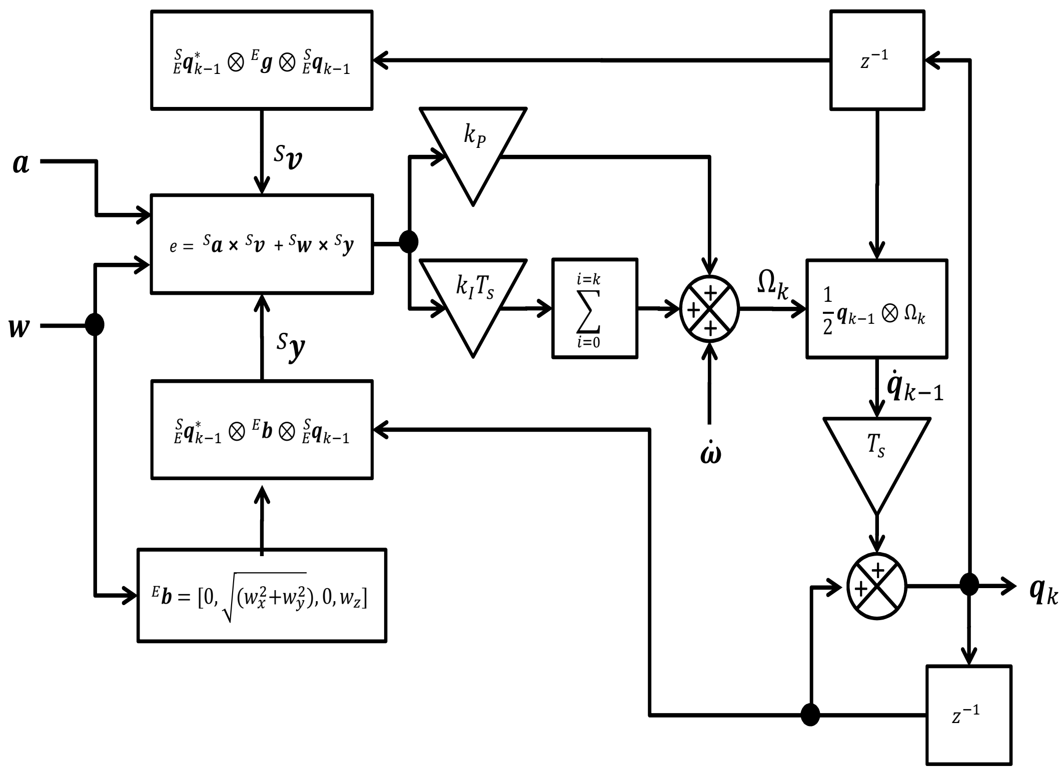

Figure 3.5: System flowchart of sensor fusion algorithm

The inputs into the filter consist of the calibrated measurements from the accelerometer $\boldsymbol{a}$, gyroscope $\dot{\boldsymbol{\omega}}$, and the magnetometer $\boldsymbol{w}$. The values from the accelerometer and magnetometer are also normalized. Using the previously calculated quaternion, $\boldsymbol{q}_{k-1}$ where k represents the current sample, an estimate of the direction of the Earth's gravity $\boldsymbol{v}$, and magnetic field $\boldsymbol{y}$, are computed from the Earth frame of reference E to the sensor's frame of reference S as shown in equations (3.16) and (3.17). The calibrated magnetometer readings $\boldsymbol{w}$ are used to create the estimate $\boldsymbol{y}$. Note that for the initial conditions,

${}^S_E\boldsymbol{q}_{k=0} = [1, 0, 0, 0]$ is used.

$$ {}^S\boldsymbol{v} = {}^S_E\boldsymbol{q}^*_{k-1} \otimes {}^E\boldsymbol{g} \otimes {}^S_E\boldsymbol{q}_{k-1} \tag{3.16} $$

$$ {}^S\boldsymbol{y} = {}^S_E\boldsymbol{q}^*_{k-1} \otimes {}^E\boldsymbol{w} \otimes {}^S_E\boldsymbol{q}_{k-1} \tag{3.17} $$

While the gravity vector $\boldsymbol{g} = [0, 0, 0, 1]$ greatly simplifies the calculations required for $\boldsymbol{v}$, the same can not be said for $\boldsymbol{y}$. The Earth's magnetic field, which is represented from the measurements by the magnetometer in $\boldsymbol{w}$, contains components along the X, Y, and Z axes while $\boldsymbol{g}$ contains only a vertical component along Z. To reduce the complexity of the estimated magnetic field $\boldsymbol{b}$, an assumption was proposed in [71] that the Earth's magnetic field can be represented by only having components in the X and Z axes. This assumption is that the Earth's magnetic fields are only directed in a strict South-North direction. Therefore, $\boldsymbol{b}$ can be represented by equation (3.18).

$$ \boldsymbol{b} = [0, \sqrt{w_x^2 + w_y^2}, 0, w_z] \tag{3.18} $$

Substituting $\boldsymbol{b}$ obtained from equation (3.18) into equation (3.17) gives us equation (3.19).

$$ {}^S\boldsymbol{y} = {}^S_E\boldsymbol{q}^*_{k-1} \otimes {}^E\boldsymbol{b} \otimes {}^S_E\boldsymbol{q}_{k-1} \tag{3.19} $$

With both estimates $\boldsymbol{v}$ and $\boldsymbol{y}$, an error e is computed by taking the sum of the cross products of the measured gravity and magnetic fields $\boldsymbol{a}$ and $\boldsymbol{w}$ as shown in equation (3.20).

$$ e = \boldsymbol{a} \times \boldsymbol{v} + \boldsymbol{w} \times \boldsymbol{y} \tag{3.20} $$

With the calculated e and $\dot{\boldsymbol{\omega}}$, a new estimated angular rate $\boldsymbol{\Omega}$ can be computed using equation (3.21) where k_P and k_I represent proportional and integral feedback factors and T_s is the sampling period in seconds.

$$ \boldsymbol{\Omega} = \dot{\boldsymbol{\omega}}_k + k_P e_k + k_I T_s \sum_{i=0}^{i=k} e_i \tag{3.21} $$

Once $\boldsymbol{\Omega}$ is obtained, the rate of change quaternion $\dot{\boldsymbol{q}}$ can be computed using equation (3.22).

$$ \dot{\boldsymbol{q}}_k = \frac{1}{2}\boldsymbol{q}_{k-1} \otimes \boldsymbol{\Omega}_k \tag{3.22} $$

Finally $\boldsymbol{q}_k$ can be determined using equation (3.23).

$$ \boldsymbol{q}_k = \boldsymbol{q}_{k-1} + \dot{\boldsymbol{q}}_{k-1} T_s \tag{3.23} $$

An important consideration for this filter is to determine an adequate and consistent sampling period for the sensors. This sampling period will be limited by the processor speed regarding the process of the incoming measurements and computing the current orientation. As well, appropriate values for k_P and k_I must be obtained in order to create a stable output.

3.7 Review of Wireless Protocols

As mentioned in Section 2.5, applying wireless connections between the sensor units and the processor unit can reduce movement restrictions upon the patient and not interfere with their daily activities. As well, it also allows patients to more easily place the sensors into their garment. These two advantages make wireless communication a better choice for the posture monitor. Since wireless systems usually require more power than a wired system, power saving techniques are employed. Furthermore, the wireless communication protocol was selected carefully in order to minimize the overall power consumption of the system. From the literature review, the three most prevalent wireless protocols are Bluetooth, IEEE 802.15.4, and ANT.

3.7.1 Bluetooth

Bluetooth is a wireless protocol that was developed by the Bluetooth Special Interest Group (SIG) [87]. Bluetooth operates in the 2.4 GHz Industrial, Science and Medical (ISM) band and is touted as easy to use and robust. The basic rate of data transfer for Bluetooth is 1 Mb/s, though using the Enhanced Data Rate can boost the throughput up to 2 - 3 Mb/s. A network of Bluetooth devices consists of one master device and at least one slave device, which the SIG refers to as a piconet. Masters and slaves are able to communicate between each other, however slaves are not able to communicate with one another directly. If there are multiple piconets, master devices can only be in charge of one piconet, but they may be slaves in another piconet. Slaves devices may be slaves in multiple piconets. When there are multiple piconets connected to each other through individual devices, the configuration is called a scatternet. Bluetooth is a popular wireless protocol among researchers designing posture monitoring systems [6, 54, 55, 88] as well as in ambulatory monitoring systems [89].

A new protocol that has been developed and claims to greatly reduce the power consumption of the classic Bluetooth protocol is called Bluetooth Low Energy (BLE) [87]. The maximum data rate for BLE is still 1 MB/s. BLE also restricts devices from belonging to more than one piconet (either the master or slaves), hence BLE does not support the scatternet topology.

3.7.2 IEEE 802.15.4

The IEEE 802.15.4 protocol (henceforth referred to as 802.15.4) is a standard for the use of wireless personal area networks (WPANs) for short range communication [90]. The standard states that 802.15.4 is designed for low-power and low-complexity applications. It can support data rates up to 250 kb/s. The 802.15.4 standard is capable of operating in the frequency bands of 868-869.6 MHz, 902-928 MHz, and most commonly between 2400-2483.5 MHz. All devices that communicate on a network have a unique ID referred to as the source address. The 802.15.4 standard also allows for multiple networks to co-exist on the same channel with the use of a personal area network (PAN) ID. The network topologies that the 802.15.4 standard supports are the star and mesh topologies. In the star topology, one device acts as a PAN coordinator and sets up the network for the remaining devices. The coordinator is capable of communicating with any of the devices in the network, however all remaining devices can only communicate with the coordinator device and not with each other. In the mesh topology, one device is the PAN coordinator and establishes the network, however all other devices on the network are free to communicate with each other. Within a network, transmitting devices are able to request that the recipient transmit an 'Acknowledgement' packet back to the transmitter so that the transmitter can be assured that the recipient received the packet [90]. The popular ZigBee protocol is actually built upon the 802.15.4 standard. The 802.15.4 standard has been used in previously posture monitoring systems [11, 12] and other types of human motion monitoring systems [75, 76]

3.7.3 ANT

The ANT protocol is a proprietary wireless protocol that was developed by Dynastream Innovations Inc. [91]. ANT operates in the 2.4 GHZ ISM band like

Bluetooth and the 802.15.4 protocols and can support up to 125 unique operating frequencies [91]. ANT is a popular protocol for use in sports and health monitoring as the protocol is designed for ultra-low power systems. A major difference between ANT and other protocols is how the communication, called the channel, is defined between a master and a slave device. Slave devices can only communicate with master devices that share the same channel. With these channels, ANT is also capable of the mesh and star topologies. Some of the integrated circuits that support ANT such as the CC2570 System-on-a-Chip (SoC) (Texas Instruments, Texas Instruments) or the nRF51422 SoC (Nordic Semiconductor, Norway) can operate with data rates up to 1 Mb/s or 2 Mb/s respectively.

3.7.4 Summary of Wireless Protocols

A brief comparison between the reviewed wireless protocols is presented in Table 3.1. Between Bluetooth, BLE, 802.15.4, and ANT, all the protocols meet the primary requirement of low power except classic Bluetooth. The distance range of all these wireless protocols between master and slave devices are over 1 m which would be acceptable for this research application. Another criteria that needs to be considered is the security features. Built-in security is an important consideration as the posture monitoring system may store patients' information. Of the remaining protocols, only ANT does not possess any built-in security features that may be required. Between 802.15.4 and BLE, the 802.15.4 standard was chosen for this research because the 802.15.4 standard is a well established protocol, has comparable power consumption to BLE, and has been implemented in numerous posture monitoring systems previously. As well, the mesh and star topologies may be useful for future expansion.

	Bluetooth	**BLE**	**802.15.4**	**ANT**
Power	High	Low	Low	Low
Data Rate	1 - 3 Mb/s	1 Mb/s	250 kb/s	1 - 2 Mb/s
Network Topology	piconet, scatternet	piconet	mesh, star	mesh, star
Security	Yes	Yes	Yes	No

Table 3.1: Comparison of wireless protocols

3.8 Summary of System Theory

As previously mentioned, the accelerometer and the gyroscope are the most commonly used sensors for posture monitoring systems. However, a disadvantage in only using those two sensors is that it is quite difficult to obtain an accurate reading of the axial rotation about the transverse plane. The addition of a 3-axis magnetometer allows for the measurement of the rotation along the transverse plane. Both the kalman and complementary filters have advantages and disadvantages. However, an important distinction between the two filters is that the kalman filter requires much more computation power for processing, which may not be suitable for a low-power portable device. Any viable posturing monitoring system that would be used by patients during their daily activities are required to operate in real-time and thus the speed of the fusion algorithm takes a higher precedence over the accuracy. Knowing the orientation of multiple sensor locations on the patient's back will allow for his/her posture to be determined. Using wireless communication allows for greater flexibility in sensor placement and the 802.15.4 standard was chosen for the wireless communication protocol.

Chapter 4

System Design[1]

4.1 System Overview

The ultimate goal of this research is to determine whether posture correcting exercises have a positive benefit for patients with mild AIS. To achieve this goal, a 3D posture monitoring system is needed to measure the posture of AIS patients in real-time and to provide feedback when their posture is poor. Patients who adopt a more correct posture during their daily activities may be less susceptible to curve progression and may not require more intensive treatments such as bracing or surgery. The posture monitor can also measure patient compliance which can provide information for researchers to evaluate the effectiveness of exercise-based treatment. This research involves designing a 3D posture monitoring system that will be used as a research tool to study the effects of exercise on AIS patients with mild scoliosis. The design and development process of the sensor and master units are discussed in this chapter. The sensor and master units communicate wirelessly. The sensor units are attached to specific areas in a tight fitting garment worn by the patient.

A block diagram of the developed system is shown in Figure 4.1. The sensor units obtain orientation data from specific locations on the patient. The master unit processes the data from the sensor units to determine the patient's posture, provides feedback to the patient if his/her posture is deemed to be 'poor', and stores the patient's posture information for further analysis. A total of five sensor units are used in the developed system.

[1]Material in this chapter has been presented at the *University of Alberta Faculty of Engineering Research Symposium 2013*

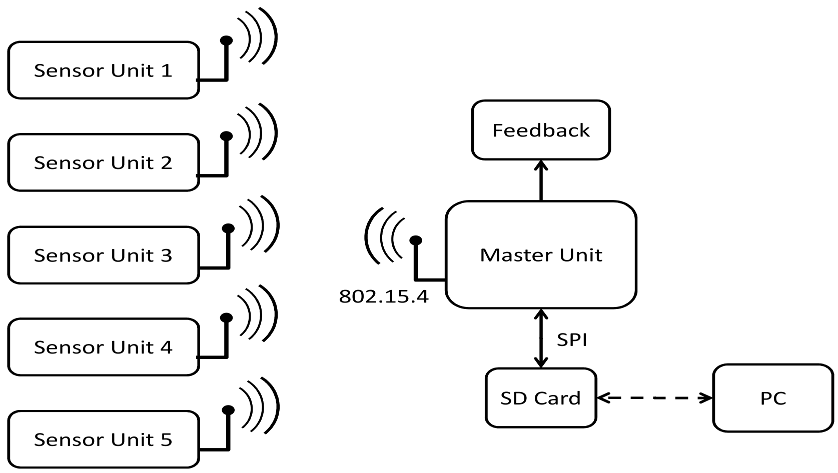

Figure 4.1: Block diagram of full system

4.2 Hardware of the Sensor Unit

The block diagram of the sensor unit is showed in Figure 4.2. Each sensor unit contains a microcontroller, MEMS type sensors (a 3-axis accelerometer, a 3-axis gyroscope, and a 3-axis magnetometer), and a battery. The MEMS type sensors offer the advantage of low-power consumption and are available in small package sizes. A sensor fusion algorithm running in the sensor unit takes the acquired measurement data and calculates the sensor unit's orientation at its respective location on the patient. The sensor unit transmits the computed orientation data to the master unit wirelessly when requested.

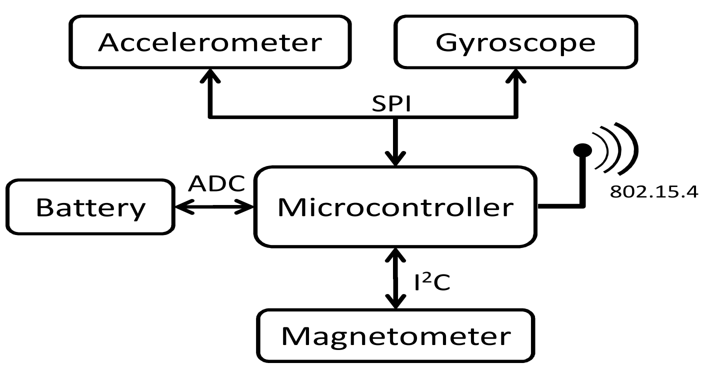

Figure 4.2: Block diagram of sensor

The dominating design features of the sensor unit are its physical size and low-power consumption. A large unit size could interfere with the daily activities of the patient, but a small form factor limits the capacity of the battery. Small capacity batteries need to be recharged more frequently. However, a small unit size may be barely noticeable and improve patient compliance. For this research, it was decided that the size of the sensor unit was more important that its battery life. Posture training sessions should only last for a few hours per day to minimize the effects of fatigue on the patient, so there would be ample opportunity for the sensor units to be recharged.

4.2.1 Microcontroller

The key hardware component for the sensor unit is the onboard microcontroller. The microcontroller is responsible for obtaining data from the three different MEMS sensors and executing the sensor fusion algorithm to compute the orientation quaternion. The microcontroller chosen for the sensor unit was the CC2530 (Texas Instruments, Texas). The CC2530 is a SoC that contains a built-in 2.4 GHz 802.15.4 radio transceiver and an 8-bit 8051 core microcontroller. The dimensions of the CC2530 are 6 mm x 6 mm. The CC2530 operated at 32 MHz and the maximum output power of the radio transceiver is 4.5 dBm. The CC2530 was configured to transmit at its maximum power and the maximum current consumption is approximately 34 mA.

The CC2530 also has up to 256 kB of programmable flash, a 12-bit ADC with up to eight channels, and up to 21 general purpose input/output (GPIO) pins which include the pins used for the ADC. The ADC was used to monitor the battery voltage. A voltage divider was required to halve the voltage from the battery as the input potential to any one pin on the CC2530 must be less than 3.3 V. Two 200 kΩ resistors were used to form the voltage divider to minimize the current consumption of the divider. The GPIO pins can be configured to run multiple peripheral interfaces including universal asynchronous receiver/transmitter (UART) and serial peripheral interface (SPI) communication. The SPI was used to communicate with the accelerometer and gyroscope. The magnetometer communicated to the CC2530 using inter-integrated circuit (I^2C) communication. As the CC2530 does not have a native I^2C interface, two GPIO pins were used to create the communication protocol using a technique known as 'bit-banging'. The CC2530 can be sent into a deep sleep mode where the current consumption drops down to 0.4 μA. When in deep sleep mode, both the radio transceiver and the core are turned off.

4.2.2 Sensors

The accelerometer and gyroscope chosen for the sensor unit was the LSM330DLC (STMicroelectronics, Geneva). This integrated circuit contains both a 3-axis digital accelerometer and a 3-axis digital gyroscope, which reduced the space requirements by combing both sensors into a single 4 mm x 5 mm package. The current consumption of the accelerometer and gyroscope during normal operations is 11 μA and 6.1 mA respectively. As both the accelerometer and gyroscope communicated with the microcontroller via a single SPI bus, it was not possible to access the data from both sensors at the same time. Two separate write and read cycles were required to send and receive data from both sensors. The accelerometer has a measurement range of between $\pm 2\ g$ up to $\pm 16\ g$ with a sensitivity ranging from 1 mg to 12 mg respectively. Accuracy of the sensor units is important so the settings for the accelerometer were set to have a measurement range of $\pm 2\ g$ with a sensitivity of 1 mg. The gyroscope settings were set to have an angular rate range of ± 500 degrees per second (dps) with a sensitivity of 0.0175 dps. The data from the accelerometer and gyroscope were sampled at 50 Hz, which was the fastest sampling rate that the microcontroller could handle from the available fixed sampling rates available in the accelerometer settings. The accelerometer generated an external interrupt after every sample, which triggered the microcontroller to sample all three sensors. This allowed the CC2530 to have a consistent 50 Hz sampling rate across the all three sensors. A consistent sampling rate was especially important for the gyroscope as this helped to minimize drift errors.

The magnetometer sensor that was chosen for the sensor units was the HMC5883L (Honeywell, New Jersey). This integrated circuit has dimensions of 3 mm x 3 mm and consumes 100 μA of current. The magnetic sensor field was kept at the default setting of ± 1.3 Gauss (G) which provided a sensitivity of 1090 least significant bit (LSB) / G. The magnitude of the earth's magnetic field on the surface ranges from 0.25 G to 0.65 G.

4.2.3 Power Supply

Lithium Polymer (LiPo) batteries are popular for battery powered applications because they are rechargeable and they have a very high energy density in a small form factor. The CC2530, LSM330DLC, and HMC5883L all can be operated at 3.3 V. Using the MCP1700 (Microchip, Arizona) low dropout regulator, the nominal voltage (3.7 V) of the LiPo was converted to a consistent 3.3 V power supply. The MCP1700 can output up to a maximum of 250 mA and its quiescent current is 1.6 μA. Also, only two external capacitors were required for operation, making its space requirements minimal.

The selection of the size of the LiPo battery depends upon the required current consumption of the onboard electronics and the desired run time for the sensor unit. During the full operation, the maximum current consumption is approximately 40 mA. The sensor units were designed to have a run time of at least two hours for one training session. Therefore, a 110 mAh LiPo battery was chosen based on the above requirements. In theory, this battery can operate the sensor unit for 2.75 hours before requiring to be recharged. The battery dimensions are 28 mm x 12 mm x 5.7 mm (L x W x H). This battery also contains a built-in protection circuit to prevent over charging and discharging.

4.2.4 Battery Charging Circuit

To charge the battery, the lithium ion battery charger STBC08 (STMicroelectronics, Geneva) was used to charge a single cell LiPo battery. This integrated circuit has hardware adjustable charging current and two status pins that can be used to monitor the charging status of the attached battery. The STBC08 can accept input voltages up to 10 V and can provide charging currents up to 800 mA. To minimize the dimensions of the sensor unit, the charging circuit was built off-board. As well, the charging circuitry for all five sensor units was placed together on a single PCB to use a common power supply. Figure 4.3 is an image of the completed board. The board contained five STBC08 battery chargers, five sets of red and green status light emitting diodes (LEDs), five male micro-USB A connectors, and a single female micro-USB A connector. Each male micro-USB A connector was used to connect to a single sensor unit. The charge current for each battery was set to 67 mA in order to charge the battery in under approximately two hours. A standard 5 V, 500 mA transformer was used to provide power for charging. When a sensor unit was connected to the powered sensor charger board, both the red and green LEDs would turn on. When the battery had been fully charged, the red LED turned off. If no battery was connected to the charger board, the red LED would turn on but not the green LED.

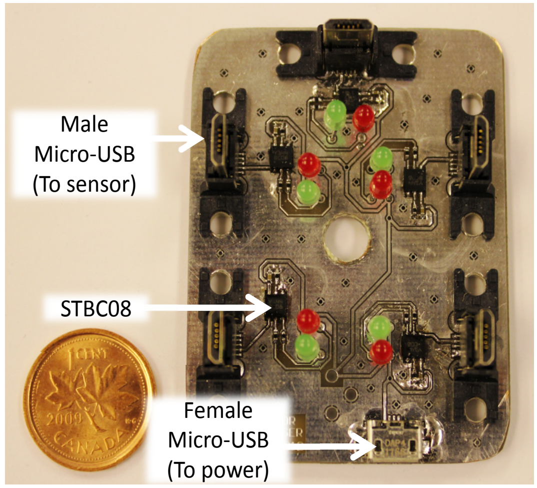

Figure 4.3: Battery charging circuit board

4.2.5 Dimensions of the Sensor Unit

A PCB was created for the sensor unit. In order to minimize the size of the sensor unit, the maximum dimensions of the PCB were set to be 31.1 mm x 18.3 mm, which allowed for the battery to be placed underneath the PCB. Final schematics and PCB layouts of the sensor unit are available in Appendix A.1 and B.1 respectively. Figure 4.4 shows a completed sensor unit. Using a 3D model of the sensor unit, a custom enclosure was designed to house the sensor unit. The enclosure prevented damage to the sensor units and allowed them to be easily integrated into a garment. The enclosure for the sensor unit has dimensions of 42.5 mm x 23.2 mm x 14.4 mm (L x W x H) and the bottom half of the enclosure is shown in Figure 4.4.

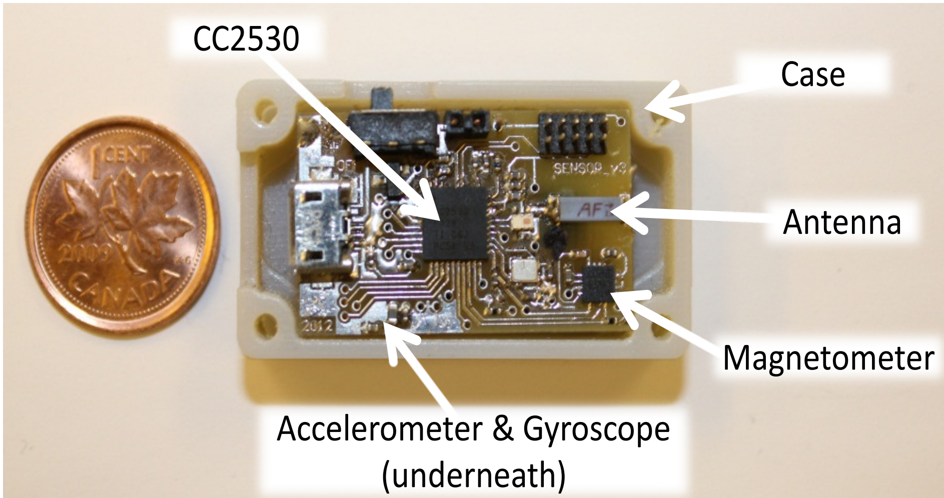

Figure 4.4: Complete sensor unit

4.3 Firmware Design for Sensor Unit

The firmware for the sensor unit was written in C and can be divided into two main operating modes; normal mode and sampling mode.

4.3.1 Normal Mode

The normal mode of operation for the sensor unit is shown in Figure 4.5. When the sensor unit is turned on, it first loads the radio settings including the source and destination addresses, the PAN ID, and the channel into the CC2530. In order to prevent multiple posture monitoring system that are in close proximity from interfering with each other, each posture monitor is assigned a unique PAN ID.

Next, the gyroscope, magnetometer, and accelerometer are initialized and checked to ensure that they are connected and working correctly. If one or more of the sensors fails to initialize, an error message is broadcast to the master unit. After broadcasting the error message, the sensor unit goes into deep sleep and no further action is taken. If all three sensors are successfully initialized, a radio packet is then broadcast out. This packet is used to 'check-in' with any available master unit operating with the same PAN ID. The check-in sequence will be described in Section 4.5. The sensor unit then loads calibration settings for each sensor that is stored in the onboard flash memory. If no calibration settings have been saved, default settings are then loaded for each sensor. After setting the calibration values, the sensor unit enters a while loop where it waits for commands from either the master unit (if the sensor successfully checked in) or from the Windows Interface if the check-in failed. The Windows Interface will be discussed in Section 4.6.

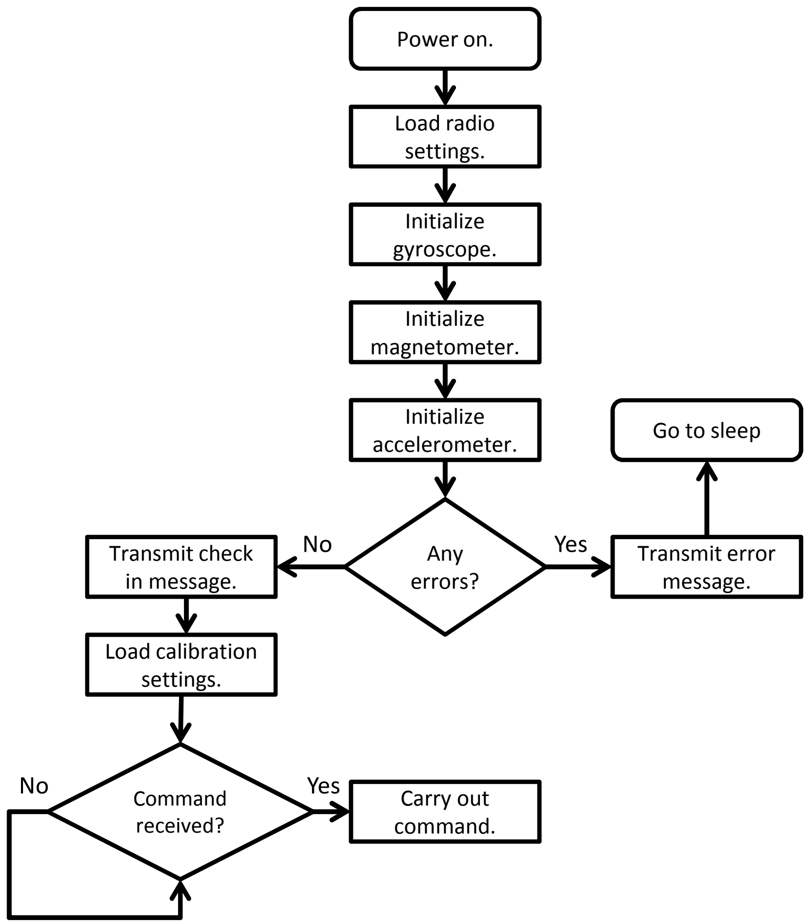

Figure 4.5: Sensor unit normal mode flow chart

The most notable operations that can be performed in normal mode are setting the calibration values for the accelerometer, gyroscope, magnetometer, and the settings for the radio. Each sensor possess calibration values that are used to compensate the raw measurement data before it is processed by the fusion algorithm. Depending on the environment, these calibration values may need to be altered to improve performance. Notably, the magnetometer sensor requires regular calibrations due to hard and soft iron effects in the surrounding environment. Instead of changing the firmware itself to take into account new calibration parameters, the sensor unit stores the calibration values in the onboard flash memory of the CC2530. This allows for only one version of the firmware to be flashed onto each sensor unit, and then each sensor unit can be calibrated individually. The same principle is applied to the radio settings. Storing both calibration and radio settings in the non-volatile flash memory allows sensor units to preserve those settings when they are turned on and off.

If the sensor unit does check-in with a master unit, the sensor unit waits for commands from the master unit. These commands are not as numerous as those available from the Windows Interface. The master unit can only request the battery status of the sensor unit, request the calculated quaternion, and put the sensor unit into sampling mode which is described in the next section.

4.3.2 Sampling Mode

In sampling mode the sensor unit is continuously sampling the data from the three sensors based on the timing provided by the accelerometer interrupt. The flow chart of the sensor unit's sampling mode is shown in Figure 4.6. The sensor unit saves its current quaternion when requested by the master unit. Each sensor unit calculates is own quaternion and transmits it wirelessly to the master unit.

The two sensor units that are on the shoulders of the patient swap their X and Y axes (i.e. pitch becomes roll and roll becomes pitch). The reason for this has to do with gimbal lock discussed in Section 3.5.2. With the default axes of the sensor shown in Figure 4.7, the sensor units use pitch ϕ to measure the slope of the shoulders. If the patient were to bend along the sagittal plane, roll θ measurements from the two shoulder units would go to $\pm 90°$, which would introduce large errors into ϕ. These errors would then cause an incorrect shoulder posture to be detected. If the X and Y axes are swapped for the shoulder sensor units, the slope of the shoulders would be instead measured from the θ angle. Therefore, movement along the sagittal plane would only affect ϕ and not θ, providing a more accurate measurement of the shoulder asymmetry.

The sensor unit samples the data in the three MEMS sensors when the interrupt from the accelerometer is triggered. The microcontroller obtains the measurement data from the magnetometer, gyroscope, and accelerometer in that order. After the microcontroller has obtained the data from the three

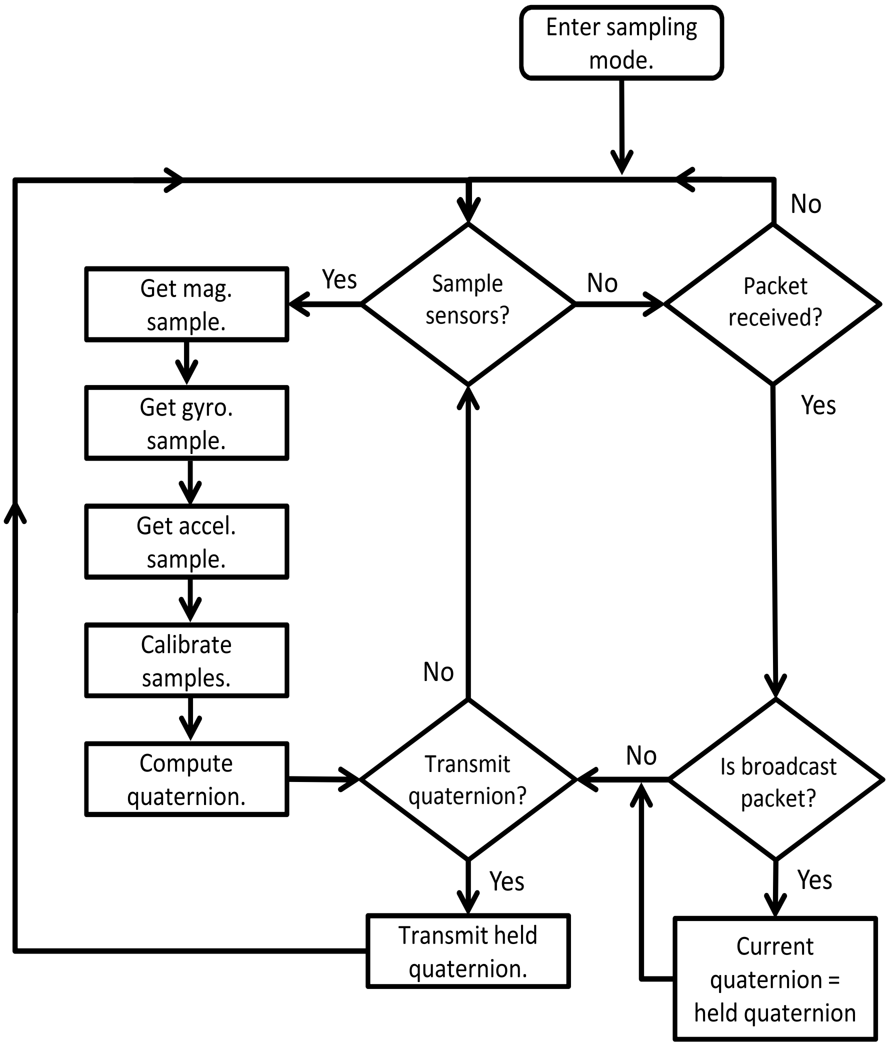

Figure 4.6: Sensor unit sampling mode flow chart

sensors, that data is processed into a quaternion using a complementary filter. The complementary filter that is used is based upon a C implementation by S.O.H Madgwick [92] of the filter proposed by Mahony *et al.* in [86]. The code has been optimized by pre-calculating repeated equations to decrease the execution time of the filter. With the microcontroller operating at 32 MHz, the filter takes approximately 6.1 ms to run. Factoring in the time required to sample the three sensors, it takes approximately 8.1 ms to calculate a new quaternion from start to finish. Once the filter has finished, the microcontroller will check to see if it needs to transmit a quaternion to the master unit. If not, the sensor unit will wait for either the next interrupt to begin sampling the sensors again, or for an incoming packet from the master unit. If the sensor unit receives a packet, it will check to see if it is a broadcast packet. If the

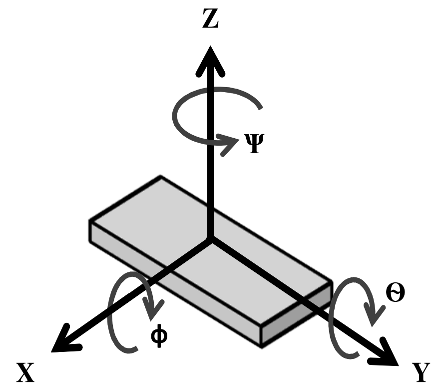

Figure 4.7: Default axes for sensor unit

packet is a broadcast packet, the sensor unit will hold the current quaternion for later transmission to the master unit. Otherwise, the sensor unit checks to see if the master unit has requested the held quaternion.

4.4 Hardware of the Master Unit

Each posture monitor only requires one master unit in order to facilitate the operation of the system. While the actual orientation estimates are calculated via a distributed computing network across the five sensor units, the master unit is responsible for obtaining the orientation estimates from each sensor unit to determine if the patient's posture is acceptable or if feedback is required. Besides the feedback function, the master unit also records each orientation estimate from each sensor unit, a time stamp, and any errors in the patient's posture for later review. As the master unit performs a different role than that of the sensor units, so the hardware and firmware design of the master unit are different from the sensor unit. As well, the master unit allows the patient to control the posture monitoring system during set up. This increases the mobility and flexibility of the posture monitor. In order to control the system, a user interface is required on the master unit. A LCD screen and buttons allows the patient to interact with the master unit and receive visual feedback. The following section outlines the hardware and firmware of the master unit.

Selection of the hardware for the master unit was driven by its role in the posture monitoring system as the central unit that must obtain and process large packets of data from multiple sensor units. The master unit is also responsible for providing feedback and storing posture information from each training session. Figure 4.8 shows a block diagram of the hardware for the master unit.

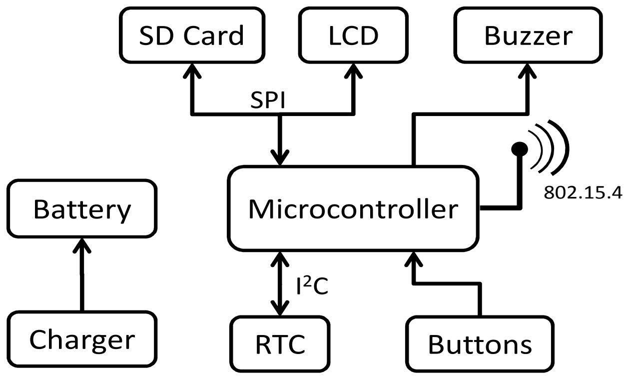

Figure 4.8: Master unit block diagram

4.4.1 Microcontroller

The workload of the master unit is much heavier than that of a single sensor unit and so a more powerful microcontroller was chosen. The STM32W108 (STMicroelectronics, Geneva) possess a 32-bit ARM® Cortex™-M3 processor to handle the large computational load. As well, the STM32W108 possesses a built-in 2.4 GHz 802.15.4 transceiver to communicate with the sensor units. The processor operated at 24 MHz and the radio transceiver was transmitting at the maximum power of 8 dBm in order to ensure that the maser unit was able to communicate with the sensor units. The STM32W108 has dimensions of 7 mm x 7 mm, has 24 GPIO pins, and possesses hardware peripherals for SPI and I^2C communication protocols. The SPI peripheral was used to communicate with the LCD screen and the microSD card. The I^2C interface was used to communicate with the real-time clock (RTC). The STM32W108 consumes up to 43.5 mA when the radio transmit power is set for 7 dBm and the CPU is running at 24 MHz.

4.4.2 LCD Screen

The largest component of the master unit was the LCD screen. The Nokia 5110 Graphic LCD was chosen for it's small board size of 45 mm x 45 mm with a 84 x 48 pixel screen that allows for six lines with twelve characters per line to be displayed at one time. The LCD was controlled by the STM32W108 using

SPI and two extra GPIO pins. The LCD draws approximately 0.49 mA when turned on. Three push buttons were used to control the cursor on the LCD screen. These buttons were used to trigger interrupts in the STM32W108, providing the patient with near instantaneous response from the interface.

4.4.3 MicroSD Card

The master unit stored the received data from the sensor units in a text file format in a microSD card. The text file format was chosen as it is a fairly universal file type and can be opened easily in many different operating systems. Using a microSD card allowed for the stored data to be easily transferred to a PC directly. The microSD card was chosen because of its small size and a large storage capability. A M41T62 RTC (STMicroelectronics, Geneva) was used to add timestamps to the sensor data stored in the microSD card. As well, the file system module [93] required a time stamp when it was modifying a file stored in the microSD card. This RTC was chosen because it contains a built-in 32.768 kHz crystal, consumes 50 μA, and has dimensions of 1.5 mm x 3.2 mm.

4.4.4 Visual and Audio Feedback

Two types of feedback could be provided by the master unit; visual and/or audio. Visual feedback was provided from the LCD screen and audio feedback was provided from a small buzzer. The advantage of using visual feedback is that the feedback can be provided to specific patient posture problems. For example, if the posture was deemed to be incorrect because of a large kyphotic angle, the LCD screen could display a message to indicate bad posture for the kyphotic measure. However, the disadvantage in visual feedback is that the patient is required to view the LCD screen frequently during the training session, which would severely interfere with the patient's daily activities. The buzzer provides audio feedback, which is less specific than visual feedback, but it interferes less in the patient's daily activities. Audio and visual feedback can be customized for the needs of individual patients.

4.4.5 Power Supply

Power for the master unit was provided by a 400 mAh LiPo battery regulated by a MCP1700. Unlike the sensor unit, the master unit possessed its own charging circuitry so a power supply could be connected to the master unit directly to charge the battery. In theory, a fully charged battery could allow the master unit to operate for approximately nine hours.

4.4.6 Dimensions of the Master Unit

A custom PCB was also designed for the master unit. Final schematics of the master unit are available in Appendix A.2 and A.3 while the PCB layout is available in B.2. The size of the PCB was restricted to match the size of the LCD screen. This allowed for the PCB to be mounted underneath the LCD screen to minimize the size of the master unit. As well, a custom enclosure was designed to house the master unit. The final dimensions of the enclosure are 51.9 mm x 51.6 mm x 20.3 mm (L x W x H) and is shown in Figure 4.9.

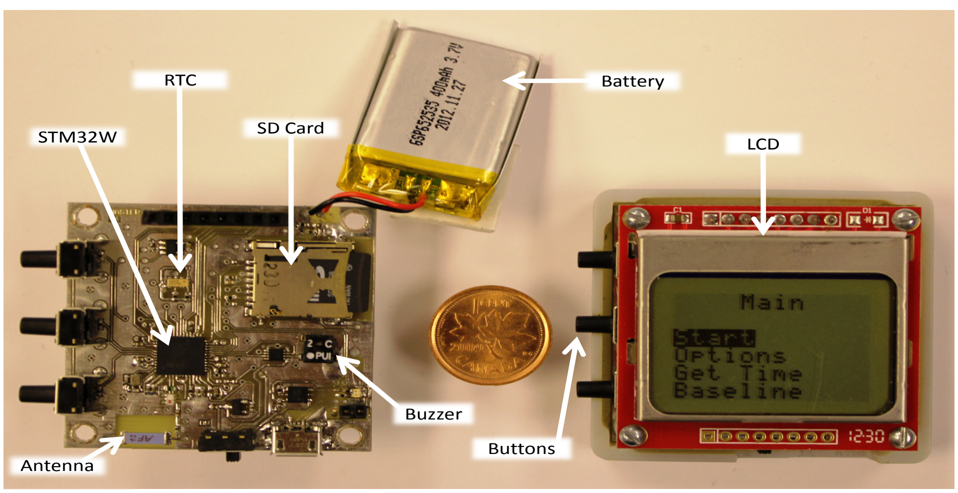

Figure 4.9: Complete master unit without and with LCD screen

4.5 Firmware Design for Master Unit

The master unit is the central node of a wireless distributed computing network and as such the firmware was designed to reflect its central role in the posture monitoring system. In a similar manner to the sensor unit, the master firmware can be divided into two main operating modes called normal mode and sampling mode. The firmware for the master unit was written in C.

4.5.1 Normal Mode

Normal mode is the default mode when the master unit is turned on. The block diagram of the master unit's normal mode is shown in Figure 4.10. When the master unit is turned on, the unit initializes the microSD card. Then either the default radio settings or the settings stored in the microSD card are loaded. Once the radio has been initialized, the master unit displays the current firmware version and the PAN ID before initializing the RTC. After, the master unit displays the main screen which is shown in Figure 4.9. In Figure 4.10, the grey blocks denote a screen shot that is shown to the user while white blocks denote an internal process. Navigation between the screen shots is performed using push buttons located on the side of the master unit (shown in Figure 4.9). From the different screens, options are displayed that allow the user to start a session, setting and viewing the current time in the RTC, checking the status of the microSD card, and checking the status of currently connected sensor units without the need of a PC.

After the master unit has entered the main screen, sensor units are able to check-in. The check-in process is illustrated in Figure 4.11 and is performed internally by the master unit. The check-in procedure acts to associate a specific sensor unit with a master unit. When the master unit receives a request from a sensor unit, the master unit checks to see if it has an available spot in its network. A master unit only can check-in five sensor units into its network at one time. If no spot is available, the master unit does not reply to the request. Otherwise, the master unit checks to see if it is already engaged in checking in another sensor unit. If there is a check-in already in process, the master unit ignores the new check-in request from the sensor unit. Otherwise, the master unit transmits back to the requesting sensor unit a new source address between 0x01 and 0x05. When the new source address is sent out by the master unit, a timer is initiated. If the requesting sensor unit responds to the master unit with the correct source address, the timer is disabled and the sensor unit has successfully checked-in with the master. If not, the master unit cancels the check-in process and frees up the previously sent out source address for another sensor unit.

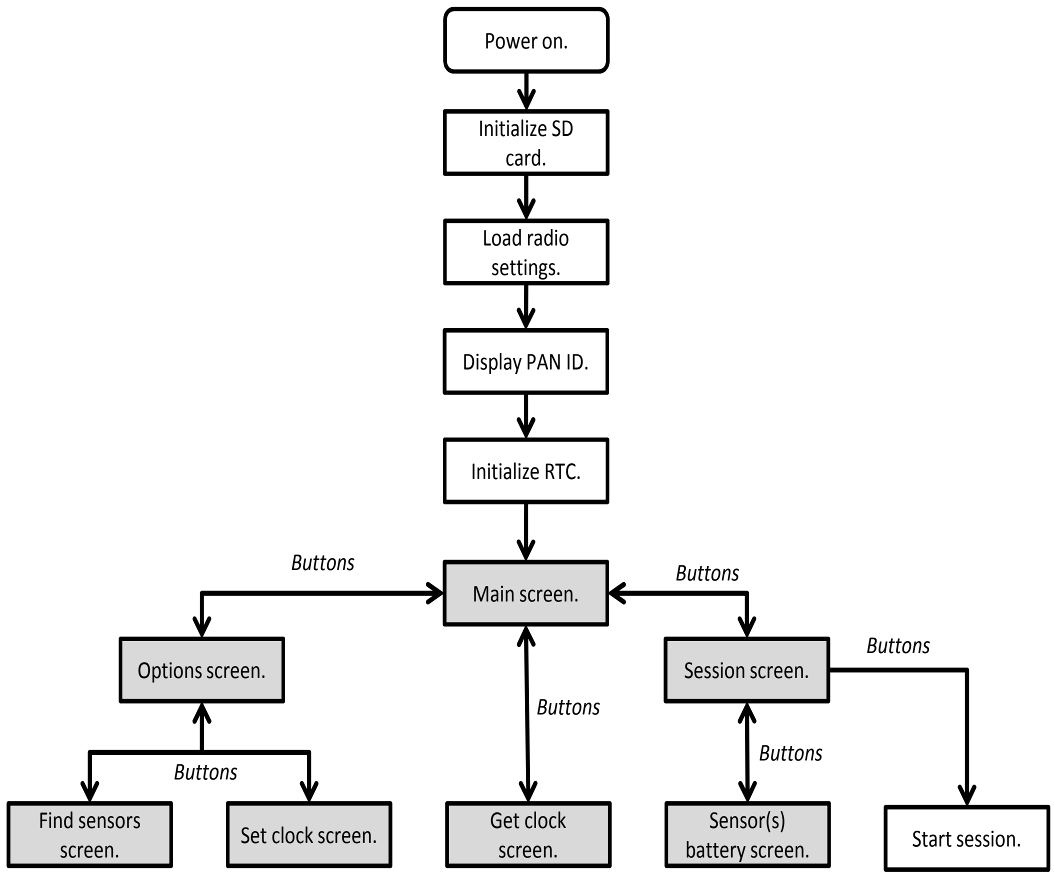

Figure 4.10: Master unit normal mode block diagram

4.5.2 Sampling Mode

Sampling mode is where the master unit routinely polls the sensor units for their orientation information in order to determine the patient's posture (Figure 4.12). The master unit enters sampling mode when a session is started from the *Session screen*. When the session begins, the master unit checks if the microSD card is available. If there is no microSD card, the master unit displays an error message on the LCD screen and returns to the *Main screen*. If the microSD card is present, the threshold values for each posture measurement and the type of feedback for the session are then loaded into the master unit from the microSD card. These thresholds are used to determine whether the patient's posture is good or bad. If the threshold values are invalid, an error message is displayed on the LCD screen and the master unit returns to the *Main screen* in normal mode.

After all the initialization steps have been completed, the system begins by

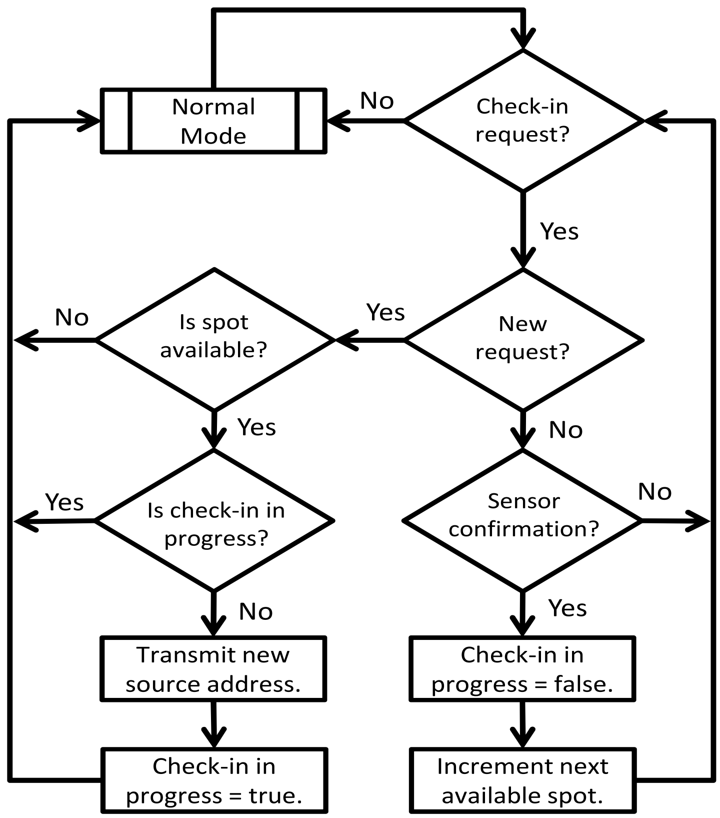

Figure 4.11: Check-in procedure for master unit

asking the patient to assume a correct posture and hold it for ten seconds. During this time, the master unit is acquiring a baseline reading of each sensor unit. This baseline reading is necessary as it is very difficult to place the sensor units in the exact same locations for every session. Mathematically, this is equivalent to zeroing the measurements from the sensor units. The baseline reading is acquired by averaging ten samples taken from the sensor unit during the ten seconds that the patient is maintaining a correct posture.

Before the posture measurements are computed, an internal timer is started to interrupt every two seconds. Two seconds was chosen because that sampling frequency provides the master unit with sufficient time to poll all five sensor units, calculate the patient's posture, provide feedback if required, and write the data to the microSD card. When the timer reaches 0, it triggers an interrupt to acquire a new sample. The master unit first broadcasts a command to all the sensor units to hold their current quaternion. Then, the master unit requests the currently held quaternion from each sensor unit in sequence from sensor unit one (S1) to sensor unit five (S5). The location of the sensor units

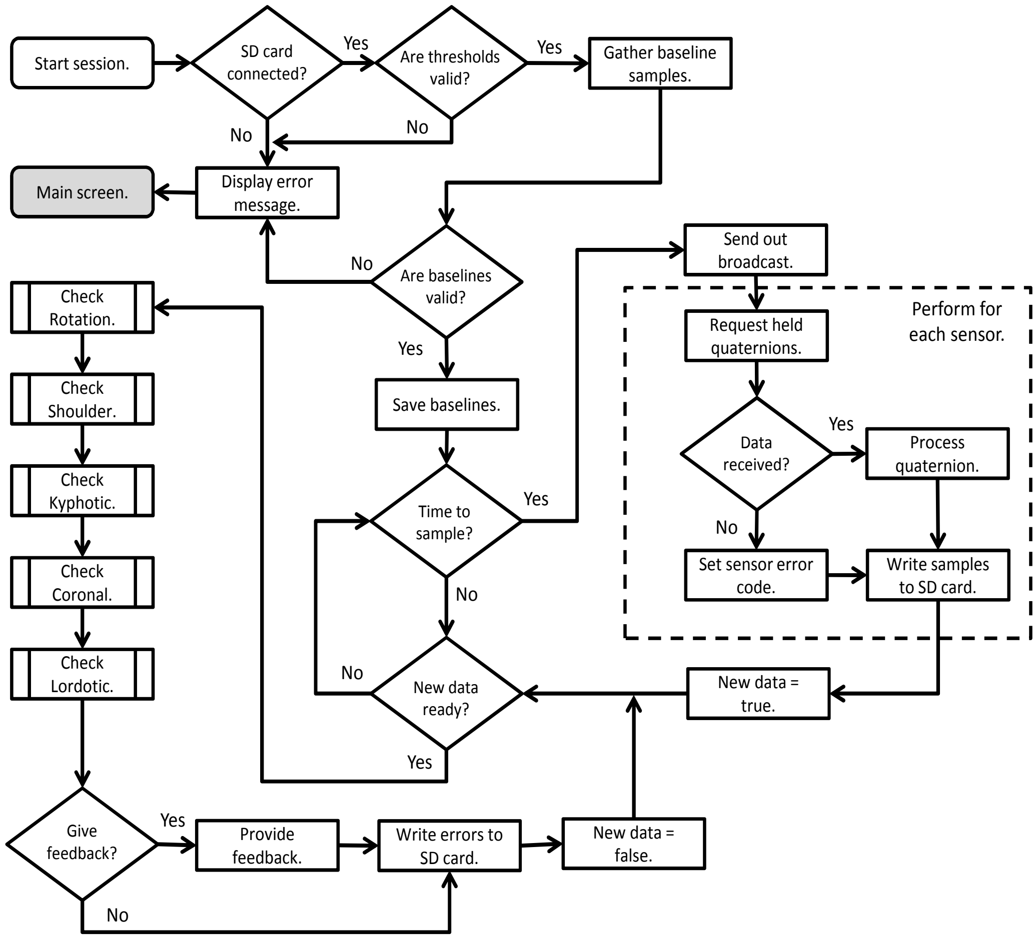

Figure 4.12: Master unit sampling mode flow chart

on the patient are shown in Figure 4.13. If no quaternion is received, an error code is logged for that specific sensor. Otherwise, the received quaternion is converted to its equivalent Euler angles as described in Chapter 3.

After all requests have been made, the Euler angles from each sensor unit are then written to the microSD card including a time stamp obtained from the RTC. Sensor units which did not transmit a quaternion had blank samples written to the microSD card. Once the samples have been stored, the patient's posture is computed. As seen in Figure 4.12, there are five different calculations performed to evaluate the patient's posture.

The *Check Rotation* subroutine is tasked with computing the amount of rotation the patient has along the transverse plane. The baseline reading obtained by the master unit relates to the direction that the patient was facing. A different approach was taken for computing the angle about the transverse plane.

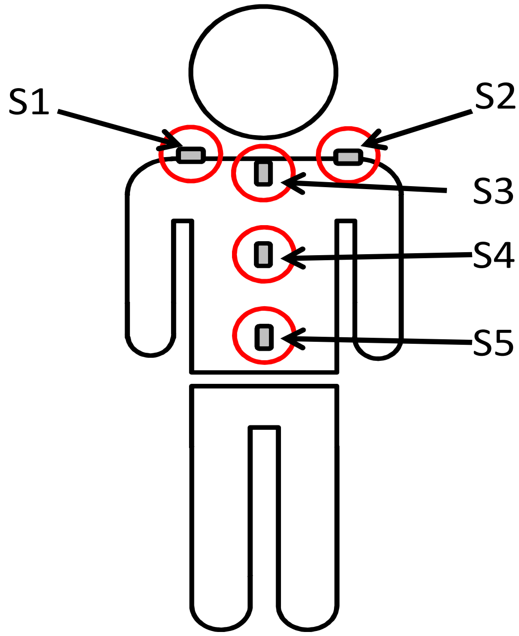

Figure 4.13: Sensor unit locations on patient

The yaw angles (ψ) from S3 and S5 are used to compute the rotation of the torso as shown in Figure 4.14. The logic flowchart for the rotation angle calculation is shown in Figure 4.15 and the *Angle Calculator* algorithm performed is shown in Algorithm 1.

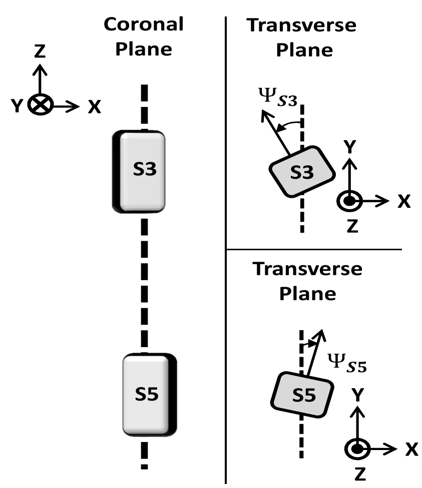

Figure 4.14: Calculation of the *Check Rotation* posture measure

The rotation is calculated by first computing the current rotation angle of S3 and S5. This is performed using Algorithm 1. A decreasing yaw angle indicates the patient is turning to his/her right while and increasing yaw angle indicates a left turn. If the sign of the measured yaw and baselines are not

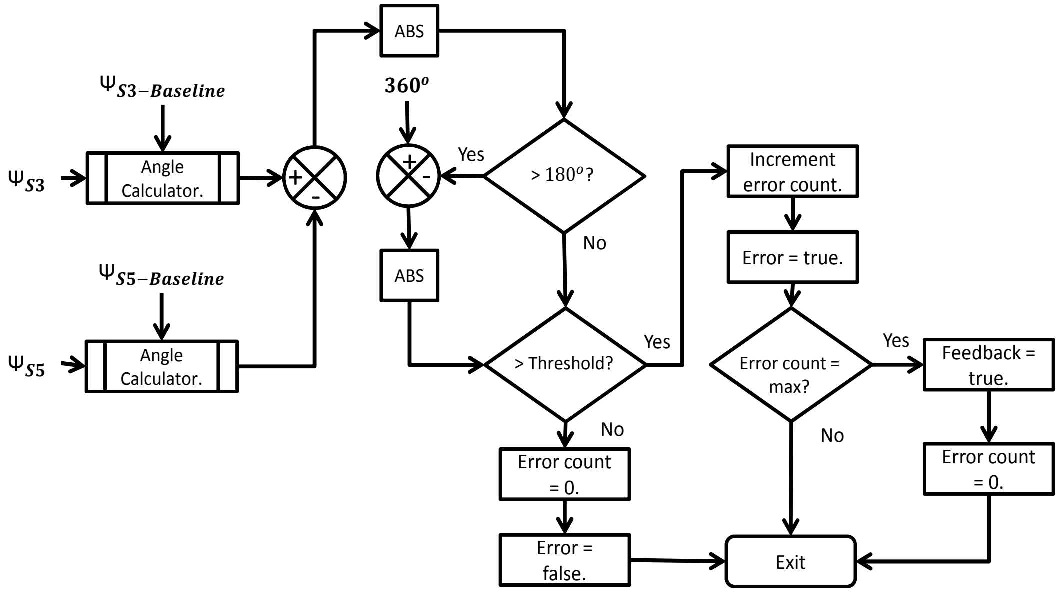

Figure 4.15: Rotation posture calculation flowchart

the same, their absolute values are added together. Otherwise, the absolute difference between the measured yaw and baseline value is computed. The absolute difference between the absolute value for both S3 and S5 is then taken and compared to 180°. If the result is greater than 180°, the result is then subtracted from 360°. This procedure is to ensure that no false positives (i.e: incorrect posture) are detected at the discontinuity points between -180°and 180°. For example, suppose the yaw baselines obtained for a patient during their session for S3 and S5 were $\Psi_{S3-Baseline} = 179°$ and $\Psi_{S5-Baseline} =$ -176° and the measured yaw values for one sample were $\Psi_{S3} = 173°$ and $\Psi_{S5} =$ 174°. The resulting angle computed for S3 and S5 are 6° and 350° respectively. The absolute difference between 6° and 350° is 344°. As 344° > 180°, the final result for the amount of rotation detected by the master unit would be 360°-344°= 16°.

Algorithm 1 Angle Calculator subroutine

if $((\Psi < 0)$ AND $(\Psi_{Baseline} > 0))$ OR $((\Psi > 0)$ AND $(\Psi_{Baseline} < 0))$ **then**
  return $|\Psi| + |\Psi_{Baseline}|$
else
  return $|\Psi - \Psi_{Baseline}|$
end if

The *Check Shoulder* subroutine is responsible for computing the patient's shoulder posture. The shoulder posture is calculated using the roll angles

(θ) of S1 and S2 as shown in Figure 4.16. Figure 4.17 shows a general logic flowchart for calculation of the shoulder posture, where A is θ_{S1} and B is θ_{S2}. These roll angles first have their respective baseline values subtracted from them before finding their absolute difference. If the difference is greater than the shoulder threshold, a counter is incremented. If the counter reaches a pre-defined maximum, feedback is requested and the counter is reset. Otherwise, the counter is reset and no incorrect posture is recorded.

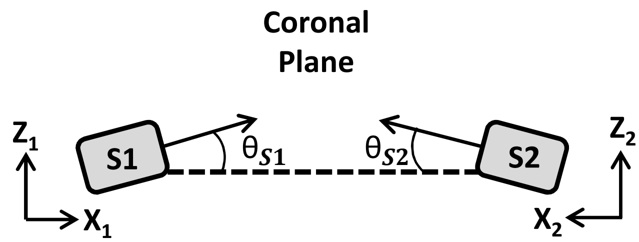

Figure 4.16: Calculation of the *Check Shoulder* posture measure

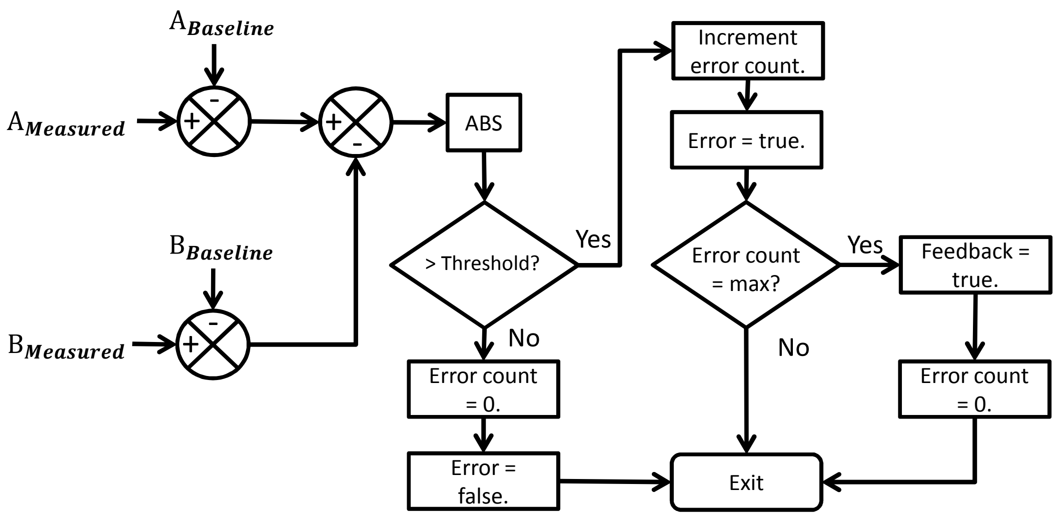

Figure 4.17: General posture calculation flowchart

The *Check Kyphotic* subroutine computes a proxy kyphotic angle using the pitch angles (ϕ) from S3 and S4 on the patient's back as shown in Figure 4.18. The proxy kyphotic angle takes into account the baseline values for S3 and S4 so the reported angle is not the medically defined kyphotic angle. The logic flowchart for calculating the proxy kyphotic angle is shown in Figure 4.17, where ϕ_{S1} and ϕ_{S2} are represented by A and B respectively. After the baselines have been subtracted, the absolute difference is calculated and compared to the kyphotic threshold. If the threshold value is exceeded, a counter is incremented and, if the counter has reached the maximum value, feedback is requested.

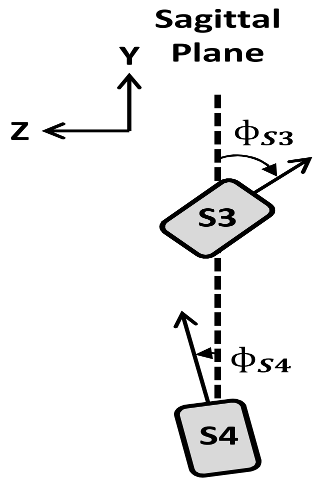

Figure 4.18: Calculation of the *Check Kyphotic* posture measure

The *Check Coronal* subroutine is used to check the patient's posture along the coronal plane using θ from S3, S4, and S5 as shown in Figure 4.19 and the subroutine logic shown in Figure 4.20. After subtracting the baselines, the absolute difference for S3 and S4 (referred to as *Upper*) is compared to a threshold. If the difference is greater than the threshold, a counter is incremented. If the counter reaches a maximum value, the counter is reset and feedback is requested for the patient. If *Upper* is less than the threshold, the absolute difference is computed for S4 and S5 (*Lower*) and compared to the same threshold as for *Upper*. If *Lower* is greater than the threshold, the counter is incremented. If the maximum value is reached, the counter is reset and feedback is requested. Otherwise, the coronal counter is reset and no incorrect posture is recorded.

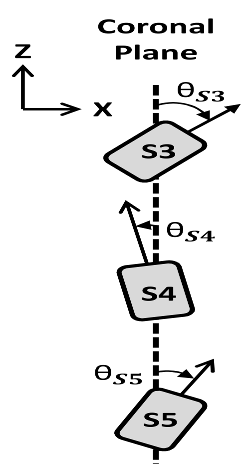

Figure 4.19: Calculation of the *Check Coronal* posture measure

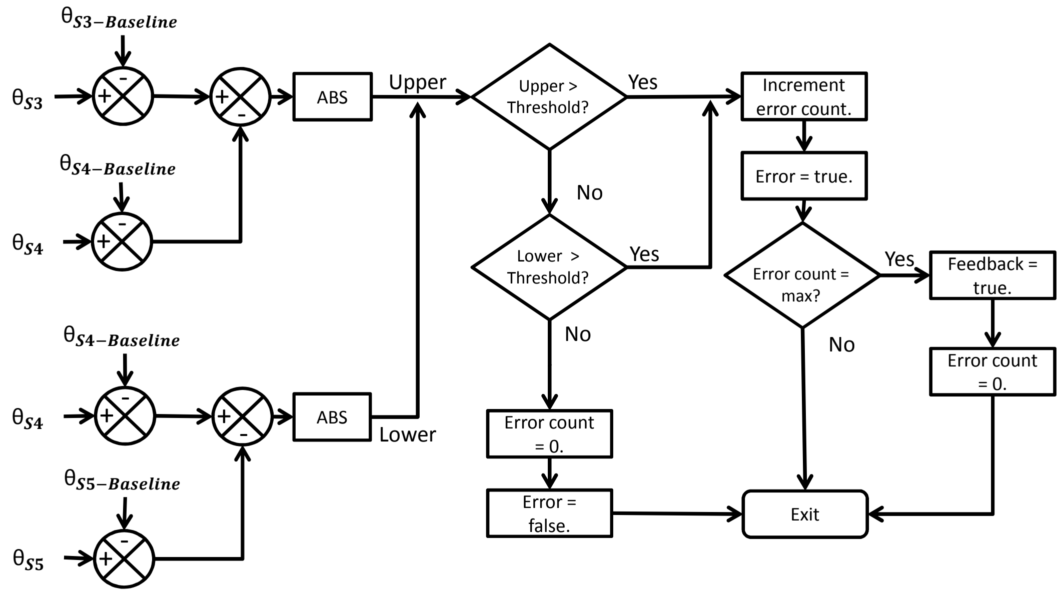

Figure 4.20: Coronal posture calculation flowchart

The *Check Lordotic* subroutine is used to compute a proxy lordotic angle in a similar manner to *Check Kyphotic*. *Check Lordotic* uses ϕ_{S4} and ϕ_{S5} (Figure 4.21) in the calculations shown in Figure 4.17, where A is ϕ_{S4} and B is ϕ_{S5}. If the absolute difference is greater than the lordotic threshold, a lordotic counter is incremented. If the counter is equal to a maximum value, feedback is requested for the patient and the counter is reset. If the difference is less than the threshold, the counter is reset.

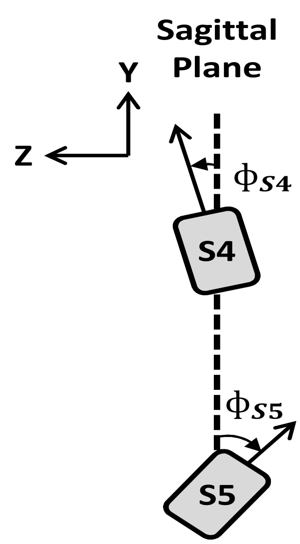

Figure 4.21: Calculation of the *Check Lordotic* posture measure

Immediately after the completion of the individual posture measure subroutines, a feedback counter is incremented for every instance in which a subroutine requested feedback for the patient. If audio feedback has been enabled for the session, the number of feedback requests is then forwarded to the buzzer. For example, if feedback has been requested from two of the posture measurement subroutines, the buzzer would beep twice. The patient knows that if he/she hears multiple audio beeps, his/her posture has deviated significantly from good posture. The buzzer can emit a maximum of five beeps when providing feedback. If visual feedback is enabled, the feedback is applied immediately after each posture measure subroutine has completed and corresponds to the calculation performed. For example, if *Check Kyphotic* returned that feedback is required, the LCD screen would display “KYP ERROR”. Visual feedback provides a more detailed explanation for patients as to what component of their posture requires correcting.

4.6 Windows Interface

While the user interface on the master unit is sufficient for initiating training sessions and checking the status of sensor units, it is unable to handle changing radio parameters for the master and sensor units. Furthermore, loading the calibration settings to the sensor units and processing the results of the patient's sessions are required to be done on a PC. The Windows Interface is used by the patient and therapist to address the limitations of the master unit. The program was written in C#. The different user controls are grouped into tabs in order to ease user navigation of the different available options. In order to access any sensor unit or master unit settings, the patient must first connect to an 802.15.4 radio USB dongle (Figure 4.22) through the *File* drop down menu. The dongle provides radio communication between the posture monitor units and the Windows Interface. The ‘Calibration Settings’ tab (shown in Figure 4.23) provides a way to transmit new calibration settings to the sensor unit. The user can input new scale and offset factors for the accelerometer and gyroscope. For the magnetometer, a new soft iron matrix and hard iron matrix can be loaded. It is also possible to obtain the currently loaded settings from each sensor unit. This function provides an easy method for updating the settings when the sensor units are brought into an area with a different magnetic fields caused by electronic equipment or other metal objects.

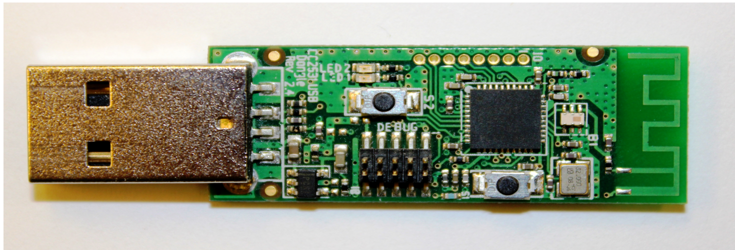

Figure 4.22: 802.15.4 USB dongle

The 'General Settings' tab (shown in Figure 4.24) allows for the default radio settings in the master and sensor units to be changed or viewed. By changing the radio settings, specifically the PAN ID, it is possible for multiple posture monitoring systems to operate in close proximity without interfering with each other.

The 'Session Information' tab (shown in Figure 4.25) provides the ability for a user to load a text file containing the results from a posture training session and perform data analysis. A percentage of the incorrect samples for the five posture measures is displayed along with the packet reception. Average values of each posture measure along with the baselines readings are also displayed. This allows operators to monitor the progress of the posture training and the effectiveness of the treatment approach.

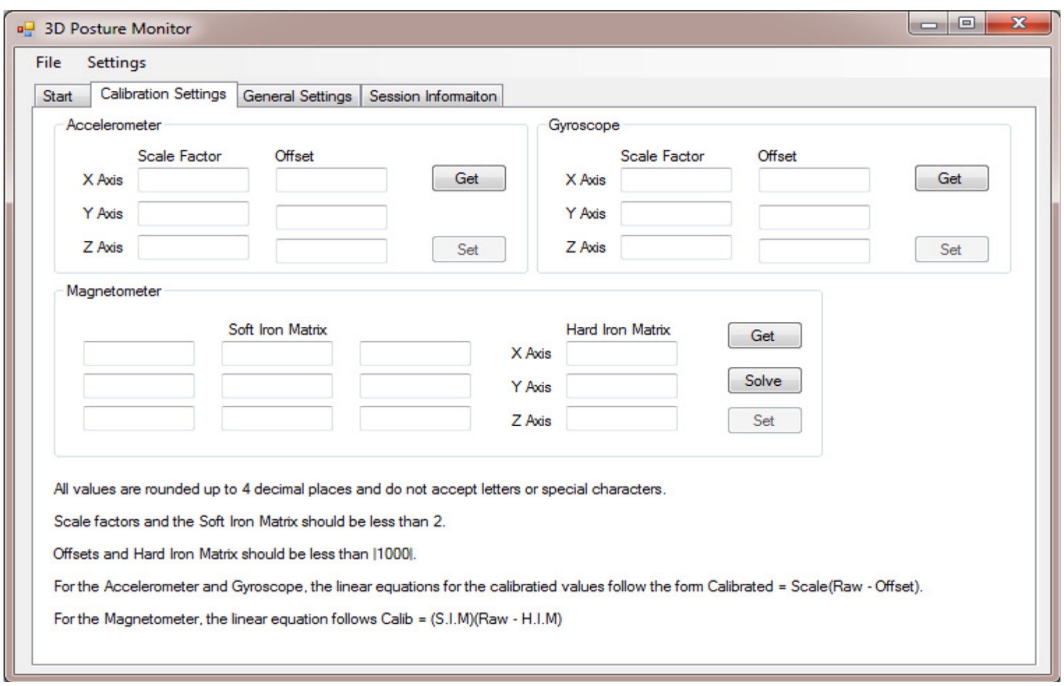

Figure 4.23: Calibration Settings tab of the Windows Interface

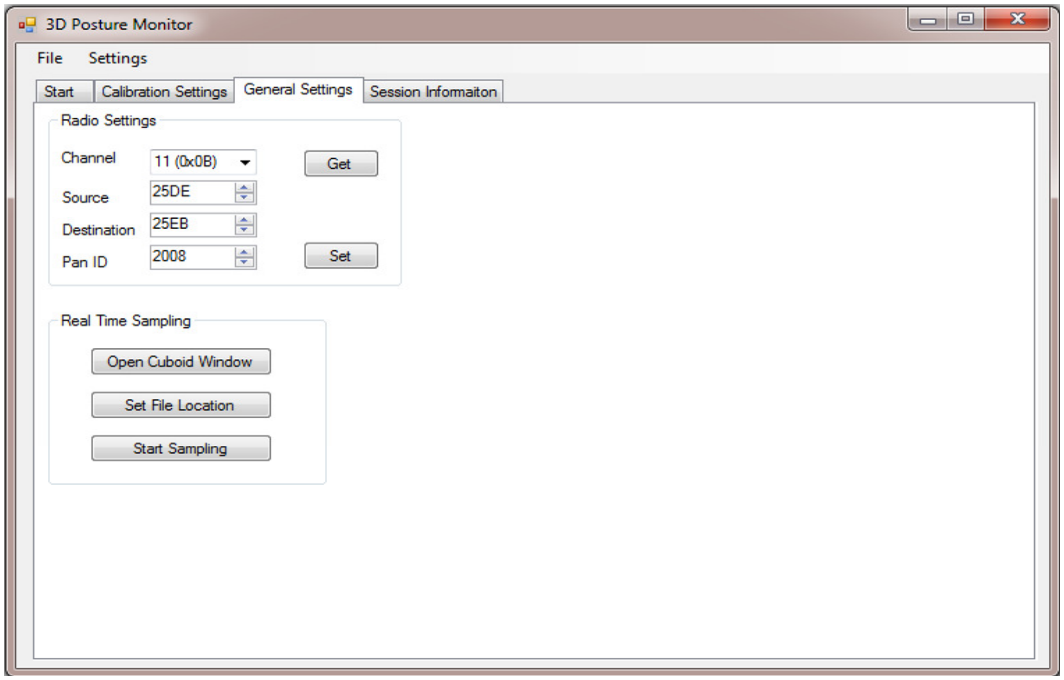

Figure 4.24: General Settings tab of the Windows Interface

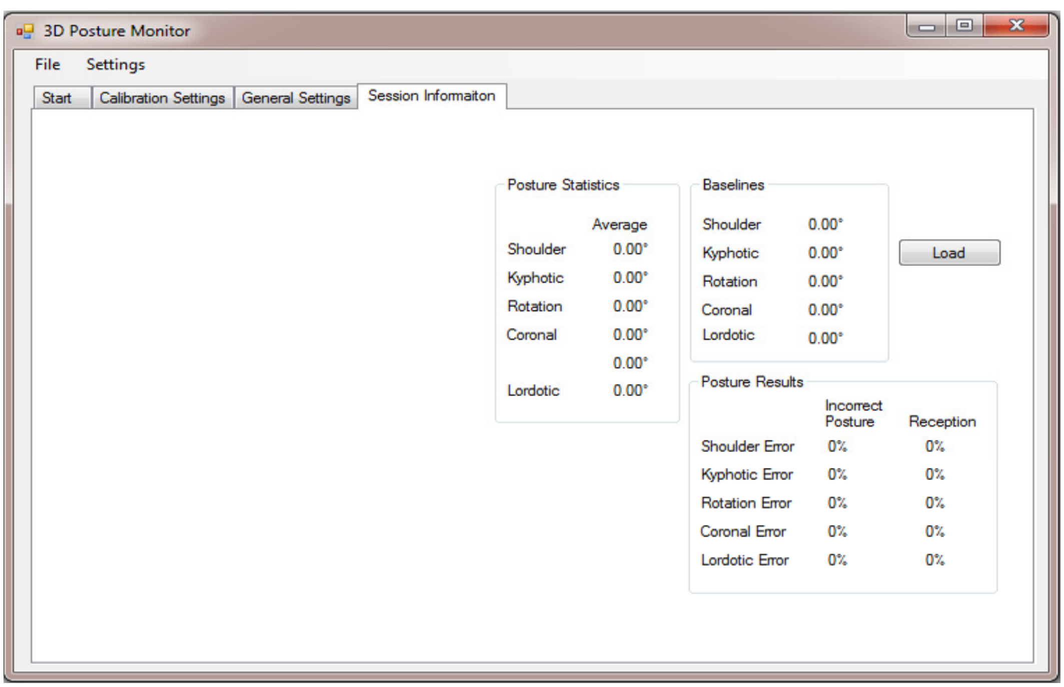

Figure 4.25: Session Information tab of the Windows Interface

Chapter 5

System Validation and Results[1]

In order to evaluate the accuracy and performance of the developed posture monitoring system, laboratory tests have been performed. For both sensor and master units, the battery life has been measured. The communication range between a sensor unit and the 802.15.4 USB dongle has been evaluated at different ranges. The static and dynamic accuracies of the orientation measurements, the stability of the orientation output, and the effects of nearby ferrous objects that affect the local magnetic field of the sensor unit have been determined. Posture training experiments have also been performed to evaluate the effects of posture training on volunteers for a short period of time. A total of three volunteers each wore the posture monitoring system for either four or five days. This chapter describes the details of the posture training experiment procedures and presents the results from each of those tests.

5.1 Laboratory Tests

5.1.1 Sensor Unit Current Consumption Test

The current consumption of the sensor units was measured using a Fluke 179 multimeter to determine the operating time of the sensor units. The multimeter was hooked up in series between the battery and the sensor unit. Three tests were performed: a) the sensor unit was running in the normal mode while no wireless data was being transmitted, b) the sensor unit was

[1]Material in this chapter has been presented at the *University of Alberta Faculty of Engineering Research Symposium 2013*

running in the normal mode while wireless data was transmitted at a rate of 50 Hz, and c) the sensor unit was running in the sampling mode while wireless data was transmitting at a rate of 0.5 Hz. For all tests, the radio transceiver was turned on. The current measurement was taken for each test after the sensor unit was operating for five minutes to allow for stabilization.

5.1.2 Master Unit Current Consumption Test

The current consumption of the master unit was measured using a Fluke 179 multimeter to determine its operating time. The current consumption was observed in two states; a) operating in normal mode while not transmitting any wireless data and b) while sampling five sensor units in sampling mode and providing only visual feedback. The multimeter was hooked up in series between the master unit and the battery. For all tests, the radio transceiver was turned on and the current measurement was obtained after five minutes of operation to allow for stabilization.

5.1.3 Sensor Unit Communication Range Test

A range test was performed to evaluate the wireless communication range between a sensor unit and the USB dongle connected to the PC. A sensor unit was configured to transmit 100 data packets containing an 18 byte payload to the Windows Interface. The sensor unit transmitted the packets at 50 Hz. The Windows Interface would display the number of packets received. The range test was performed at distances of 0 m, 1 m, 2 m, and 3 m. These distances were chosen as the expected set up for interfacing the sensor unit with the PC would keep the sensor unit within 3 m of the PC.

5.1.4 Static Pitch, Roll, and Yaw Accuracy Tests

The static accuracy test was performed by mounting a sensor unit to a rotating acrylic wheel as shown in Figure 5.1. The sensor unit was rotated counterclockwise in 10° increments through a full 360° rotation. The senor unit continuously computed its orientation and transmitted the data wirelessly to the Windows Interface. The USB dongle was located within 2 m of the sensor unit for each test. The angle was recorded at every 10° rotation. The test was carried out for pitch, roll, and yaw measurements using the same sensor unit and repeated three times for each measurement to confirm repeatability. The readings from the wheel were compared to the measurements from the sensor unit.

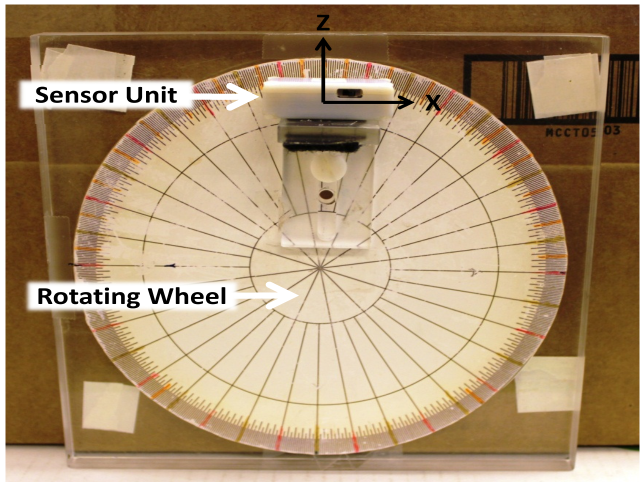

Figure 5.1: Static accuracy test setup for sensor unit

5.1.5 Stability Test

To determine the stability of the pitch, roll, and yaw measurements, a sensor unit was placed on a desk for a long period of time in the laboratory. The sensor unit transmitted its orientation to the master unit at a frequency of 0.5 Hz for a period of 60 minutes. The data acquisition began ten seconds after the sensor unit began calculating its orientation in order for the orientation angles to have reached a steady state. The master unit recorded the orientation information in a text file stored in the microSD card. The master unit and the sensor unit were within 30 cm of each other for each test. The test was repeated three times with the same sensor unit.

5.1.6 Magnetic Distortion Test

This test was conducted to determine the effect of moving a large ferrous object towards the sensor unit. The sensor unit was placed on a flat surface with the Z axis perpendicular to the surface. A piece of wood with markings every 2.54 cm up to 50.8 cm was placed next to the sensor unit as seen in Figure 5.2. The sensor unit was calibrated in the area of the test with the iron more than 2 m away in order to not include the effects of the iron in the calibration parameters for the magnetometer. For each test, a large piece of iron was placed 50.8 cm away from the sensor unit and was decremented 2.54 cm per step to bring the iron closer to the sensor unit. The iron would remain at each step for ten seconds. During the entire test, the sensor unit was transmitting its orientation to the Windows Interface at a frequency of 50 Hz. The sensor unit was located approximately 1.5 m away from the USB dongle at all times during each test. The test was repeated a total of three times in the same location in a laboratory environment with the same sensor unit.

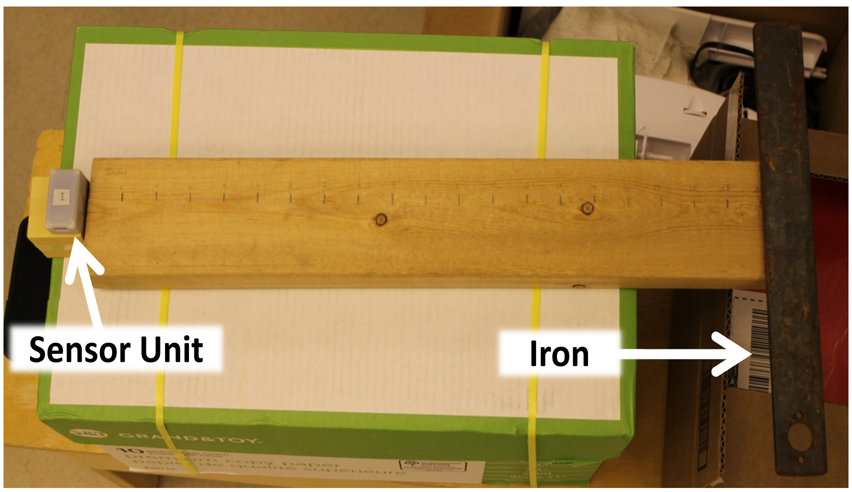

Figure 5.2: Setup for magnetic distortion test

5.1.7 Dynamic Pitch, Roll, and Yaw Accuracy Tests

The dynamic accuracy test was performed to evaluate the sensor unit's performance in a dynamic situation. The experiments were performed in a motion capture (gait) laboratory shown in Figure 5.3, which contains eight high-end motion camera systems (Motion Analysis, Santa Rosa), only which four are shown in the figure. The gait laboratory uses the cameras to track the movement of reflective spherical markers which are affixed to the point of interest as shown in Figure 5.4. Infrared light is reflected off the markers and captured by the cameras. The cameras sample the reflective light at 120 Hz and have a positional accuracy of 0.5 mm. The three-dimensional coordinates of each marker is obtained from processing all of the data acquired from the eight cameras. Before the tests, the camera system was calibrated by a trained technician. A custom lid was created for the sensor unit (Figure 5.4) that allowed for the markers to be placed along its X, Y, and Z axes. Each marker had a diameter of 20 mm and was placed 43.6 mm away from the center of the sensor unit's case. The gait laboratory has many metal objects which can affect the readings of the magnetometer. A magnetometer calibration was performed on the sensor unit while in the center of the gait laboratory, where all tests were carried out.

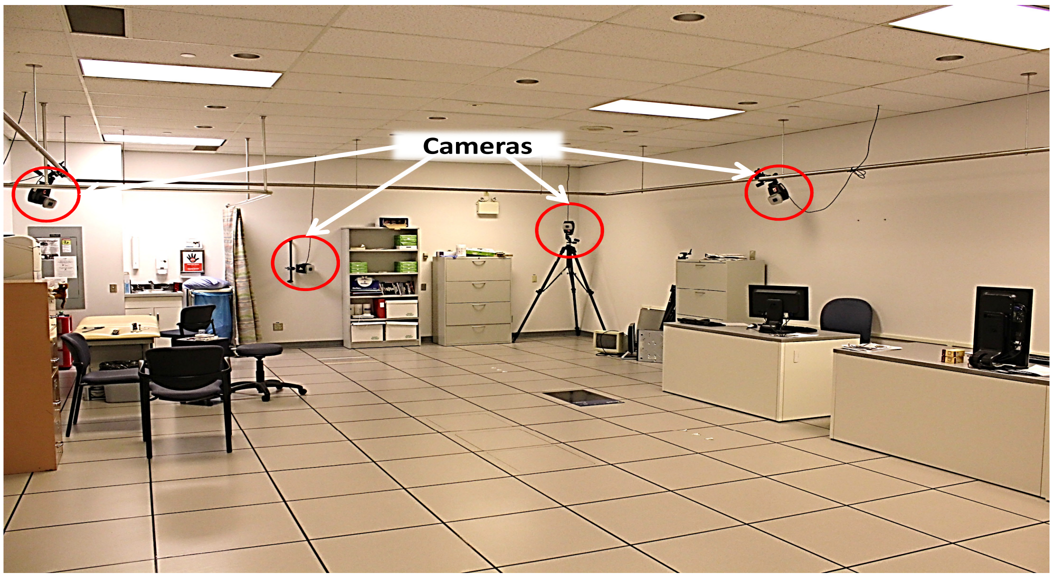

Figure 5.3: Motion capture camera (gait) laboratory

Two sets of dynamic tests were performed. For the first test, the sensor unit was held by a volunteer and rotated to known orientations where it was held still for approximately ten seconds. The sensor unit was held at a starting position by the volunteer in such a way that its X and Y axes were parallel with the ground. The sensor unit was held in this starting position for ten seconds. The sensor unit was then slowly rotated about the X axis to 90° and held there for ten seconds. After, the sensor unit was slowly rotated back about the x axis to -90° and held still for another ten seconds. The sensor unit was then rotated back to the starting position for a further ten seconds. This procedure was repeated for roll (about the Y axis) and yaw (about the Z axis). For the yaw test, the sensor unit was first rotated to -90° and then to 90°. This procedure was repeated a total of three times.

The second test involved continuously rotating the sensor along the X, Y, and Z axes. A volunteer held the sensor unit in same starting position used in the first test. The volunteer then applied a smooth, slow rotation about the X axis from 90° to -90° and repeated it. The volunteer would then rotate the sensor unit about the Y axis from -90° to 90° twice and the same for along the Z axis. This procedure was repeated a total for four times. The same sensor unit was used for both tests.

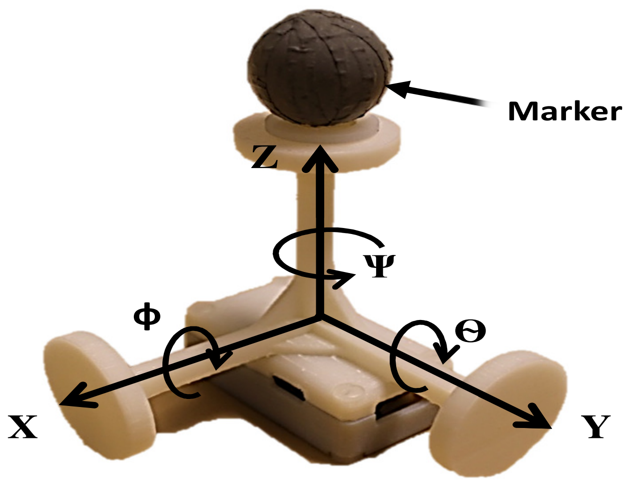

Figure 5.4: Custom lid for sensor unit for dynamic accuracy tests

5.2 Posture Monitor Tests

The purpose of the posture monitor tests are to evaluate the ability of the master unit and sensors units to work together to correctly identify a subject's posture and to provide feedback when correction was required. These tests also evaluate the reliability of the system as a whole. A total of three posture tests were performed with volunteers wearing the posture monitoring system in a laboratory environment. Figure 5.5 is an image of where the five sensor units were located on a volunteer. S1 and S2 were placed on the volunteer's shoulders so that their X axes would run parallel with the sagittal plane and the Z axes were perpendicular to gravity. S3 was placed in the upper thoracic region around T1, S4 was placed in the middle of the back around T11-T12, and S5 was placed in the mid lordotic region around L2-L3. The sensor units were calibrated for each volunteer in the area where the posture monitoring sessions were conducted.

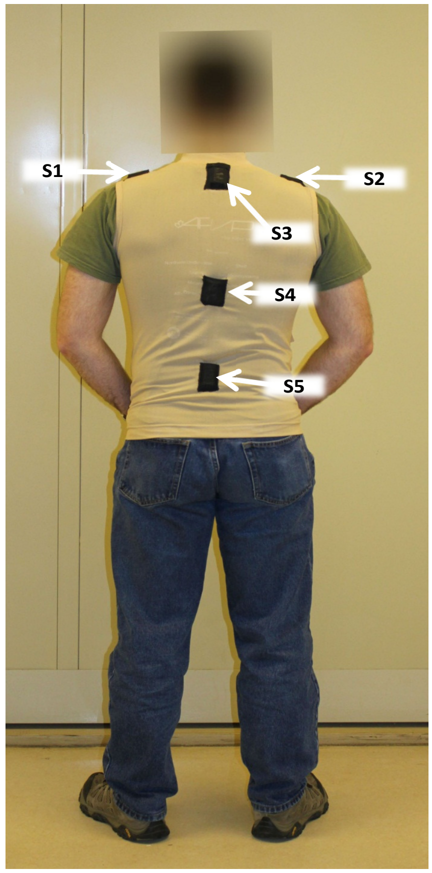

Figure 5.5: Sensor unit locations on garment used in posture monitor tests

5.2.1 Posture Monitor Test 1

The first posture monitor test evaluated the complete system and aided in the development of a testing protocol for future experiments. Two healthy adult volunteers with no scoliosis wore the posture monitoring system for two hours per day for five consecutive days. During the two hour session, the volunteers were primarily sitting and working on a computer. Each volunteer wore a tight-fitting garment with custom pockets to hold the five sensor units. No feedback was provided on the first or second day in order to acquire a baseline of the volunteers' posture when they are sitting down. Audio and visual feedback was provided to the volunteers on days three and four at the fifth incorrect consecutive posture sample. No feedback was provided to the volunteers on the fifth day and the purpose of this was to evaluate the learning effects from the third and fourth days. The thresholds for each volunteer were kept constant throughout the week and each volunteer wore the same sensor units and master unit. The master unit sampled the volunteer's posture at a frequency of 0.5 Hz. Only four posture measures were performed during the five day tests; shoulder posture, kyphotic, rotation about the transverse plane, and coronal measure.

5.2.2 Posture Monitor Test 2

The second test involved two volunteers wearing the posture monitoring system for two hours per day for four consecutive days. The test procedure was based on the procedures used in [12] and [13] where volunteers would wear the system for a total of four days and only be provided feedback on the two middle days. The first day and last day had no feedback. The second and third days had audio and visual feedback provided when the fifth consecutive poor posture sample was detected. The master unit sampled all five posture measurements at a rate of 0.5 Hz. The master unit was placed on a desk less than 30 cm away from the volunteer at the start of the test.

5.2.3 Posture Monitor Test 3

The third test was designed to build upon the findings in the second test by examining the posture of a volunteer after not wearing the system for three consecutive days. This test followed the same set up as the second posture monitor test by having each volunteer wear the system for five days, four of which were consecutive. The second and third days were the only days where audio and visual feedback was provided. The volunteers then did not wear the system for three consecutive days after the fourth day to minimize their feedback memory. On the fifth experiment day, the volunteers wore the system again without any feedback. The thresholds for both volunteers were kept constant throughout all five days of posture monitoring. The master unit sampled all five posture measures at a frequency of 0.5 Hz. The approximate distance between the master unit and the sensor units was 40 to 50 cm.

5.2.4 Baseline Repeatability Test

After the three posture monitor tests, it was realized that the initial baseline readings obtained from the volunteers during each session had some variability. One reason was that the garment might not have been donned the exact same way between the tests. Any minor shift might affect the orientation of the sensor units. In order determine how much variability can be expected from a subject donning the posture monitoring garment between sessions, a repeatability test was performed. A volunteer donned the posture monitoring system and assumed a correct posture to allow the system to obtain a baseline. This procedure was repeated a total of three times with three separate volunteers. The volunteers wore the same posture monitoring system for each of their three tests and sat in the same location in a laboratory environment.

5.3 Laboratory Test Results

5.3.1 Sensor Unit Current Consumption Test Results

The current consumption of the sensor unit for each test is shown in Table 5.1.

Normal Mode (No TX)	Normal Mode (50 Hz TX)	Sampling Mode (0.5 Hz TX)
35.3 mA	35.9 mA	35.5 mA

Table 5.1: Current consumption of sensor unit

It can be seen that there was no significant difference of current consumption between the three tests conducted. According to the manufacturer datasheet of the LiPo battery, the battery can source 22 mA for five hours. Taking that information, the sensor unit would be capable of operating for three hours on a single charge which is sufficient for the requirements of this system.

5.3.2 Master Unit Current Consumption Test Results

The measured current consumption of the master unit in normal mode and sampling mode was 49.7 mA and was 62.2 mA respectively. The higher current consumption in sampling mode was due to the frequent wireless transmissions between the master unit and the sensor units. From the manufacturer datasheet, the master unit is capable of operating for approximately six hours with the 400 mAh LiPo battery.

5.3.3 Sensor Unit Communication Range Test Results

During the range tests for the sensor unit, no packet loss was recorded at any distance between 0 m and 3 m. At each distance, the Windows Interface correctly received all 100 numbered packets. It is expected that during the system set up, the sensor units will not be more than 3 m away from the USB dongle.

5.3.4 Static Pitch, Roll, and Yaw Accuracy Test Results

The average accuracy of the sensor unit's pitch, roll, and yaw measurements were $1.4°\pm0.03°$, $3.0°\pm0.39°$, and $5.5°\pm0.78°$ respectively. For each of the trials the sensor unit started at the same spot, which was considered to be 0°. The results are presented in Figure 5.6.

The results show that yaw was less accurate than either pitch or roll, but all three have $R^2 > 0.99$. The high correlation meant that the calculated values from the sensor unit was close to the measured values from the rotating wheel. A possible reason for the reduced accuracy of the yaw measurement could be that the calibration of the sensor unit was not sufficient to completely remove the effects of nearby metal present in the surrounding testing environment. Figure 5.6c did have a more pronounced sinusoidal curve when compared to the plot for pitch and roll.

Figure 5.7 provides a summary of measurement errors for the three tests for pitch, roll, and yaw. It can be seen that nearly 50% of yaw errors were greater than 5° in magnitude. All pitch errors were less than 3° while roll had 55% of errors less than 3°.

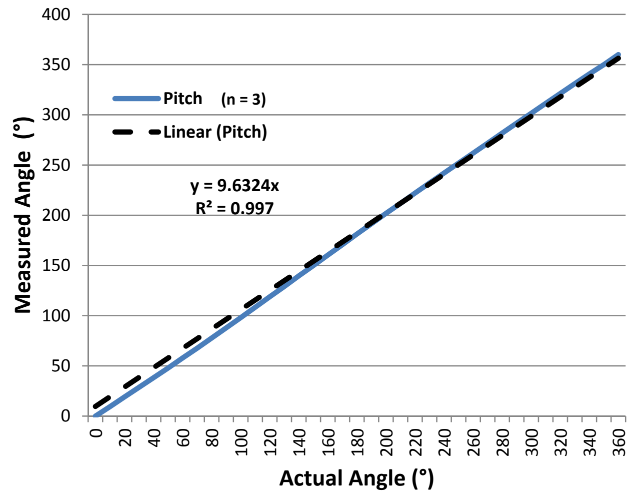

(a) Pitch (ϕ)

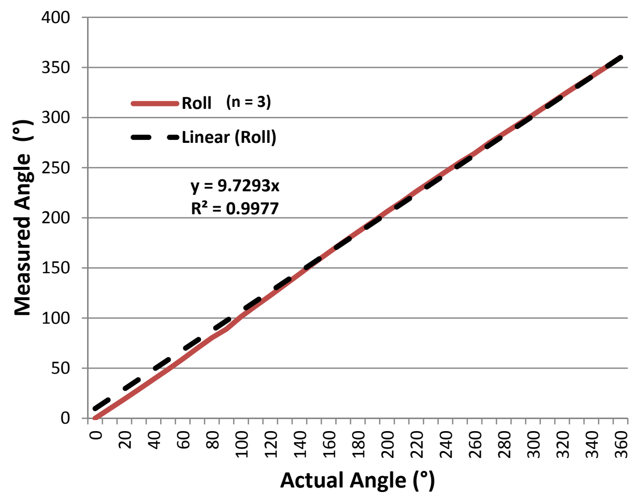

(b) Roll (θ)

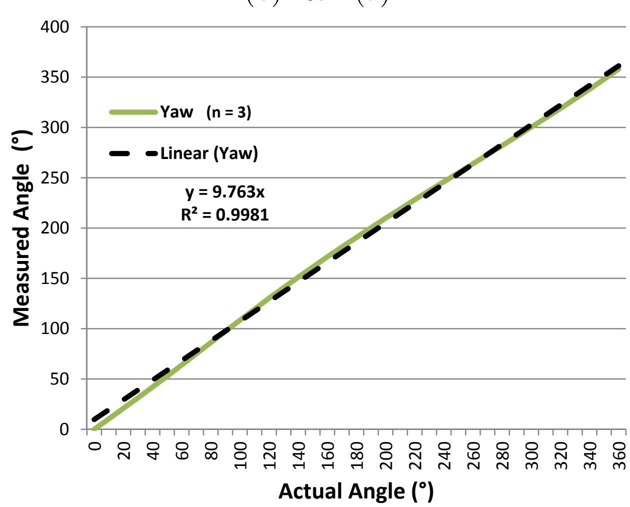

(c) Yaw (ψ)

Figure 5.6: Results of the static accuracy tests

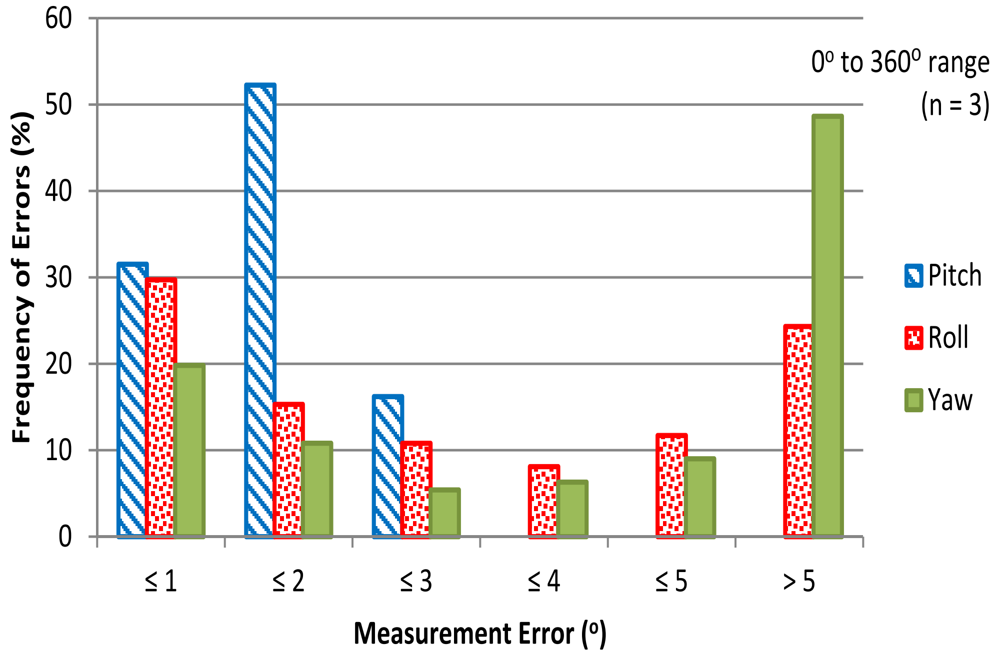

Figure 5.7: Error frequency for sensor static tests

5.3.5 Stability Test Results

The results of the stability test are summarized in Table 5.2. For both pitch (ϕ) and roll (θ), all three tests had 0.5° or less in change between the first sample and the last sample over the 60 minute period. Pitch and roll were very stable. Yaw (ψ) experienced a greater change in angle during the tests. Both test 1 and 3 saw the yaw angle only change by less than 2°, but test 2 had a change of 9° between the start and end samples. This discrepancy might have been due to environmental effects, but this phenomenon did not exist in test 3. The average difference between the maximum and minimum values over all three tests for pitch, roll, and yaw were 1.5°±0.4°, 0.8°±0.2°, and 5.0°±4.0° respectively.

	Test 1			Test 2			Test 3		
	ϕ	θ	ψ	ϕ	θ	ψ	ϕ	θ	ψ
Start	2.4°	0.4°	31.5°	2.4°	0.3°	-128.0°	1.8°	0.3°	57.1°
End	2.8°	0.2°	33.4°	2.0°	-0.2°	-137.0°	1.3°	0.1°	58.9°
Avg.	2.8°	0.3°	33.0°	2.0°	-0.1°	-134.6°	1.5°	0.1°	58.4°
Max.	4.2°	0.6°	33.7°	2.7°	0.6°	-127.5°	2.3°	0.5°	59.2°
Min.	2.1°	0.0°	31.4°	1.5°	-0.5°	-138.1°	1.1°	-0.3°	57.0°
Diff.	2.1°	0.6°	2.3°	1.2°	1.1°	10.7°	1.2°	0.8°	2.1°

Table 5.2: Summary of results for sensor unit stability tests

5.3.6 Magnetic Distortion Test Results

The results for the yaw measurement of the magnetic distortion test are shown in Figure 5.8 and the pitch and roll results are shown in Figure 5.9. For all three tests, the starting yaw angles were all within 3° of each other after the steady state had been reached. The first noticeable changes to the yaw appeared when the piece of iron was 27.9 cm away from the sensor unit. When the iron moved closer to the sensor, yaw would experience a sharp decrease before it leveled out. Once the iron was placed next to the sensor unit, the yaw measurements had changed by a minimum of 70° from the initial measurement.

These tests showed the severe effect on the magnetometer's measurements in the surrounding environment due to additional soft iron effects. These additional soft iron effects can heavily distort the yaw measurements of the sensor units. For each test, the pitch and roll remained very stable though small spikes of a few degrees did occur when the iron was moved closer as shown in Figure 5.9. In Test 1, the huge spike in both pitch and roll at the end of the test was due to sensor unit being turned off.

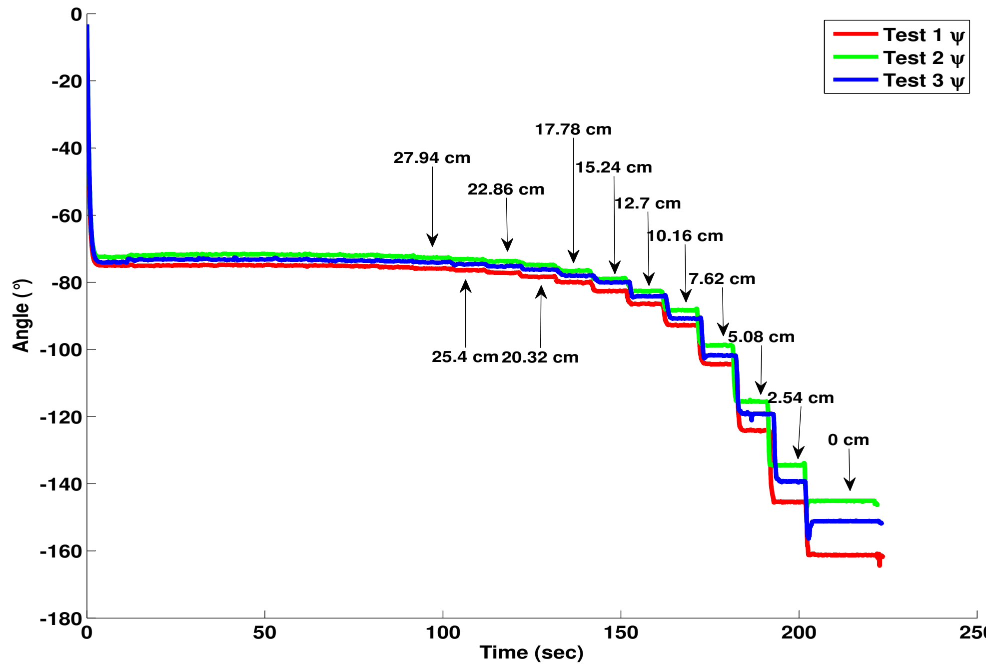

Figure 5.8: Effect of proximity of ferrous object on yaw (ψ) measurement

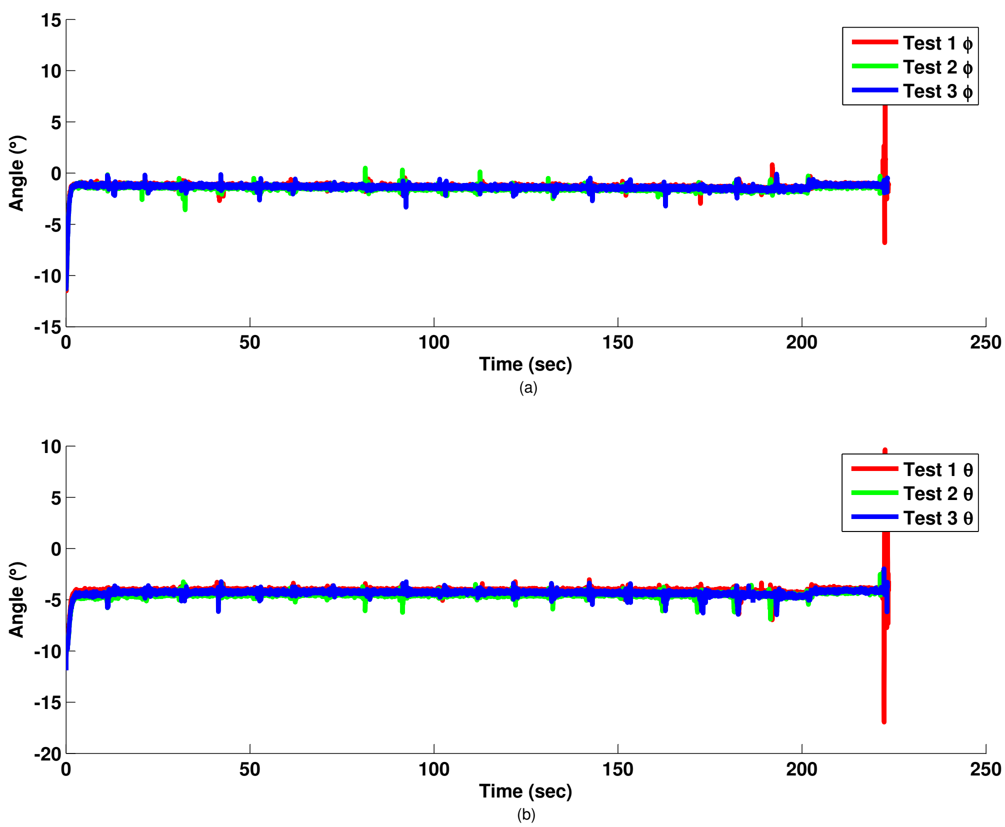

Figure 5.9: Effect of proximity of ferrous object on (a) pitch (ϕ) measurement and (b) roll (θ) measurement

5.3.7 Dynamic Pitch, Roll, and Yaw Accuracy Test Results

A summary of the results of dynamic accuracy test 1 are shown in Table 5.3. These accuracies follow a similar pattern to the results of the static test. Figure 5.10 shows a comparison between the angles captured by the sensor unit and the gait laboratory.

Trial	ϕ	θ	ψ
1	3.1°	4.9°	4.2°
2	2.8°	3.1°	7.6°
3	4.4°	5.0°	4.3°
Average	3.4°	4.4°	5.4°
Std. Dev.	0.7°	0.9°	1.6°
# of Samples	12247	11479	11374

Table 5.3: Summary of results for dynamic accuracy test 1

From Figure 5.10, the computed angles from the sensor unit, especially during the 20 seconds of motion for pitch (10 - 30 seconds), roll (33 - 53 seconds), and yaw (60 - 80 seconds), were comparable to measurements from the gait laboratory. Even though the sampling rate of the sensor unit was 50 Hz and the motion capture camera system was 120 Hz, the sensor unit was able to respond to the orientation changes quickly and maintained that new orientation.

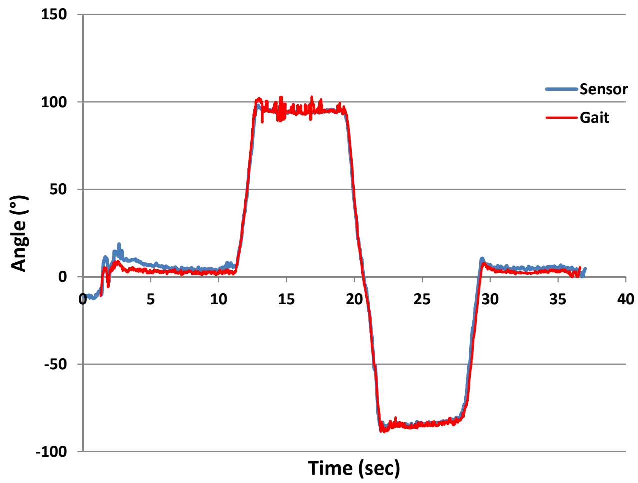

(a) ϕ from trial 1

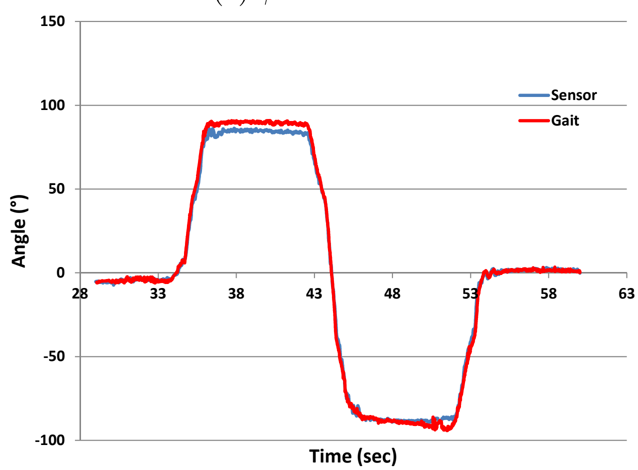

(b) θ from trial 2

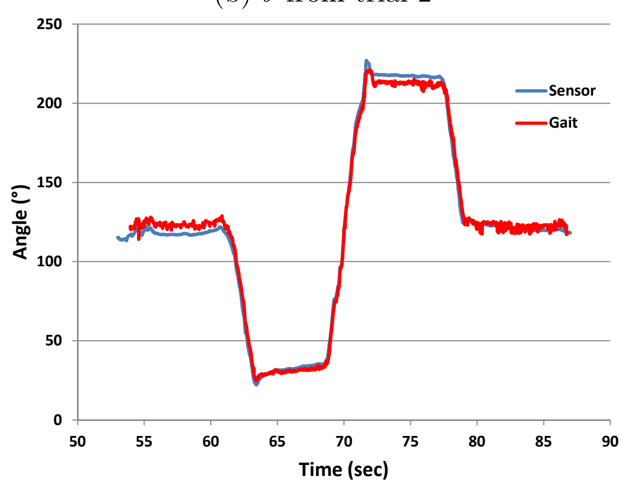

(c) ψ from trial 1

Figure 5.10: Comparison of measurements from sensor unit and gait laboratory during dynamic accuracy test 1

The overall results from the second dynamic accuracy test are presented in Table 5.4. No value is reported for the yaw accuracy of trial 1 as the Windows Interface stopped receiving orientation data from the sensor unit half-way through, hence that result is not included in the further analysis. The standard deviation for roll (θ) was almost double for dynamic test 2 compared to the first dynamic test.

Trial	ϕ	θ	ψ
1	4.0°	3.7°	
2	3.8°	3.5°	5.2°
3	3.9°	2.8°	5.1°
4	3.4°	6.7°	4.7°
Average	3.8°	4.2°	5.0°
Std. Dev.	0.2°	1.5°	0.2°
# of Samples	11960	9285	7720

Table 5.4: Summary of results for dynamic accuracy test 2

From the results of dynamic accuracy test 2 shown in Figure 5.11, the sensor unit was able to accurately maintain its correct orientation when it was continuously moving. Of special note on Figure 5.11b are the two points (inside the dashed circles) where the measurement data from the gait laboratory was restricted to a range between ±90°, the same range that was present in the sensor units for computing roll. Pitch and yaw measurements from the gait laboratory were restricted to a range of ±180°, which were same range present in the sensor units. This was done in order to more accurately compare the data from the sensor unit and the gait laboratory. These accuracies from this test were close to and consistent with the results from dynamic test 1.

Both dynamic tests showed that the sensor units were able to maintain their accuracy when experiencing motion. These results demonstrate that the posture monitoring system should be able to capture the posture of patients during their training sessions as most of the time it is expected that they will be in a sitting position.

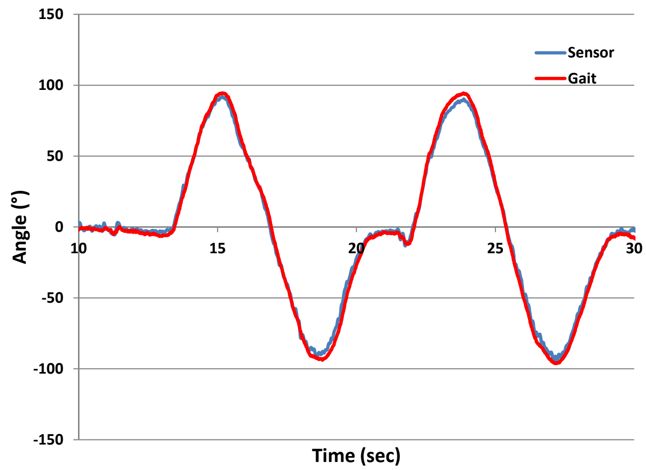

(a) ϕ from trial 2

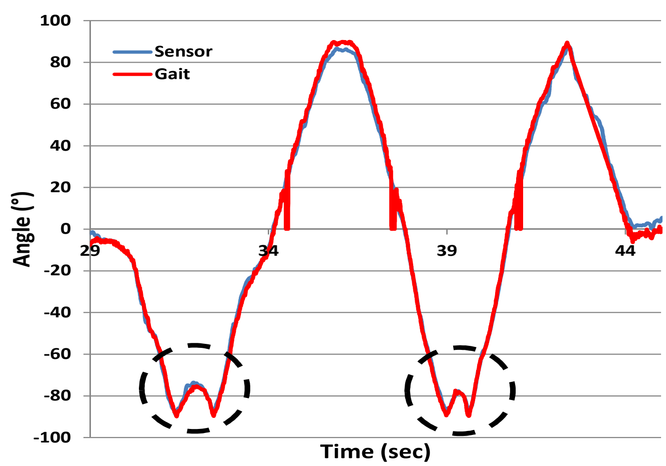

(b) θ from trial 2

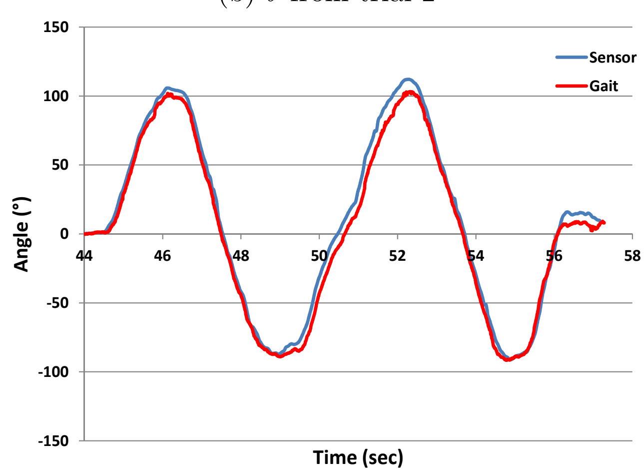

(c) ψ from trial 3

Figure 5.11: Comparison of measurements from sensor unit and gait laboratory during dynamic accuracy test 2

5.4 Posture Monitor Test Results

All volunteers in each of the posture monitor tests used the same thresholds for the posture measures. The threshold for the shoulder, coronal, and lordotic measures was set to 10°, the kyphotic measure threshold was set to 6°, and the rotation measure threshold was set to 15°. There was a minimum of two weeks between each posture monitoring test where volunteers did not wear the system to prevent earlier posture training sessions from influencing future tests.

5.4.1 Posture Monitor Test 1 Results

Figure 5.12 shows the posture error frequency of volunteer 1 for posture monitor test 1. The shaded cells on the table for day 3 and 4 indicate days which feedback was provided to the volunteer. On day 1, the frequency of kyphotic errors was quite high while the remaining three measures were low. On the second day however, the number of kyphotic errors dropped significantly, though no feedback was provided. This could have been the result of the volunteer making a subconscious effort to improve his posture. When feedback was provided on day 3 and 4, the posture measures were similar to those from day 2, which means that when the volunteer was aware of his posture, he spent more time in a correct posture. On day 5, the kyphotic measure errors saw an increase of approximately 24%, while the remaining measures were relatively unchanged when compared to day 4. However, the frequency of kyphotic errors on day 5 was 41% lower than on day 1, implying that memory effects might be present for the kyphotic measure.

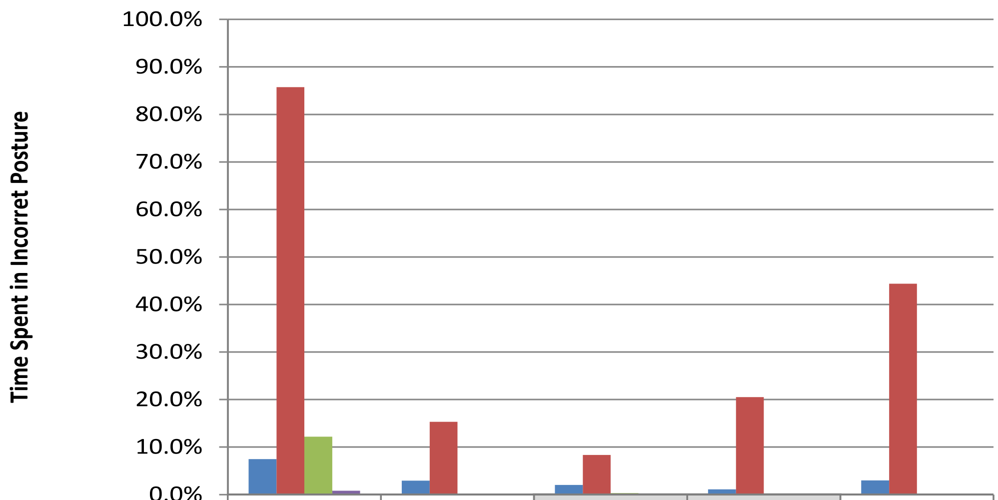

	Day 1	Day 2	Day 3	Day 4	Day 5
Shoulder Error	7.5%	2.9%	2.0%	1.1%	3.0%
Kyphotic Error	85.7%	15.3%	8.4%	20.5%	44.4%
Rotation Error	12.2%	0.1%	0.3%	0.1%	0.1%
Coronal Error	0.8%	0.0%	0.2%	0.0%	0.1%

Figure 5.12: Posture error frequency results of posture monitor test 1 for volunteer 1

The results for volunteer 2 are shown in Figure 5.13. On day 3, the sensor units located on the upper back (S3) and middle back (S4) experienced a malfunction and no usable data was obtained from them by the master unit. The results of this error affected the calculation of the kyphotic, rotation, and coronal measures. To show this, 0% values were placed in the table for those affected measures. This malfunction also occurred on day 5 with S5 located on the volunteer's lower back, resulting in no usable information for the rotation and coronal measures. However, from the data that was successfully captured, some phenomenon were observed. The kyphotic and rotation error frequencies on day 1 and day 2 were relatively consistent and when compared to the measures on day 4 when feedback was provided, a large improvement can be observed. The coronal measure results did not vary greatly between day 1, 2, and 4. When the volunteer wore the posture monitoring system again on day 5, the frequency of kyphotic errors did increase compared to day 4, but not as high as day 1 and 2. However, the frequency of shoulder errors jumped to nearly 80% on day 5 which was larger than the results of either day 1 or 2. This was the result of the orientation of the two shoulder sensor units (S1 and S2) not swapping their X and Y axes as discussed in Section 4.3.2. The two sensor units on the shoulders were orientated so that the Y axis ran parallel with the coronal plane and the X axis ran parallel with the sagittal plane. The master unit used the pitch values from S1 and S2 to compute the shoulder measure of the volunteer, which worked correctly as long as the volunteer did not bend over too far (near 90° approximately) along the sagittal plane. The 90° bending resulted in gimbal lock and inaccurate values for both pitch and roll. Since volunteer 2 bent over quite a bit on day 5, the results caused the master unit to interpret his shoulder posture as being incorrect. This problem was corrected in posture monitor tests 2 and 3 by switching the X and Y axes of S1 and S2.

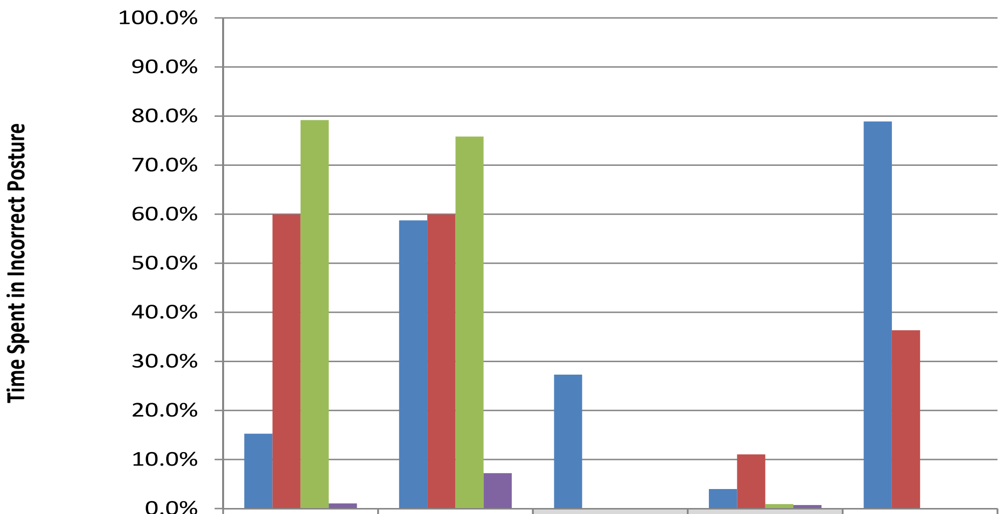

	Day 1	Day 2	Day 3	Day 4	Day 5
Shoulder Error	15.3%	58.7%	27.3%	4.0%	78.9%
Kyphotic Error	60.0%	60.0%	0.0%	11.0%	36.4%
Rotation Error	79.2%	75.8%	0.0%	0.9%	0.0%
Coronal Error	1.1%	7.2%	0.0%	0.7%	0.0%

Figure 5.13: Posture error frequency results of posture monitor test 1 for volunteer 2

From the first posture monitor test, it seems that the kyphotic error may be corrected if the volunteers either pay attention to the state of their posture, or if they are provided with regular reminders, in the form of feedback, when their posture is poor and in need of correction.

5.4.2 Posture Monitor Test 2 Results

Figure 5.14 shows the frequency of posture errors for volunteer 1 during the second posture monitor test. The shoulder, coronal, and rotation posture measures did not vary greatly between days with or without feedback. However, it can be seen that the frequency of incorrect kyphotic and lordotic posture measures were significantly reduced on day 2 and 3, when feedback was provided, compared to day 1. On day 4, the frequency kyphotic errors did increase though not to the same level as seen on day 1. Lordotic errors on day 4 increased approximately 11% from day 3. Overall, there was approximately a 20% and 81% reduction in kyphotic and lordotic errors respectively between day 1 and day 4.

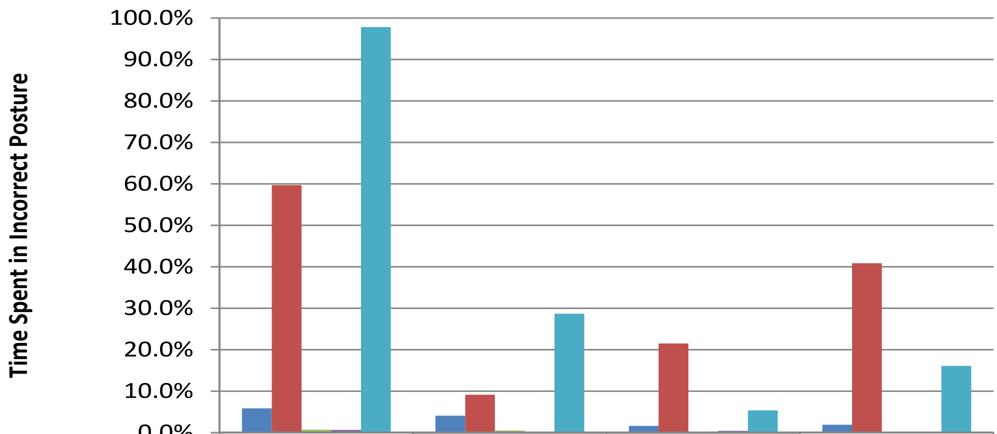

	Day 1	Day 2	Day 3	Day 4
Shoulder Error	5.9%	4.1%	1.6%	1.9%
Kyphotic Error	59.7%	9.1%	21.5%	40.9%
Rotation Error	0.7%	0.5%	0.0%	0.0%
Coronal Error	0.7%	0.2%	0.4%	0.1%
Lordotic Error	97.8%	28.7%	5.4%	16.1%

Figure 5.14: Posture error frequency results of posture monitor test 2 for volunteer 1

The average posture measures for volunteer 1 per day are shown in Table 5.5. The threshold column shows the thresholds that were used by the system to determine incorrect posture. It can be seen for volunteer 1 that both the kyphotic and lordotic measures were above their respective thresholds on day 1 and therefore the volunteer spent the majority of the session in incorrect posture for these two measures. The difference between the average lordotic measure and its threshold was much higher than for the average kyphotic measure and this was reflected in a higher error frequency for the lordotic measure on day 1. When feedback was applied, the average values for the posture measures dropped below their respective thresholds and fewer incorrect posture samples were recorded. These results agree with the results in Figure 5.14.

	Threshold	Day 1	Day 2	Day 3	Day 4
Shoulder	10.0°	4.0°	4.0°	3.8°	3.1°
Kyphotic	6.0°	6.6°	3.2°	4.4°	5.2°
Rotation	15.0°	3.2°	3.6°	1.5°	0.9°
Coronal Top	10.0°	2.4°	0.8°	0.7°	0.7°
Coronal Bot.	10.0°	1.0°	1.3°	1.8°	0.8°
Lordotic	10.0°	25.1°	8.8°	5.8°	6.0°

Table 5.5: Average posture measures for volunteer 1 for posture monitor test 2

The results for volunteer 2 during the second posture monitor test are shown in Figure 5.15. Volunteer 2 had a high frequency of kyphotic, rotation, and lordotic errors during his first day with the posture monitor and all these measures had a reduction in error frequency when feedback was applied on day 2 and 3. On the final day, the kyphotic, rotation, and lordotic measures still had a lower frequency of errors than day 1. The frequency kyphotic, rotation, and lordotic errors improved by approximately 23%, 55%, and 40% respectively between day 1 and day 4. The frequency of shoulder errors showed a slight improvement on day 4 when compared to day 1 as well.

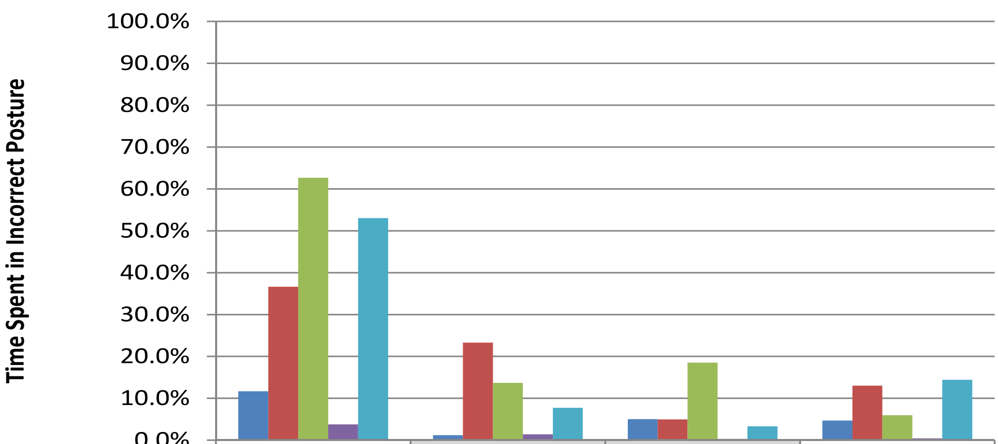

	Day 1	Day 2	Day 3	Day 4
Shoulder Error	11.7%	1.2%	5.0%	4.7%
Kyphotic Error	36.6%	23.3%	5.0%	13.0%
Rotation Error	62.7%	13.7%	18.5%	6.0%
Coronal Error	3.8%	1.4%	0.3%	0.4%
Lordotic Error	53.0%	7.7%	3.3%	14.4%

Figure 5.15: Posture error frequency results of posture monitor test 2 for volunteer 2

The results for volunteer 2 in Table 5.6 show that on the first day, the kyphotic, rotation, and lordotic measures were near or above the set thresholds and so more incorrect postures were detected. With feedback on day 2 and 3, the average posture measures dropped below the thresholds, meaning fewer incorrect posture samples which is consistent with the results from Figure 5.15.

	Threshold	**Day 1**	**Day 2**	**Day 3**	**Day 4**
Shoulder	10.0°	4.8°	2.8°	4.9°	3.8°
Kyphotic	6.0°	5.7°	4.1°	2.5°	3.1°
Rotation	15.0°	19.5°	5.8°	9.0°	4.8°
Coronal Top	10.0°	1.8°	2.0°	2.3°	1.9°
Coronal Bot.	10.0°	3.2°	1.5°	1.5°	1.9°
Lordotic	10.0°	11.8°	4.6°	3.9°	5.9°

Table 5.6: Average posture measures for volunteer 2 for posture monitor test 2

This posture monitor test showed that both volunteers were able to reduce the number of poor posture samples detected by the master unit with two days of posture training with feedback. Their kyphotic and lordotic average posture measures and error frequencies were improved between the first and last days of the test. The shoulder and coronal measures for both volunteers experienced limited to no significant changes. The sagittal posture problems (i.e: kyphotic and lordotic measures) appear to be easier to improve compared to the other measures.

The master unit only calculated a posture measure if the orientation information from all the sensor units involved in that posture measure were successfully received. Table 5.7 shows the success rate for the posture monitoring system in being able to calculate each posture measure. The most reliable posture measure was the shoulder measure with a 97.4%±1.2% success rate because the two sensor units on the volunteers' shoulders (S1 and S2) had the clearest line of sight to the master units. The remaining three sensor units were located on the back of the volunteers and the body absorption of the high frequencies used by the wireless protocol of the system might have had some effect at the lower reception rates for the remaining posture measures. The coronal measure had the worst reception rate at 89.1%±5.3% because it required that the master unit successfully receive the orientation data from all three sensor units on the back (S3, S4, and S5).

	Shoulder	Kyphotic	Rotation	Coronal	Lordotic
Average	97.4%	91.5%	93.8%	89.1%	92.5%
Std. Dev.	1.2%	4.2%	2.6%	5.3%	4.2%

Table 5.7: Average packet reception during posture monitor test 2

To determine the communication loss, the overall data set and time stamps from the master unit were used. The average packet loss for volunteers 1 and 2 over the four day test were 2.2%±1.4% and 3.3%±1.1% respectively. This showed that the communication between the master and sensor units was reliable when worn.

5.4.3 Posture Monitor Test 3 Results

The results of the third posture monitor test for volunteer 1 are shown in Figure 5.16. The vertical line between day 4 and 5 indicates that there are three days separating those two sessions. Volunteer 1 had a significant improvement in reducing the number of posture errors throughout the five days with the system. He had a very high number of shoulder and lordotic errors without feedback on his first day, but when feedback was applied on days 2 and 3, both measures had a significant reduction in error frequency. On day 4 the shoulder measure saw nearly a 70% reduction in error frequency compared to day 1. The lordotic measure saw a decrease of approximately 82% from day 1 to day 4. With no feedback provided to the volunteer on day 4, the posture measures remained relatively close to the measures on day 2 and 3, except for the shoulder measure which increased approximately 11% from day 3. From day 4 to 5, the shoulder measure error frequency dropped 10% back to the frequency observed on day 3. The kyphotic and lordotic measures increased 21% and 24% respectively from day 4 to 5. However, the shoulder and lordotic measures still had an error frequency reduction of 80% and 60% respectively from day 1 to day 5.

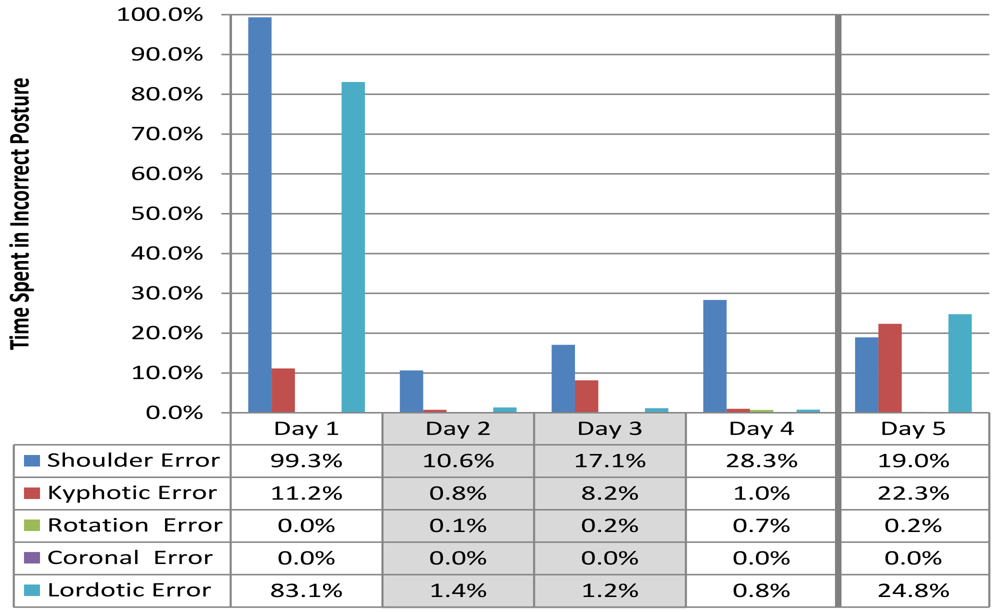

Figure 5.16: Posture error frequency results of posture monitor test 3 for volunteer 1

The average posture measures for volunteer 1 are also shown in Table 5.8. The volunteer's average shoulder and lordotic posture measures dropped by approximately 27° and 10° respectively when feedback was provided on day 2. These drops were consistent with the frequency error reduction of posture errors from Figure 5.16. The shoulder and kyphotic measures remained fairly consistent throughout day 3, 4, and even on day 5 after not wearing the system for three days. The coronal and rotation measures remained relatively unchanged during the five days of the test.

	Threshold	**Day 1**	**Day 2**	**Day 3**	**Day 4**	**Day 5**
Shoulder	10.0°	32.0°	5.3°	6.0°	7.6°	6.5°
Kyphotic	6.0°	3.0°	2.0°	3.8°	1.8°	3.8°
Rotation	15.0°	3.5°	4.8°	2.4°	5.7°	2.4°
Coronal Top	10.0°	2.6°	0.8°	1.9°	1.1°	1.7°
Coronal Bot.	10.0°	1.4°	2.5°	0.7°	1.3°	1.7°
Lordotic	10.0°	15.8°	5.1°	4.9°	3.0°	7.5°

Table 5.8: Average posture measures for volunteer 1 for posture monitor test 3

The results for volunteer 2 are shown in Figure 5.17. The time reported in a poor posture on the first day without any feedback was quite high for the shoulder, kyphotic, and lordotic measures, but once feedback was provided on day 2 and 3, the frequency of incorrect posture dropped dramatically. There was a 62%, 45%, and 58% reduction in errors for the shoulder, kyphotic, and lordotic measures respectively on day 2 compared to day 1. Between the three days separating the posture sessions on day 4 and day 5, there was a noticeable increase in the total number of poor posture errors that the system detected. While the shoulder error frequency rose approximately 24% between day 4 and 5, the seven days between day 1 and day 5 saw a 50% reduction in shoulder errors. The kyphotic errors were also reduced by 30% from day 1 to day 5 and the lordotic errors fell 47% during that same time period.

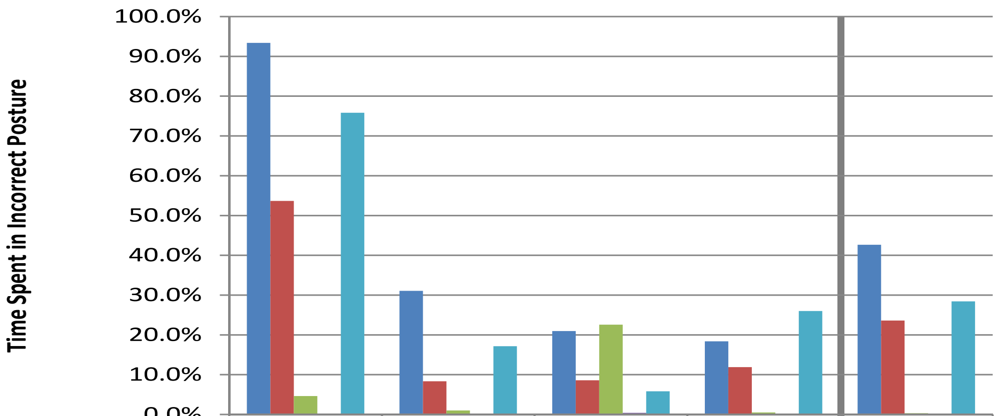

	Day 1	Day 2	Day 3	Day 4	Day 5
Shoulder Error	93.4%	31.1%	21.0%	18.4%	42.6%
Kyphotic Error	53.7%	8.3%	8.6%	11.9%	23.6%
Rotation Error	4.6%	1.0%	22.6%	0.5%	0.3%
Coronal Error	0.2%	0.1%	0.4%	0.1%	0.1%
Lordotic Error	75.8%	17.2%	5.8%	26.0%	28.4%

Figure 5.17: Posture error frequency results of posture monitor test 3 for volunteer 2

Table 5.9 also provides a summary of the average posture measures for volunteer 2. Volunteer 2 had a large average kyphotic measure on day 1, which was reflected in the large frequency of incorrect kyphotic posture samples. The average shoulder measure was reduced by approximately 14° from day 1 to day 2. The average lordotic measure also was reduced from day 1 to 2 by approximately 7° when feedback was applied. There was a slight rise of 7° in the average rotation angle between day 2 and day 3 and this was also shown by more rotation measure errors reported by the system. On day 5, the average posture measures were similar to those observed on day 4 except that the average shoulder measure increased approximately 4°.

The results from the third posture monitor test were comparable with and

	Threshold	Day 1	Day 2	Day 3	Day 4	Day 5
Shoulder	10.0°	22.3°	8.3°	6.8°	5.9°	9.5°
Kyphotic	6.0°	6.8°	2.7°	3.1°	3.1°	4.1°
Rotation	15.0°	6.9°	4.6°	12.0°	3.6°	4.6°
Coronal Top	10.0°	2.3°	1.3°	1.5°	2.7°	1.5°
Coronal Bot.	10.0°	2.3°	1.4°	1.5°	1.0°	1.7°
Lordotic	10.0°	15.4°	6.2°	4.4°	7.9°	7.3°

Table 5.9: Average posture measures for volunteer 2 for posture monitor test 3

built upon the results observed in posture monitor test 2. There was a significant drop in incorrect shoulder and lordotic posture errors for both volunteers between day 1 and day 2 when feedback was applied, and these measures remained lower than the first day for the remaining testing days. The feedback provided to the volunteers was shown to aid them in recognizing and correcting their posture. The average shoulder measure for both volunteers corresponds closely with the posture error frequency results. Average measures that were closer to the threshold had a higher number of incorrect posture samples. This highlights the importance of acquiring a proper baseline of good posture for the training sessions because the posture monitoring system was quite proficient at helping to maintain the volunteers' posture within the thresholds of the acquired baseline.

To determine the communication loss again in posture monitor test 3, the average packet reception rate was calculated from all of the data obtained. Table 5.10 shows the successful rate of communication for the system. While the overall success rate for each of the posture measures was lower than those from the second posture monitor test, the results still show that the shoulder measure had the best success rate while the coronal measure was the worst.

	Shoulder	Kyphotic	Rotation	Coronal	Lordotic
Average	94.0%	88.7%	86.7%	84.1%	91.7%
Std. Dev.	5.2%	9.2%	9.3%	11.3%	6.5%

Table 5.10: Average packet reception during posture monitor test 3

The average packet loss between the master unit and the sensors units over the five days test was 1.2%±0.5% and 6.3%±3.9% for volunteers 1 and 2 respectively. Possible reasons for the higher packet loss for volunteer 2 could be that the volunteer may have rotated his chair when working without also moving the master unit along. The rotation of the chair may have placed the back of the chair between the master unit and sensors units, which disrupted the packet transmission between the units.

5.4.4 Baseline Repeatability Test Results

Baseline values for each posture measure were calculated each time the volunteer donned the posture monitoring system. The average baseline measures and the standard deviations for each volunteer over the three trials are shown in Table 5.11, Table 5.12, and Table 5.13 respectively.

Measure	Average	Std. Dev.	Max.	Min.
Shoulder	34.0°	2.6°	36.5°	30.4°
Kyphotic	38.9°	2.0°	40.6°	36.2°
Rotation	9.9°	5.7°	17.7°	4.3°
Coronal Top	3.0°	1.1°	3.8°	1.5°
Coronal Bot.	0.8°	0.6°	1.5°	0.1°
Lordotic	9.3°	3.1°	12.9°	5.3°

Table 5.11: Baseline repeatability posture measures for volunteer 1

Measure	Average	Std. Dev.	Max.	Min.
Shoulder	35.5°	7.4°	45.1°	27.0°
Kyphotic	38.4°	2.42°	40.4°	35.0°
Rotation	17.1°	4.3°	23.1°	12.8°
Coronal Top	10.2°	3.3°	14.2°	6.2°
Coronal Bot.	4.2°	0.8°	2.1°	3.2°
Lordotic	2.4°	0.8°	3.5°	1.8°

Table 5.12: Baseline repeatability posture measures for volunteer 2

Measure	Average	Std. Dev.	Max.	Min.
Shoulder	30.0°	0.5°	30.5°	29.4°
Kyphotic	36.3°	1.3°	37.9°	34.6°
Rotation	12.1°	3.5°	16.8°	8.5°
Coronal Top	3.5°	1.3°	4.9°	1.7°
Coronal Bot.	2.0°	1.2°	3.6°	0.9°
Lordotic	2.3°	0.9°	3.0°	1.0°

Table 5.13: Baseline repeatability posture measures for volunteer 3

From the results, it is clear that there are deviations in the acquired baselines between training sessions due to donning of the garment. These variations may effect the feedback frequency of the posture monitoring system, which can influence the determination of the effectiveness of the posture training treatment of AIS. For example, the average rotation measure deviation between all three volunteers was $\pm 4.5°$. For all three volunteers, the difference between the maximum and minimum rotation baseline values was approximately $10°$. Volunteer 2 experienced a $18°$ difference in the shoulder baseline measures between the maximum and minimum baselines acquired. Both volunteer 1 and 3 had significantly smaller difference for the shoulder baselines compared to the results for volunteer 2. These large differences may be the result of the placement of the sensor units in the garment or the way that the garment was worn. This implied that obtaining a consistent baseline between sessions was also affected by the volunteer himself. Care must therefore be taken in the placement of the sensor units on volunteers to ensure their consistent placement in order to have comparable baselines between sessions. From these results, there are many factors that affect the repeatability of baseline measurements and they have to be addressed on an individual basis.

Chapter 6

Conclusions and Future Recommendations

6.1 Conclusions

The objective of this thesis was to develop a 3D posture monitoring system to investigate if posture training can be used to improve human posture. This research was motivated by the lack of available treatments for AIS patients with mild curves, which is defined as a Cobb angle under 25°, and the lack of clinical evidence for or against using exercise treatments. AIS patients with mild curves can only wait for their curve to deteriorate to a certain severity before active treatments, such as a brace, are provided. Some studies have shown that exercise-based treatment may be an effective way of treating mild AIS. Also, exercise-based treatment may be combined with brace treatment to improve the brace treatment outcome. However, literature suggests that exercise-based treatment does not have enough supporting evidence for its effectiveness. Patient compliance is difficult to measure if the exercises are not performed under supervision. Without correct compliance data, the treatment effectiveness can not be accurately determined. An electronic system that can monitor and respond to changes in a patient's posture while monitoring his/her compliance would be useful for patients and researchers alike.

The developed wireless distributed computing network consisted of five orientation sensor units in a tight-fitting garment and a master processing unit. The sensor units, located on the shoulders and along the spinal column, calculated their three-dimensional orientation at their respective locations while the master unit computed the subject's posture using orientation data obtained from the sensor units. The master unit also provided feedback if the calculated posture was poor and recorded session information for later analysis. The literature describes previously developed posture monitoring systems that can monitor posture along the sagittal and/or coronal planes, but the system developed for this thesis is the first portable posture monitor that can monitor along all three planes, providing a more complete representation of human posture.

The master unit and sensor units were tested individually and together. The static accuracy of the sensor units were $1.4°\pm0.03°$, $3.0°\pm0.39°$, and $5.5°\pm0.78°$ for pitch, roll, and yaw respectively. Dynamic accuracies for pitch, roll, and yaw were found to be $3.8°\pm0.2°$, $4.2°\pm1.5°$, and $5.0°\pm0.2°$ respectively. These accuracies were sufficient to monitor human posture as 5° of accuracy is usually used as an acceptable accuracy in clinical settings. Testing showed that there was minimal drift to the output orientation calculated by the sensor units, though yaw was dramatically affected by a close proximity to metal. With a fully charged battery, the master unit was found to be able to operate for approximately six hours and the sensor units were able to operate for more than two hours, providing sufficient time for a single training session before requiring the units to be recharged.

The healthy adult volunteers that took part in the posture monitoring tests did not have any significant posture problems along the coronal or transverse planes. This resulted in minimal to no correction being required along those planes and hence no definite conclusions could be made regarding posture correction of the coronal or rotation measures using feedback. However, these volunteers did experience periods of very poor posture along the sagittal plane and with their shoulders. When feedback was provided, the shoulder, kyphotic, and lordotic measures saw very large reductions in error frequency. There were also some memory effects for the volunteers, which suggests that good posture can be taught. The maximum average packet loss for all volunteers was $6.3\%\pm3.9\%$, which demonstrated the reliability of the posture monitor's wireless network.

Further research is needed to determine the long-term effects of the posture monitoring system, specifically with participants who are diagnosed with AIS. These participants will evaluate:

a) How comfortable is the system?

b) Which feedback methods (visual and/or audio) are better?

c) How user friendly is the master unit's user interface?

d) The effectiveness of the system in correcting poor posture.

Feedback from this study will allow for further improvements to the posture monitor and prepare the system for future long-term clinical trials.

6.2 Future Recommendations

Recommendations for future improvements to the posture monitor include miniaturization of the system, improving the orientation accuracy measurements, increasing battery life, and providing instantaneous feedback.

Future research should consider updating the sensor units with the latest MEMS sensors. With many new advances in MEMS technology, specifically in the areas of fabrication, it will soon be possible to utilize a single integrated circuit that combines a 3-axis accelerometer, a 3-axis gyroscope, and a 3-axis magnetometer. Using the new integrated circuit will be able to save size by reducing the number of components that the sensor units require. These MEMS sensors may also offer more accuracy and lower power consumption than the sensors that are currently available.

Any wireless sensor system can greatly benefit from advances in battery technology. The current sensor units are only able to operate for a period of less than three hours on a single charge. If smaller, more energy-dense batteries become available, future researchers may want to utilize them to lengthen the time that posture monitoring sessions may be worn for or to reduce the frequency that the sensor units need to be recharged.

Posture training is only one exercise that may be used in an exercise-based treatment. Future work could include developing the posture monitoring system to be able to identify movements that the patient is currently performing. This would allow for instantaneous feedback to the patient if he/she is performing more complex exercises such as those used in the Schroth Method. Instantaneous feedback would allow the patient to perform more exercises without the need for supervision for form correction.

Bibliography

[1] M. A. Asher and D. C. Burton, "Adolescent idiopathic scoliosis: natural history and long term treatment effects," *Scoliosis*, vol. 1, no. 2, 2006.

[2] M.-L. B. Lenssinck *et al.*, "Effect of bracing and other conservative interventions in the treatment of idiopathic scoliosis in adolescents: A systematic review of clinical trials," *Physical Therapy*, vol. 85, no. 12, pp. 1329–1339, 2005.

[3] L. A. Rinsky and J. G. Gamble, "Adolescent idiopathic scoliosis," *Western Journal of Medicine*, vol. 148, no. 2, pp. 182–191, 1988.

[4] J. Lonstein, "Adolescent idiopathic scoliosis," *The Lancet*, vol. 344, pp. 1407–1412, November 1994.

[5] L. Dunne *et al.*, "A system for wearable monitoring of seated posture in computer users," in *Proceedings of the 4th International Workshop on Wearable and Implantable Body Sensor Networks*, vol. 132, 2007, pp. 203–207.

[6] E. Sardini, M. Serpelloni, and M. Ometto, "Smart vest for posture monitoring in rehabilitation exercises," in *2012 IEEE Sensors Application Symposium*, February 2012, pp. 1–5.

[7] M. Bazzarelli *et al.*, "A wearable computer for physiotherapeutic scoliosis treatment," *IEEE Transactions on Instrumentation and Measurement*, vol. 52, no. 1, pp. 126 – 129, February 2003.

[8] M. Bazzarelli *et al.*, "A low power hybrid posture monitoring system," in *Proceedings of the Canadian Conference on Electrical and Computer Engineering*, vol. 2, 2001, pp. 1373–1377.

[9] M. Bazzarelli *et al.*, "A low power portable electromagnetic posture monitoring system," in *Proceedings of the 18th IEEE Instrumentation and Measurement Technology Conference*, May 2001, pp. 619–623.

[10] E. Lou *et al.*, "Smart garment to help children improve posture," in *Proceedings of the 28th IEEE Engineering in Medicine and Biology Society Annual International Conference*, August - September 2006, pp. 5374–5377.

[11] E. Lou *et al.*, "Development of a smart garment to reduce kyphosis during daily living," *Medical & Biological Engineering & Computing*, vol. 50, pp. 1147–1154, 2012.

[12] W. Y. Wong, "Development of a posture monitoring system," Ph.D. dissertation, The Hong Kong Polytechnic University, November 2007.

[13] W. Y. Wong and M. S. Wong, "Smart garment for trunk posture monitoring: A preliminary study," *Scoliosis*, vol. 3, no. 7, May 2008.

[14] W. Y. Wong and M. S. Wong, "Measurement of postural change in trunk movements using three sensor modules," *IEEE Transactions on Instruments and Measurement*, vol. 58, no. 8, pp. 2737 – 2742, August 2009.

[15] F. H. Martini, M. J. Timmons, and R. B. Tallitsch, *Human Anatomy, 4th Edition*. Pearson Education Inc.

[16] U. Gille. Lateral view of the vertebral column. [Date Accessed Feb. 27, 2013]. [Online]. Available: http://commons.wikimedia.org/wiki/File:Gray_111_-_Vertebral_column-coloured.png

[17] "Three-dimensional terminology of spinal deformity," Scoliosis Research Society, [Accessed Apr. 22, 2013]. [Online]. Available: www.srs.org/professionals/glossary/SRS_3D_terminology.htm

[18] Y. Mrabet. Planes of human anatomy. [Date Accessed Mar. 17, 2013]. [Online]. Available: http://commons.wikimedia.org/wiki/File:Human_anatomy_planes.svg

[19] S. L. Weinstein *et al.*, "Adolescent idiopathic scoliosis," *The Lancet*, vol. 371, pp. 1527–1537, May 2008.

[20] S. Weinstein *et al.*, "Health and function of patients with untreated idiopathic scoliosis: a 50-year natural history study," *Journal of the American Medical Association*, vol. 289, no. 5, pp. 559–567, 2003.

[21] M. Bialek, "Conservative treatment of idiopathic scoliosis according to FITS concept: presentation of the method and preliminary, short term radiological and clinical results based on SOSORT and SRS criteria," *Scoliosis*, vol. 6, no. 25, 2011.

[22] E. Kenanidis *et al.*, "Adolescent idiopathic scoliosis and exercising - is there truly a liaison?" *SPINE*, vol. 33, no. 20, pp. 2160–2165, 2008.

[23] S. Upadhyay *et al.*, "New prognostic factors to predict the final outcome of brace treatment in adolescent idiopathic scoliosis," *SPINE*, vol. 20, no. 5, pp. 537–545, 1995.

[24] I. Busscher, F. H. Wapstra, and A. G. Veldhuizen, "Predicting growth and curve progression in the individual patient with adolescent idiopathic scoliosis: design of a prospective longitudinal cohort study," *BMC Musculoskeletal Disorders*, vol. 11, no. 93, May 2010.

[25] S. C. Mordecai and H. V. Dabke, "Efficacy of exercise therapy for the treatment of adolescent idiopathic scoliosis: a review of the literature," *European Spine Journal*, vol. 21, pp. 382–389, 2012.

[26] T. G. Lowe *et al.*, "Etiology of idiopathic scoliosis: Current trends in research," *The Journal of Bone and Joint Surgery*, vol. 82-A, no. 8, pp. 1157–1168, 2000.

[27] H.-R. Weiss *et al.*, "Physical exercises in the treatment of idiopathic scoliosis at risk of brace treatment - SOSORT consensus paper 2005," *Scoliosis*, vol. 1, no. 6, May 2006.

[28] D. Reichel and J. Schanz, “Developmental psychological aspects of scoliosis treatment,” *Pediatric Rehabilitation*, vol. 6, no. 3-4, pp. 221–225, 2003.

[29] J. R. Cobb, “Outline for the study of scoliosis,” *AAOS Course Lectures*, vol. 5, pp. 261–275, 1948.

[30] J. L. Jaremko *et al.*, “Comparison of cobb angles measured manually, calculated from 3-d spinal reconstruction, and estimated from torso asymmetry,” *Computer Methods in Biomechanics and Biomedical Engineering*, vol. 5, no. 4, pp. 277–281, 2002.

[31] M. S. Goldberg *et al.*, “Observer variation in assessing spinal curvature and skeletal development in adolescent idiopathic scoliosis,” *SPINE*, vol. 13, no. 12, pp. 1371–1377, 1988.

[32] Skoliose-Info-Forum.de. Cobb angle measurement in scoliosis. [Date Accessed Mar. 17, 2013]. [Online]. Available: http://commons.wikimedia.org/wiki/File:Scoliosis_cobb.gif

[33] M. H. Pope, A. F. Stokes, and M. Moreland, “The biomechanics of scoliosis,” *CRC Critical Reviews in Biomedical Engineering*, vol. 11, no. 3, pp. 157–188, 1984.

[34] F. Canavese and A. Kaelin, “Adolescent idiopathic scoliosis: Indications and efficacy of nonoperative treatment,” *Indian Journal of Orthopaedics*, vol. 45, no. 1, pp. 7–14, Jan. 2011.

[35] T. Maruyama *et al.*, “Conservative treatment for adolescent idiopathic scoliosis: can it reduce the incidence of surgical treatment?” *Pediatric Rehabilitation*, vol. 6, no. 3-4, pp. 215–219, 2003.

[36] Scoliosis Research Society. [Accessed Apr. 22, 2013]. [Online]. Available: ”http://www.srs.org/professionals/education_materials/SRS_bracing_manual/”

[37] B. Richards *et al.*, “Standardization of criteria for adolescent idiopathic scoliosis brace studies: Srs committe on bracing and nonoperative management,” *SPINE*, vol. 30, no. 18, pp. 2068–2075, 2005.

[38] E. M. Bunge *et al.*, “Patient’s preferences for scoliosis brace treatment,” *SPINE*, vol. 35, no. 1, pp. 57–63, 2010.

[39] S. Negrini *et al.*, “Specific excercises reduce brace prescription in adolescent idiopathic scoliosis: A prospective controlled cohort study with worst-case analysis,” *Journal of Rehabilitation Medicine*, vol. 40, no. 6, pp. 451–455, June 2008.

[40] H.-R. Weiss and R. Klein, “Improving excellence in scoliosis rehabilitation: A controlled study of matched pairs,” *Pediatric Rehabilitation*, vol. 9, no. 3, pp. 190–200, 2006.

[41] V. Mooney, J. Gulick, and R. Pozos, “A preliminary report on the effect of measured strength training in adolescent idiopathic scoliosis,” *Journal of Spinal Disorders*, vol. 13, no. 2, pp. 102–107, 2000.

[42] C. Lehnert-Schroth, “Introduction to the three-dimensional scoliosis treatment according to schroth,” *Physiotherapy*, vol. 78, no. 11, pp. 810–815, June 1992.

[43] M. Jelaĉić *et al.*, "Barcelona scoliosis physical therapy school - BSPTS - based on classical schroth principles: short term effects on back asymmetry in idiopathic scoliosis," in *Scoliosis*, vol. 7, no. Suppl 1, 2012, Oral Presentation, p. O57.

[44] S. Negrini *et al.*, "Effectiveness of complete conservative treatment for adolescent idiopathic scoliosis (bracing and exercises) based on SOSORT management criteria: results according to SRS criteria for bracing studies - SOSORT award 2009 winner," *Scoliosis*, vol. 4, no. 19, 2009.

[45] S. Negrini, "Approach to scoliosis changed due to cause other than evidence: Patients call for conservative (rehabilitation) experts to join in team orthopedic surgeons," *Disability and Rehabilitation*, vol. 30, no. 10, pp. 731–741, 2008.

[46] M. Hawes, "Impact of spine surgery on signs and symptoms of spinal deformity," *Pediatric Rehabilitation*, vol. 9, no. 4, pp. 318–339, 2006.

[47] S. Negrini *et al.*, "Exercises reduce the progressive rate of adolescent idiopathic scoliosis: Results of a comprehensive systematic review of the literature," *Disability and Rehabilitation*, vol. 30, no. 10, pp. 772–785, 2008.

[48] R. L. Barrack *et al.*, "Proprioception in idiopathic scoliosis," *SPINE*, vol. 9, no. 7, pp. 681–685, 1984.

[49] Z. Ding *et al.*, "Inertial sensor-based guidance system for upperlimb posture correction," *Medical Engineering & Physics*, vol. 35, no. 2, pp. 269–276, 2013.

[50] N. Farra *et al.*, "A mobile sensing and imaging system for real-time monitoring of spine health," *Journal of Medical Imaging and Health Informatics*, vol. 1, pp. 238–245, March 2011.

[51] G. Devedžić *et al.*, "Identification of anatomical landmarks for intelligent postural sensing," in *2012 Mediterranean Conference on Embedded Computing*, 2012, pp. 70–73.

[52] J. Baek and B.-J. Yun, "Posture monitoring system for context awareness in mobile computing," *IEEE Transactions on Instruments and Measurement*, vol. 59, no. 6, pp. 1589–1599, June 2010.

[53] H. J. Luinge and P. H. Veltink, "Inclination measurement of human movement using a 3-d accelerometer with autocalibration," *IEEE Transactions on Neural Systems and Rehabilitation Engineering*, vol. 12, no. 1, pp. 112–121, March 2004.

[54] D. Curone *et al.*, "A real-time and self-calibrating algorithm based on triaxial accelerometer signals for the detection of human posture and activity," *IEEE Transactions on Information Technology in Biomedicine*, vol. 14, no. 4, pp. 1098–1105, July 2010.

[55] W. Xu *et al.*, "eCushion: An eTextile device for sitting posture monitoring," in *2011 International Conference on Body Sensor Networks*, May 2011, pp. 194–199.

[56] H. Silva *et al.*, "Wireless hydrotherapy smart-suit network for posture monitoring," in *IEEE Internatioanl Symposium on Industrial Electronics*, June 2007, pp. 2713–2717.

[57] W. Y. Wong and M. S. Wong, "Detecting spinal posture change in sitting positions with tri-axial accelerometers," *Gait & Posture*, vol. 27, pp. 168–171, 2008.

[58] T. N. Theologis *et al.*, "Quantifying the cosmetic defect of adolescent idiopathic scoliosis," *SPINE*, vol. 18, no. 7, pp. 909–912, 1993.

[59] L. G. Lenke *et al.*, "Adolescent idiopathic scoliosis - a new classification to determine extent of spinal arthrodesis," *Journal of Bone and Joint Surgery*, vol. 83-A, no. 8, pp. 1169 – 1181, 2001.

[60] A. Krawczyński *et al.*, "Clinical and radiological assessment of vertebral rotation in idiopathic scoliosis," *Ortopedia Traumatologia Rehabilitacja*, vol. 8, no. 6, pp. 602–607, 2006.

[61] M. Kumar, "MEMS: Theory and usage in industrial and consumer applications," in *National Conference on Computational Instrumentation*, March 2010.

[62] H. Harms *et al.*, "ETHOS: Miniature orientation sensor for wearable human motion analysis," in *2010 IEEE Sensors*, November 2010, pp. 1037–1042.

[63] M. Barczyk, "Nonlinear state estimation and modeling of a helicopter UAV," Ph.D. dissertation, University of Alberta, November 2012.

[64] Q. Li *et al.*, "Accurate, fast fall detection using gyroscopes and accelerometer-derived posture information," in *Sixth International Workshop on Wearable and Implantable Body Sensor Networks*, June 2009, pp. 138–143.

[65] "Magnetic sensor products," Honeywell Inc., 12001 State Highway 55, Plymouth, MN 55441.

[66] C. C. Foster and G. H. Elkaim, "Extension of a two-step calibration methodology to include nonorthogonal sensor axes," *IEEE Transactions on Aerospace and Electronic Systems*, vol. 44, no. 3, pp. 1070–1078, 2008.

[67] W. de Vries *et al.*, "Magnetic distortion in motion labs, implications for validating inertial magnetic sensors," *Gait & Posture*, vol. 29, no. 4, pp. 535–541, 2009.

[68] J. M. G. Merayo *et al.*, "Scalar calibration of vector magnetometers," *Measurement Science and Technology*, vol. 11, pp. 120–132, 2000.

[69] V. Renaudin, M. H. Afzal, and G. Lachapelle, "Complete triaxis magnetometer calibration in the magnetic domain," *Journal of Sensors*, vol. 2010, 2010.

[70] X. Yun and E. R. Bachmann, "Design, implementation, and experimental results of a quaternion-based kalman filter for human body motion tracking," *IEEE Transactions on Robotics*, vol. 22, no. 6, pp. 1216–1227, 2006.

[71] S. O. H. Madgwick, A. J. L. Harrison, and R. Vaidyanathan, "Estimation of IMU and MARG orientation using a gradient descent algorithm," in *2011 IEEE International Conference on Rehabilitation Robotics*, June 2011, pp. 1–7.

[72] E. R. Bachmann, X. Yun, and R. B. McGhee, "Sourceless tracking of human posture using small inertial/magnetic sensors," in *Proceedings. 2003 IEEE International Symposium on Computational Intelligence in Robotics and Automation*, vol. 2, July 2003, pp. 822–829.

[73] T. Beravs *et al.*, "Development and validation of a wearable inertial measurement system for use with lower limb exoskeletons," in *11th IEEE-RAS International Conference on Humanoid Robots*, October 2011, pp. 212–217.

[74] E. R. Bachmann, "Inertial and magnetic tracking of limb segment orientation for inserting humans into synthetic environments," Ph.D. dissertation, Naval Postgraduate School, December 2000.

[75] V. van Acht *et al.*, "Miniature wireless inertial sensor for measuring human motions," in *Proceedings of the 29th IEEE Engineering in Medicine and Biology Society Annual International Conference*, 2007, pp. 6278–6281.

[76] N. Abbate *et al.*, "Development of a mems based wearable motion capture system," in *2nd Conference on Human System Interactions*, 2009, pp. 255–259.

[77] D. Roetenberg, C. T. M. Baten, and P. H. Veltink, "Estimating body segment orientation by applying inertial and magnetic sensing near ferromagnetic materials," *IEEE Transactions on Neural Systems and Rehabilitation Engineering*, vol. 15, no. 3, pp. 469–471, 2007.

[78] J. Diebel, "Representing attitude: Euler angles, unit quaternions, and rotation vectors," October 2006.

[79] J. Kuipers, *Quaternions and rotation sequences.* Princeton university press Princeton, NJ, USA:, 1999.

[80] S. O. Madgwick, "Quaternions," Online, [Date Accessed Aug. 20, 2012]. [Online]. Available: http://www.x-io.co.uk/quaternions

[81] S. O. Madgwick, "An efficient orientation filter for inertial and inertial-magnetic sensor arrays," Online, [Date Accessed Aug. 16, 2012]. [Online]. Available: http://www.x-io.co.uk/open-source-imu-and-ahrs-algorithms

[82] B. Huyghe, J. Doutreloigne, and J. Vanfleteren, "3D orientation tracking based on unscented kalman filtering of accelerometer and magnetometer data," in *IEEE Sensors Applications Symposium*, 2009, pp. 148–152.

[83] Z. Shi *et al.*, "Angular velocity estimation in gyroscope-free inertial measurement system based on unscented kalman filter," in *8th World Congress on Intelligent Control and Automation*, 2010, pp. 2031 – 2034.

[84] D. Roetenberg *et al.*, "Compensation of magnetic disturbances improves inertial and magnetic sensing of human body orientation," *IEEE Transactions on Neural Systems and Rehabilitation Engineering*, vol. 13, no. 3, pp. 395 – 405, 2005.

[85] G. Welch and G. Bishop, "An introduction to the kalman filter," 2001, SIGGRAPH 2001 Course 8.

[86] R. Mahony, T. Hamel, and J.-M. Pflimlin, "Nonlinear complementary filters on the special orthogonal group," *IEEE Transactions on Automatic Control*, vol. 53, no. 5, pp. 1203–1218, 2008.

[87] *Bluetooth Specifications Version 4.0*, Bluetooth SIG, Inc. Std., Rev. 4.0, June 2010.

[88] U. J. Brush, "Design and validation of an intensity-based POF bend sensor applications in measuring three-dimensional trunk motion," Master's thesis, The Ohio State University, 2010.

[89] F. Kamal, "Using 5.9 ghz dsrc to aid the elderly in vehicular environments," Master's thesis, University of Alberta, 2013.

[90] *IEEE Standard for Local and metropolitan area networks - Part 15.4: Low-Rate Wireless Personal Area Networks (LR-WPANs)*, IEEE Std., Rev. 2, June 2011.

[91] *ANT Message Protocol and Usage*, Dynastream Innovations Inc. Std., Rev. 4.5, November 2011.

[92] S. Madgwick, "Mahonyahrs.c," [Date Accessed Aug. 20, 2012]. [Online]. Available: http://www.x-io.co.uk/open-source-imu-and-ahrs-algorithms

[93] E. Chan, "Fatfs - generic fat file system module," [Date Accessed Sept. 13, 2012]. [Online]. Available: http://elm-chan.org/fsw/ff/00index_e.html

Appendix A

Schematics

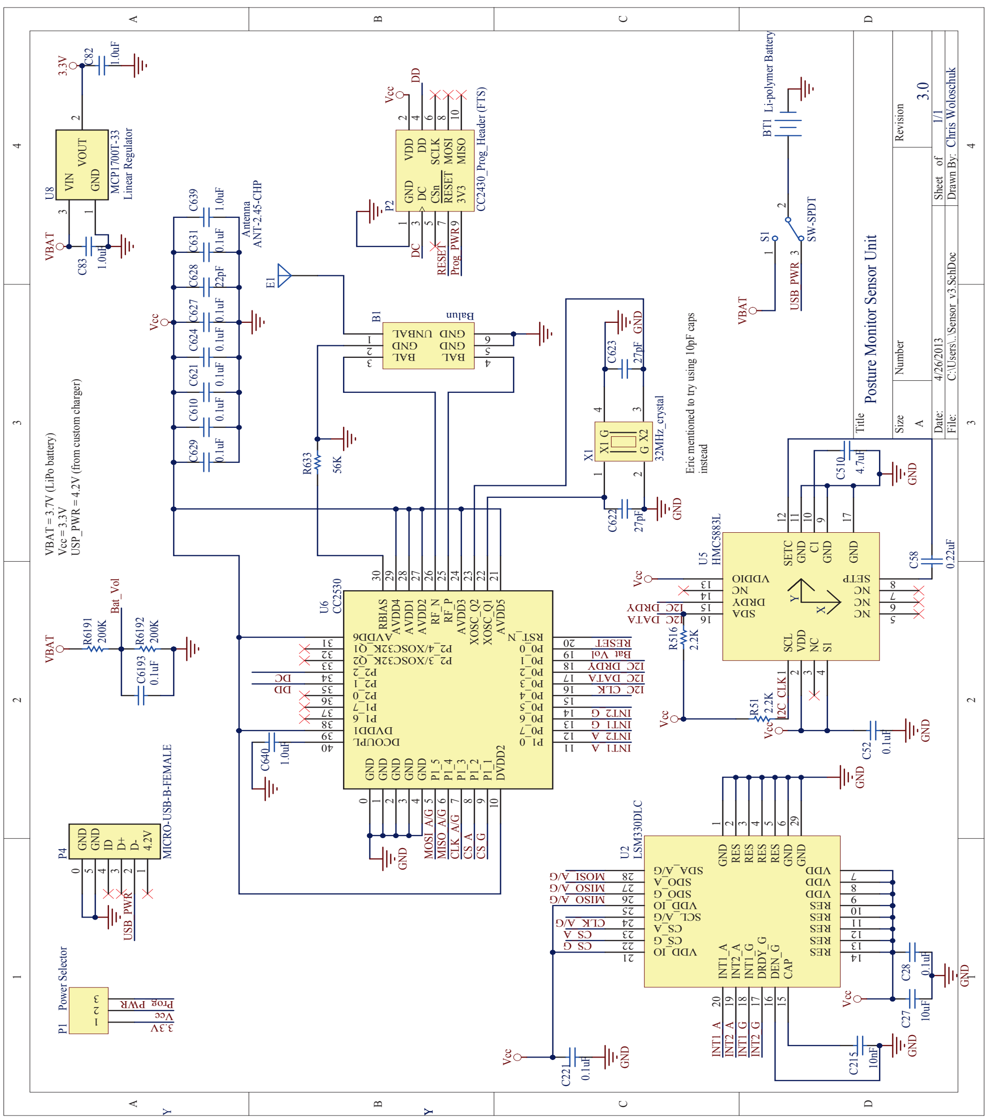

Figure A.1: Sensor unit schematic

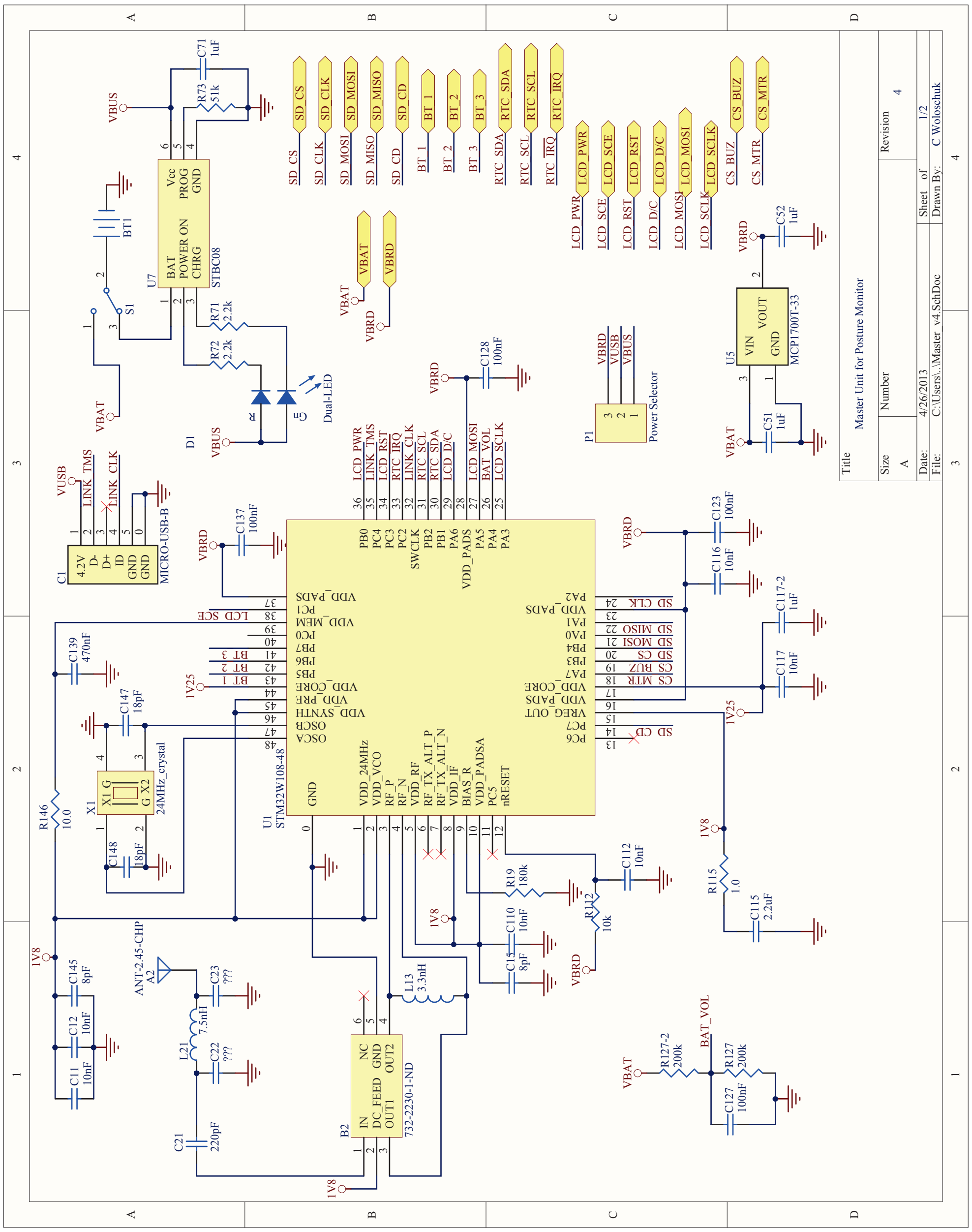

Figure A.2: Master unit schematic page 1

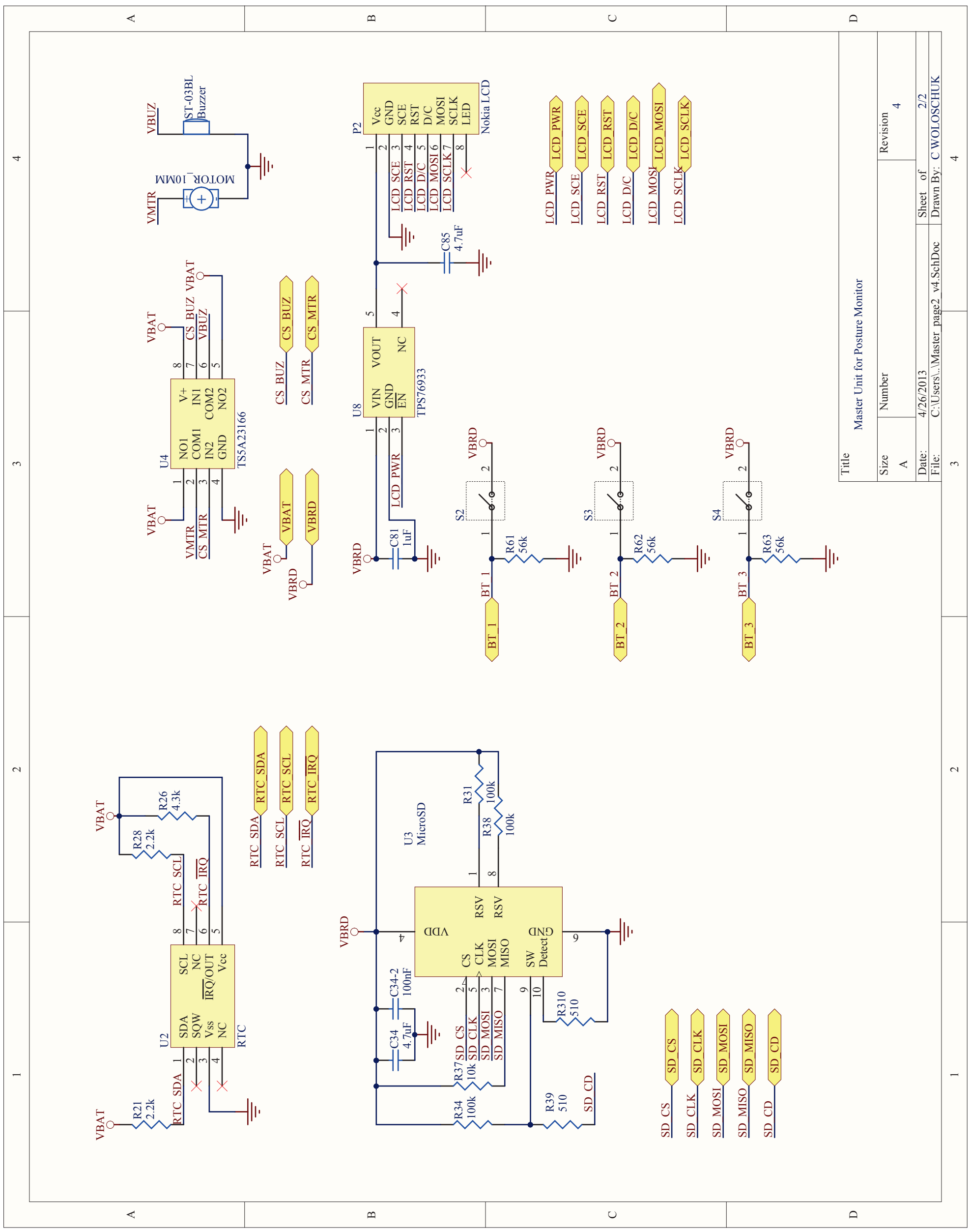

Figure A.3: Master unit schematic page 2

Appendix B

PCB Layouts

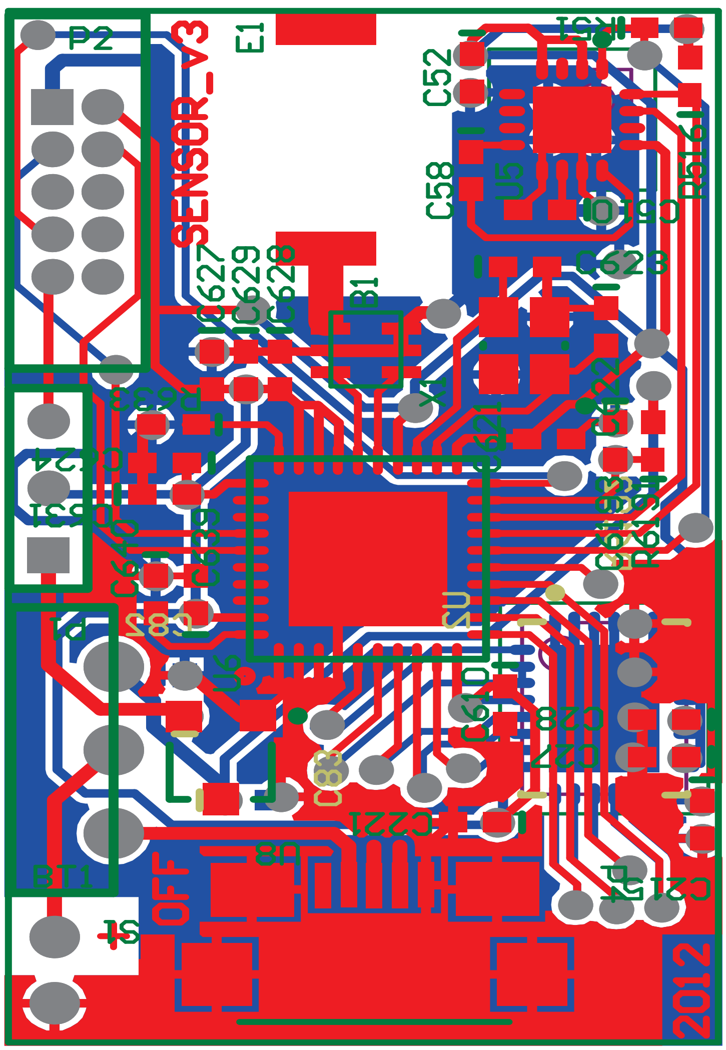

Figure B.1: Sensor unit PCB layout

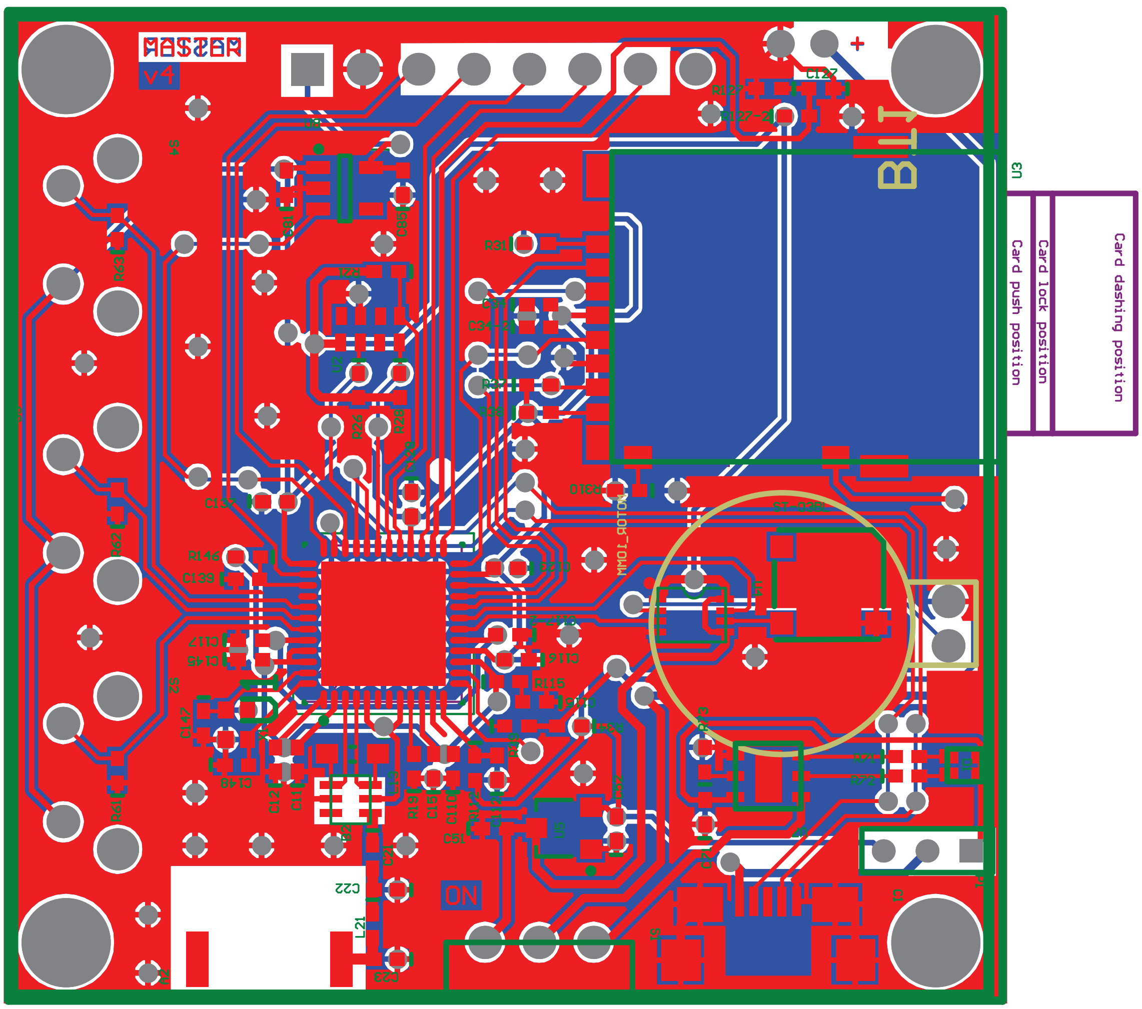

Figure B.2: Master unit PCB layout